Computational Analysis of Fission Penetrability Through Double-Humped Barriers by Exact and JWKB Methods

MARIO D'AMICO

A Thesis

in

The Department

of

Physics

Presented in Partial Fulfilment of the Requirements
for the Degree of Master of Science at
Concordia University
Montreal, Quebec, Canada

November 1992

ISBN 0-315-84646-1

Canada

Abstract

Computational Analysis of Fission Penetrability Through Double-Humped Barriers by Exact and JWKB Methods

Mario D'Amico

After the discovery of the double-humped potential barrier, researchers have derived a host of expressions for the probability of tunnelling through such a barrier. It is generally believed that the penetrabilities obtained by using the various methods do not differ sufficiently to have significant effects on the analysis of experimental data on fission. However, some have expressed doubts concerning the use of the usual JWKB method and have offered improved approximate and Exact methods for developing penetrability expressions. This thesis is devoted to the quantitative comparison of penetrabilities from these expressions, and to the investigation of effects various methods will have on spontaneous and isomeric fission half-lives.

Results from the penetrability expressions are compared in relation to the pure vibrational state energy levels, level heights, resonance widths, and the probability of penetrating the full barrier from its ground-state deformations.

ACKNOWLEDGEMENT

I wish to thank Dr R.C Sharma and the Concordia Physics Department for their guidance throughout my work.

TABLE OF CONTENTS

TABLE OF CONTENTS

LIST OF FIGURES

LIST OF FIGURES

LIST OF FIGURES

LIST OF FIGURES

LIST OF TABLES

INTRODUCTION

Prompted by the discovery of neutrons from experiments performed by Rutherford, Chadwick, Irene and Frederic Joliot-Curie; Fermi[1934][1] and co-workers initiated experiments involving irradiation of Uranium by neutrons. These experiments led Fermi to believe that it might be possible to extend the periodic table to higher atomic numbers by neutron induced processes, producing heavier elements called "transuranium elements". It was believed at this point that only heavier elements could be produced by such processes. Later investigation by Hahn and Strassman[1938][2], as well as Curie and Savitch[1938][3] produced a number of unexpected results which finally led Hans and Strassman to discover that elements of smaller atomic mass and charge could also be produced from Uranium.

Within a few weeks after this discovery, Meitner and Frisch[1939][4] proposed a model of nuclear fission in terms of a liquid-drop of the nucleus. They called the process "fission", drawing analogy from the division of biological cells . On the basis of a fluid sphere, dividing into two smaller droplets due to deformation caused by an external disturbance, they postulated that for heavy nuclei, the mutual repulsion of the electrical charges balance surface tension forces so delicately that only a small amount of external

energy is required to cause breakup of the nucleus into approximately symmetric fragments. Bohr and Wheeler[1939][5] did the pioneering work of giving a detailed qualitative description of what is known today as the Liquid Drop Model (LDM) in Nuclear Physics.

The LDM with its many successes , however, is not adequate in predicting the nuclear properties associated with the shell structure of the nucleus. To explain spin and parity of nuclei with odd number of neutrons and protons, a single particle model (SPM) is used based on the assumption that each nucleon moves in a potential resulting from the interaction of that nucleon with all the remaining ones. Calculations based on this model were performed by Mottelson , Nillson[1956][6] and Bes and Szymanski[1961][7] . By assuming a deformation dependent potential, Nillson calculated single particle energy as a function of nuclear deformation, but his model failed to explain properties for large deformation and high energies.

The problem in the SPM at high energies was resolved by Strutinsky[1967][8] who proposed a method in which shell effect was considered as small deviation from a uniform single particle energy level distribution, and was treated as a correction to the LDM energy. The combination of the LDM potential energy and shell correction energy led to a double-humped potential barrier shape like the one shown in Fig. 1 whereas, the LDM only predicts the existence of a single-humped potential barrier(dotted line). Moreover, the well

established "thorium anomaly" was theoretically resolved by Möller and Nix[9] when they introduced a mass asymmetric deformation in their calculation of fission barrier and found that for some nuclei (N~143) , the outer barrier was split into two saddle points separated by a third minimum, resulting in a triple-humped barrier.

The Strutinsky barrier was immediately successful in explaining isomeric fission and observed intermediate structure in induced fission cross sections for nuclei in the actinide region of the periodic table. A study of these nuclear processes requires the knowledge of the transmission through the double humped-barrier, which in turn requires a mathematical description of the barrier. A solution to the problem of mathematically describing the shape of the double-humped barrier was proposed by Wong and Bang[10]. They approximated the barrier with respect to the nuclear ground state, by smoothly joining three parabolic segments. In this approximation, the potential energy of a nucleus with respect to nuclear deformation, requires six parameters; three energies corresponding to the heights of the two peaks and the depth of the well; and three frequencies corresponding to the amount of curvature.

Various forms of Exact and JWKB methods have been employed in deriving expressions for the probability of tunnelling through a double-humped potential. The JWKB methods vary in their use of connection formulas, and their

approximation method. Bohm[1951][11], Merzbacher[1970][12], and Kemble[1937][13], obtained the JWKB solutions by using the asymptotic approximation and bi-directional connection formulas at the turning points. This approach has been severely criticized by Fröman[14]. Instead, he uses a convergent series expansion method to arrive at the JWBK solutions to the Schrodinger equation. The JWKB solutions based on Fröman's formalism are exact solutions and yield uni-directional connection formulas.

Unlike the asymptotic form of the JWKB method which yields simple closed form solutions for the penetrability, the Exact methods require the more complicated Weber Cylinder Parabolic Functions. In most of the known published works, Weber's functions have been approximated by using their known series expansion, by interpolating from existing tables in a limited range of parameters, or by using Taylor's expansion. In the present work, the Weber's functions are evaluated to a higher degree of accuracy through modern numerical techniques by using Airy and Hypergeometric functions. High precision is required in evaluating the Weber functions because of small fission widths at low energies. An alternative is to use Lorenzian curve fitting at resonance.

It is the purpose of the present work to offer a mathematical and a detailed numerical analysis of the various expressions available for the penetrability through a two-humped potential barrier. Four characteristics of the energy

versus probability graph are studied for varied barrier parameters, namely: pure vibrational state energy levels, level heights, level widths, and the penetrability through the full barrier from ground state energy. These results will be used to investigate the effects the differences will have on predictions of spontaneous and isomeric fission half-lives.

Chapters 1 and 2 focus on the development leading to the present-day double-humped barrier. Chapters 3 to 5 describe various mathematical expressions for penetrability through double and triple-humped barriers. Two methods, JWKB and exact are analyzed. Fröman's F matrix formalism is also discussed. Ignatyuk[1969][15] was the first to apply the asymptotic JWKB equations to the double-humped barrier. His results have been slightly expanded by Bhandari[1974-1980][16-18] for double-humped potentials. Cramer and Nix[1970][19] were the first to give exact expressions. As well, Sharma and Lebeouf[1972-1975][20-22] have expressions which take into account non zero reflection imposed by Cramer and Nix, and allowance for the initial state of the nucleus. In addition, Sharma and Leboeuf have used Fröman's F matrix to obtain a JWKB penetrability expression.

Chapter 6, describes the physical mechanism of the spontaneous and isomeric fission as relating to the Strutinsky barrier. Chapter 7, deals with the numerical techniques used, such as the methods for obtaining values for the Weber functions. Finally, in chapter 8, a detailed numerical analysis is performed for the various penetrability

expressions and the effects of their use in predicting Spontaneous and Isomeric fission half-lives is studied.

The characteristics of the penetrability are derived by varying the six barrier parameters. The maximum and minimum values of the barrier parameters are obtained from experimental data for actinide nuclei. Since many works have been published in which the experimental barrier parameters have been adjusted to agree with isomeric and spontaneous fission half-lives, we hope to investigate whether the above methods vary sufficiently to have an effect on these predictions. Also, Cramer and Nix have remarked that the energy level shifts between the exact and JWKB increase as the deformation energy increases. We wish to study whether this is generally true.

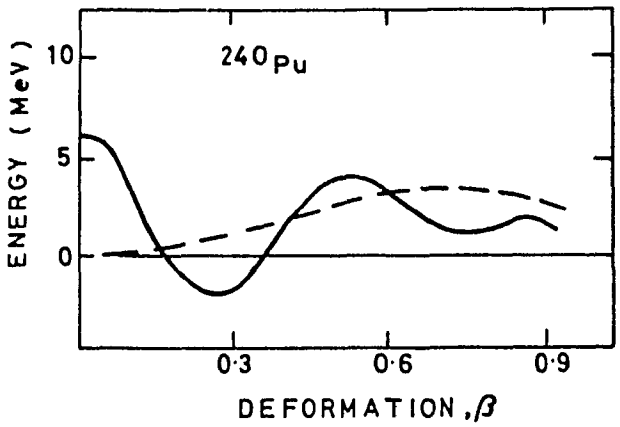

FIG. 1. The Double-Humped potential barrier as a result of the superposition of the Liquid Drop energy and the Shell-Correction Taken from S.Bjornholm and J.E. Lynn 1980.

CHAPTER 1

Nuclear Models and Fission

1.1 Collective Coordinates

In most nuclear models, it is convenient to use a macroscopic approach in which collective, rather than single-particle, degrees of freedom are used. Swiatecki and Bjornholm[23] have pointed out that three degrees of freedom is the barest minimum required to reveal the essential features of nuclear dynamics. The three degrees of freedom commonly used are nuclear stretching(c), necking(h), and mass-asymmetry. These variables are related, though vaguely, to the Legendre Polynomials. Stretching and necking coordinates (Fig. 2) are useful in the study of the excitation mechanism of the fission process, which involves a particle moving in a deformed time-dependent potential. These variables are also used in Strutinsky's Shell Correction Method.

Collective coordinates are primary tools for modelling four important nuclear collective motions (Fig. 3): vibration or compression, rotation, photonuclear resonance, and nuclear fission. Photonuclear resonance occurs when a photon approaches a nucleus resulting in the accumulation of protons in an area of the nucleus. This results in the formation of necking and stretching of the nucleus, and hence resonance. On the other hand, fission is the separation of a nucleus into

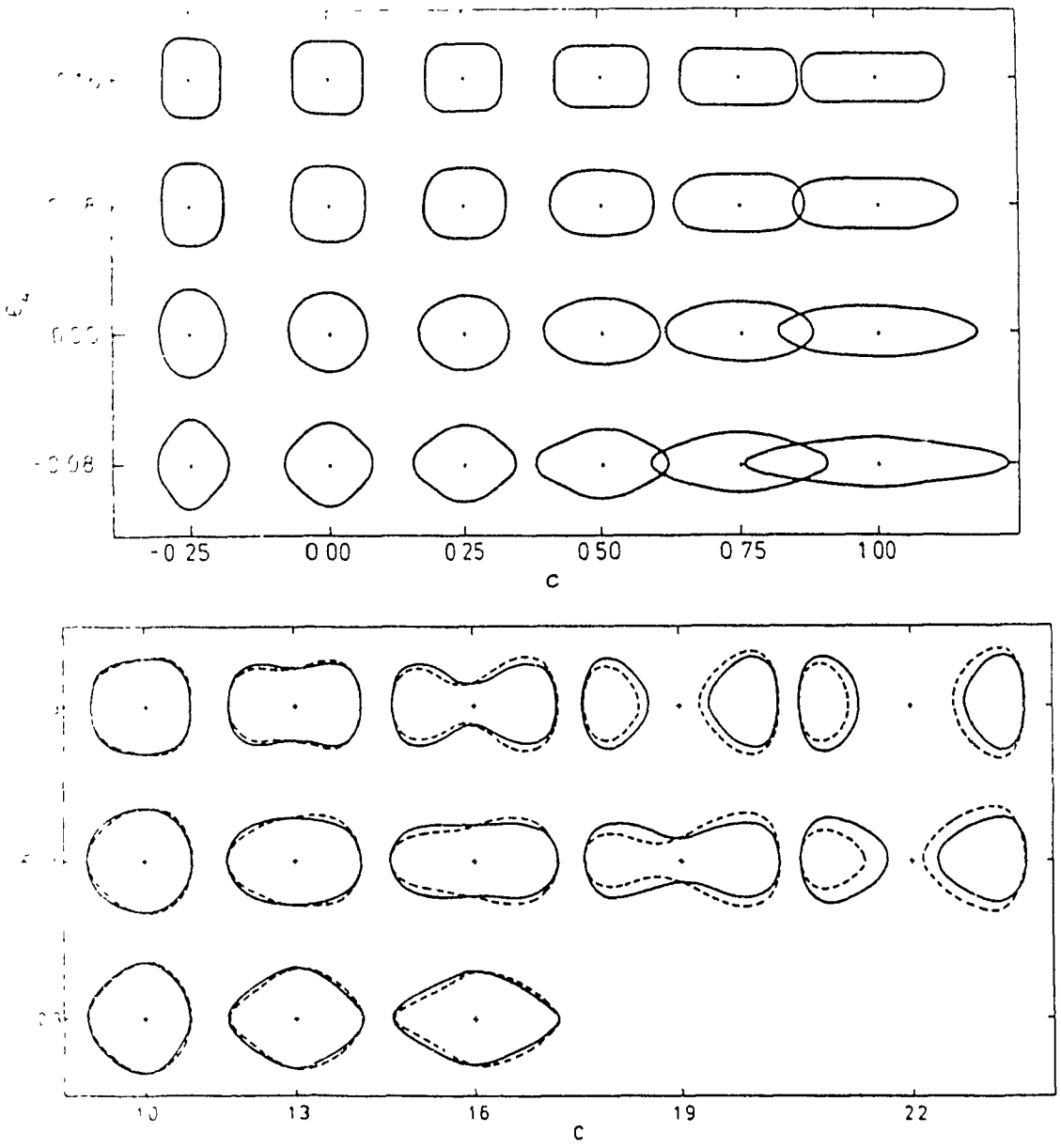

FIG. 2. Nuclear shapes corresponding to Stretch and Neck coordinates. Taken from S Bjornholm and J E Lynn 1980

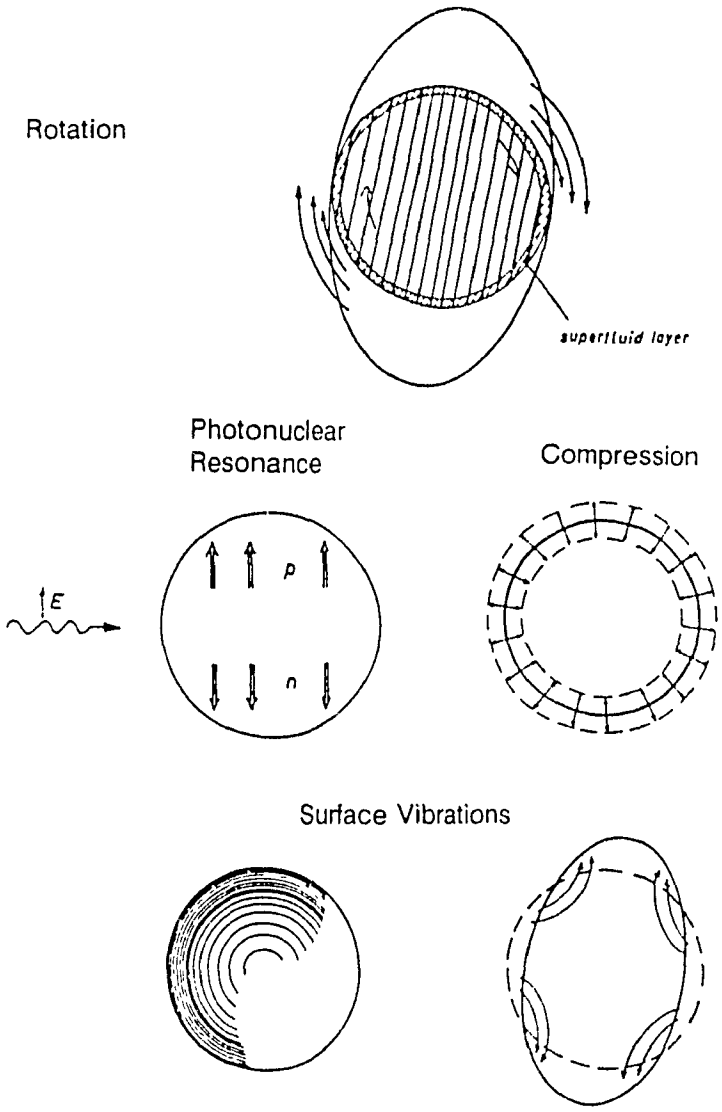

FIG. 3. Schematic figures of types of Nuclear Motions

usually two asymmetric fragments.

The LDM model was developed primarily to explain the stability of a nuclear drop with respect to distortion of the nucleus. Therefore, stretching and necking coordinates are not used in the LDM. Instead, the LDM and SPM use the Legendre Polynomials or Spherical Harmonics in the radius, R(θ), as,

$$R(\theta) = R[1+\alpha_o+\alpha_2 P_2(\cos\theta)+\alpha_3 P_3(\cos\theta)+.....] \qquad (1.10)$$

$$R(\theta) = R[1+\beta_o+\beta_2 Y_{20}(\cos\theta)+\beta_3 Y_{30}(\cos\theta)+..... \qquad (1.11)$$

The deformation parameters α and ß are related by

$$\alpha_\lambda = a_{lo}\left(\frac{4\pi}{2l+1}\right)^{1/2} = \beta_\lambda\left(\frac{4\pi}{2\lambda+1}\right)^{1/2} \qquad (1.12)$$

The potential energy of a deformed nucleus is derived in terms of nuclear deformation parameters. Fission mass asymmetry is explained by including odd α terms (Fig. 4) and even α terms are used to explain symmetric fission (Fig. 5).

1.2 The Liquid Drop Model

Bohr and Wheeler[5], using the analogy of a liquid drop, calculated the nuclear potential energy as the sum of surface energy and electrostatic energy in terms of nuclear deformation. The electrostatic energy is simply due to the coulomb effects of protons. The surface tension energy arises due to the nuclear binding forces. The total energy of a drop

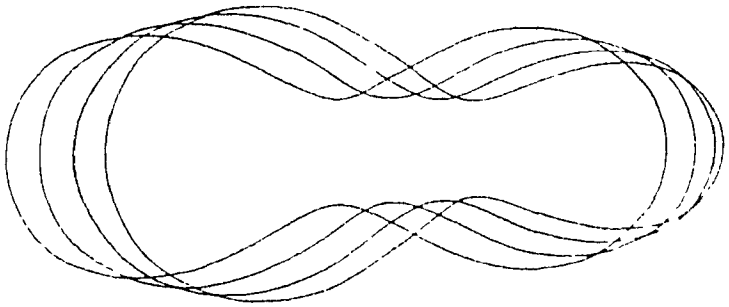

FIG. 4. Nuclear shapes corresponding to varied α_1 and fixed even α terms of the Legendre Polynomials Taken from R. Vandenbosch and R. Huizenga 1973

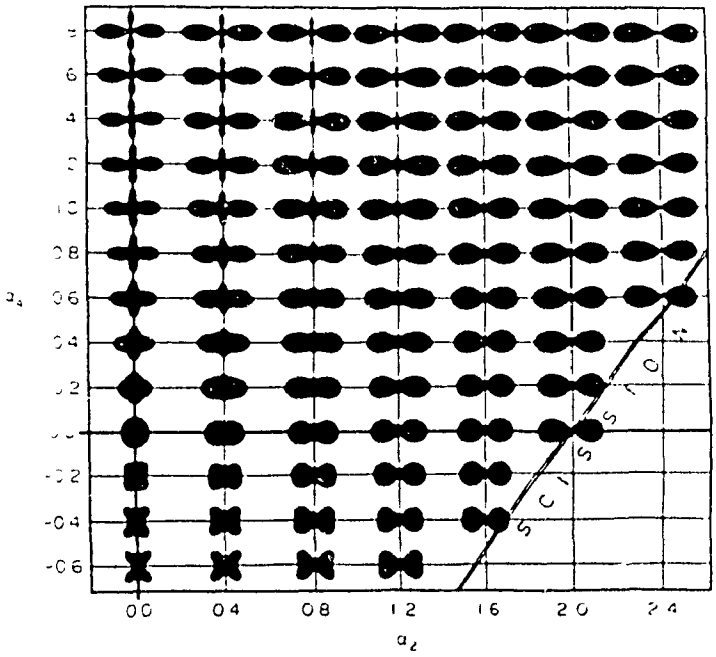

FIG. 5. Nuclear shapes corresponding to the α_2 and α_4 terms of the Legendre Polynomials Taken from R Vandenbosch and R. Huizenga 1973

is then obtained under certain assumptions. It is assumed that the drop is an incompressible fluid of volume $(4\pi/3)r_o^3A$, a uniformly distributed charge Ze, and possessing surface tension O. The energy of symmetric distortion from spherical shape to the forth order of even α is given by,

$$\Delta E_{S+E} = 4\pi r_o OA^{2/3}[2\alpha_2^2/5+116\alpha_2^3/105+101\alpha_2^4/35+2\alpha_2^2\alpha_4/35+\alpha_4^2] - 3(Ze)^2/5r_oA^{1/2}[\alpha_2^2/5+64\alpha_2^3/105+58\alpha_2^4/35+8\alpha_2^2\alpha_4/35+5\alpha_4^2/27] \quad (1.20)$$

It is obvious that for a liquid drop a point is reached when the surface is no longer able to contain the electrostatic energy. At this point the drop will easily break up. The point of instability of the nuclear drop can be obtained from Eq.(1.20) as the limiting value of (Z^2/A)

$$(Z^2/A)_{limiting} = 10(4\pi/3)r_o^3O/e^2 \quad (1.21)$$

which can be written as

$$(Z^2/A)_{limiting} = 14MeV\left(\frac{10r_o}{3e_2}\right) \quad (1.22)$$

$(Z^2/A)_{limiting}$ from Eq.(1.22) gives a value which is 17% higher than (Z^2/A) for U^{238} (35.56). Thus we can conclude that nuclei such as Uranium and Thorium lie close to the limit of stability. These results can also be used to calculate the energy at the point of scission by minimizing Eq.(1.20) with respect to α_4 to obtain,

$$\alpha_4 = -(243/594)\alpha_2^2 \qquad (1.23)$$

Let $x=(Z^2/A)/(Z^2/A)_{limiting}$, then

$$E_f = (4\pi r_o^2) OA^{2/3} [98(1-x)^3/135 - 11368(1-x)^4/34425 + \ldots] \qquad (1.24)$$

The energy in Eq. (1.20) of a nuclear droplet involves even α terms, limiting fission to symmetric shapes only. For asymmetric fission, it is necessary to include odd α terms. Cohen and Swiatecki[1963][24] investigated saddle point configurations for small odd deformations to study asymmetric mass division. They concluded that division of the nucleus, was energetically more favourable to symmetric division, which was physically untenable. Investigations continued without success, and no asymmetric equilibrium configuration with energy lower than symmetrical configurations were found.

The above failure, coupled with others prompted refinements to the LDM, including, some type of single particle effects, nonuniform charge distribution, compressibility, and a curvature dependent surface tension.

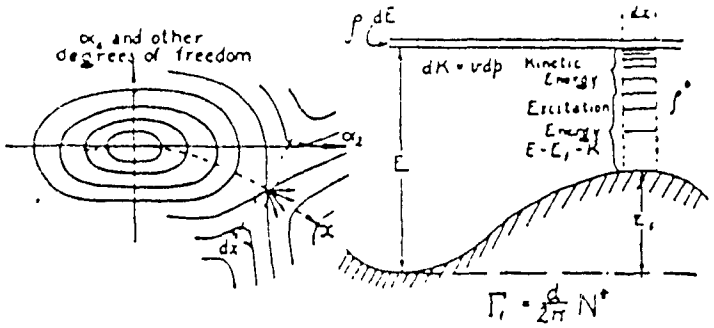

FIG. 6. Energy required to produce unstable deformations towards fission Taken from N Bohr and J A Wheeler 1939

The LDM is successful in relating mass to nuclear stability. It predicts a spherical shape in the ground state of the nucleus. The LDM also predicts a one peaked fission barrier. The probability of penetrating such a barrier is of exponential nature.

1.3 The Shell Structure of the Nucleus

The LDM inadequately predicts those effects which are associated with the shell structure of the nucleus. On the other hand, the single particle model is successful in explaining shell gaps and spin and parity of nuclei with an odd number of neutrons or protons and nuclear magic numbers (2,8,20,28,50,82,126 for neutrons and protons). In this model, it is assumed that each nucleon moves in an average potential approximately representing the interaction of one nucleon with the rest.

Investigations of static and dynamic properties of nuclei indicate periodicities in the properties of nuclei. It was first suggested by G. Gamow[1934][25] and W. Elasser[1934][26] that these properties may be due to a shell structure similar to the atomic shell structure.

Magic number effects are the strongest evidence in favour of shell structure. An element possessing a magic number of nucleons has more stable isotopes than its neighbour.

Similarly, an element possessing a magic number of neutrons has more stable isotones than its neighbour. Neutron cross sections are very low at magic numbers, indicating that shells are closed and do not absorb the incoming neutron. For the same reason, elements having only one valency neutron are good spontaneous neutron emitters.

1.4 Nillson Model

Nillson and collaborators[1955][27], used a deformed harmonic oscillator potential with $P_2(\cos\Theta)$ and $P_4(\cos\Theta)$ terms included to account for the spheroidal and the neck-constriction degrees of freedom in describing the shape. The Hamiltonian used is

$$H=\frac{p^2}{2m}+\frac{1}{2}\omega_o^2 r^2[1-2\beta Y_{20}(\theta)]-Cl.s-Dl^2 \qquad (1.40)$$

The appropriate coordinates of the system are represented by three Euler angles Θ_i, a deformation parameter ß, and the particle coordinates r'_p relative to the nuclear symmetry axiz Z'. The spin-orbit coupling is represented by the term -Cl·s, with C being constant within an oscillator shell.
Using the above hamiltonian , Nillson derived,

$$\omega_o(\beta_o)=\omega_{oo}[1+(\frac{4}{5}\pi)^{-1/2}\beta_o)^2(1-2(\frac{4}{5}\pi)^{-1/2}\beta_o)]^{-1/3} \qquad (1.41)$$

The energy map as a function of distortions is illustrated in Fig. 8. At large α_2 values, the energy started to rise rapidly.

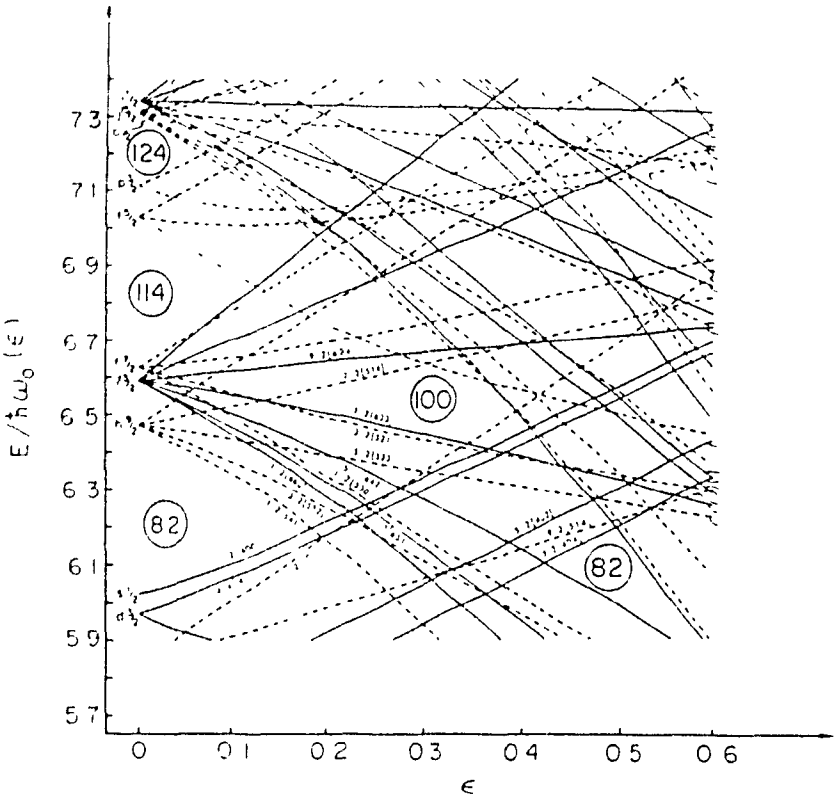

FIG. 7. Nilsson diagram for odd protons Taken from R Vandenbosch and R Huizenga 1973

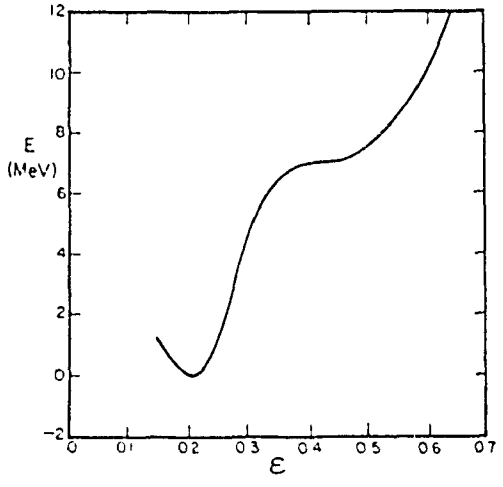

FIG. 8. Energy as a function of deformation for the Nilsson deformed shell model Taken from R Vandenbosch and R Huizenga 1973

CHAPTER 2

Strutinsky's Shell Correction Approach

At large deformations, the single particle model failed to give reasonable deformation energies. Strutinsky[1967][8] proposed a method requiring both the SPM and the LDM. In Strutinsky's approach , the total energy of the nucleus is the sum of the LDM contribution and a correction derived from single particle effects. The method assumes the total energy of the nucleus to be dominated by the smoothly varying LDM energy. The single particle contribution is derived from, the normal nonuniform SPM energy , and a modified uniform single particle energy distribution.

2.1 Strutinsky's Method

Strutinsky considered the total potential energy of a nucleus to be,

$$E=E_{LDM}+\sum_{p,n}(\delta U+\delta P) \tag{2.10}$$

Neutron and proton corrections were treated separately. The terms in the sum are correction terms. The first correction term, δU, is due to the difference between two methods of calculating single particle energies; one with nonuniform spacings and degeneracies, the other as a uniform distribution. The shell correction is therefore given by,

$$\delta U=U-\tilde{U} \tag{2.11}$$

The nonuniform energy, U ,is simply the sum of the energies of n_i particles occupying a level with energy E_i.

$$U=\sum_{\nu} 2E_i n_i \tag{2.12}$$

The uniform energy, $\tilde{U}$, uses a function (g(E)) obtained by taking weighted average of nonuniform energies using a weighting function scheme.

$$\tilde{U}=2\int_{-\infty}^{\lambda} Eg(E)\,dE \tag{2.13}$$

The second correction term, δP ,is the contribution from pairing correlation calculated by the BCS approximation[28].

Both the sum of the single particle correction, and the sum of the pairing correlation contribution, produce oscillating energies as a function of deformation. However, these contributions are out of phase. As well, the pairing energy is much lower than the single particle energy. Therefore, the pairing effect serves to decrease the amount of modulation by the single particle correction alone.

Equation (2.10), a function with respect to deformation, is dependent on the SPM and requires an assumption to be made in the choice of the average single particle potential. The shell correction approach has been used by many, differing only in the choice of average potential. Strutinsky's own calculations[1967][8] employed a deformed Wood -Saxon potential. Calculations have also been carried out using the Yukawa and Harmonic Oscillator Potential by Moller and Nix[1974][9]. These methods are widely discussed in many papers.[28-30]

2.2 Results of calculations

Strutinsky's method was very successful in predicting the nuclear binding energies. When applied to the actinide nuclei, Strutinsky discovered a secondary well or dip in the potential energy. A study of the potential energy as a function of deformation lead to a double-humped barrier as a

result of an oscillating shell correction superimposed on the liquid drop saddle point energy region.

Shell correction varies with the changing proton and neutron number, while the LDM energy varies with changing fissility parameter. The sum of both the differences gives rise to variation in double-humped barriers from nucleus to nucleus.

2.3 Double-Humped Barrier

Calculations carried out by Moller and Nix[9], using the modified harmonic oscillator shell model potential for spontaneously fissioning isomers, reveal secondary minima in the range 2-3 MeV for Th, U, Pu, Cm, Cf, and Fm.

Experimental data on spontaneous fission isomer half-lives and excitation cross-sections and intermediate structure in fission cross-sections indicate that the inner barrier is higher than the outer barrier. Early calculations in which the nuclear shape was assumed axially and reflection symmetric, showed the opposite. This discrepancy was removed qualitatively by Moller and Nix demonstrating that reflection asymmetry in the nuclear shape gave potential energy minima at elongations corresponding to the outer barrier. The method used included, adding third and fifth Legendre Polynomials, $(\alpha_3 P_3 \cos\theta)$ and $(\alpha_5 P_5 \cos\theta)$ to the deformation shapes. Fig. 9 shows parametric values of the first barrier, the second

minimum, and outer barrier for various nuclei.

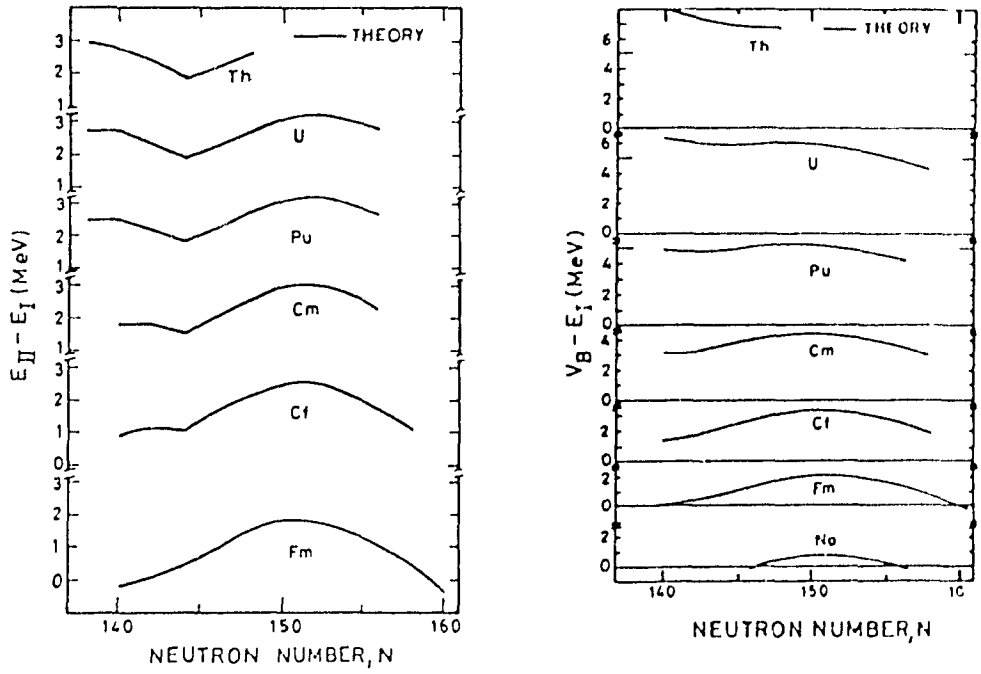

FIG. 9. Energy of the second minimum and outer barriers calculated from Strutinsky's method using a modified Harmonic oscillator shell model Taken from S Bjornholm and J E Lynn 1980

To simplify penetrability calculations, the double-humped barrier is generally constructed by connecting segments of parabolas. After the work of Wong and Bang[1969][10], Cramer and Nix[1970][19] developed an expression for the double-humped potential barrier in terms of three energies E_1, E_2, E_3 , three oscillator frequencies $\hbar\omega_1, \hbar\omega_2, \hbar\omega_3$ (Fig. 10) , and the connection points (a,b). The Strutinsky barrier also includes the first well, as shown in Fig. 11, where Sharma and Lebeouf's convention of parameters is used.

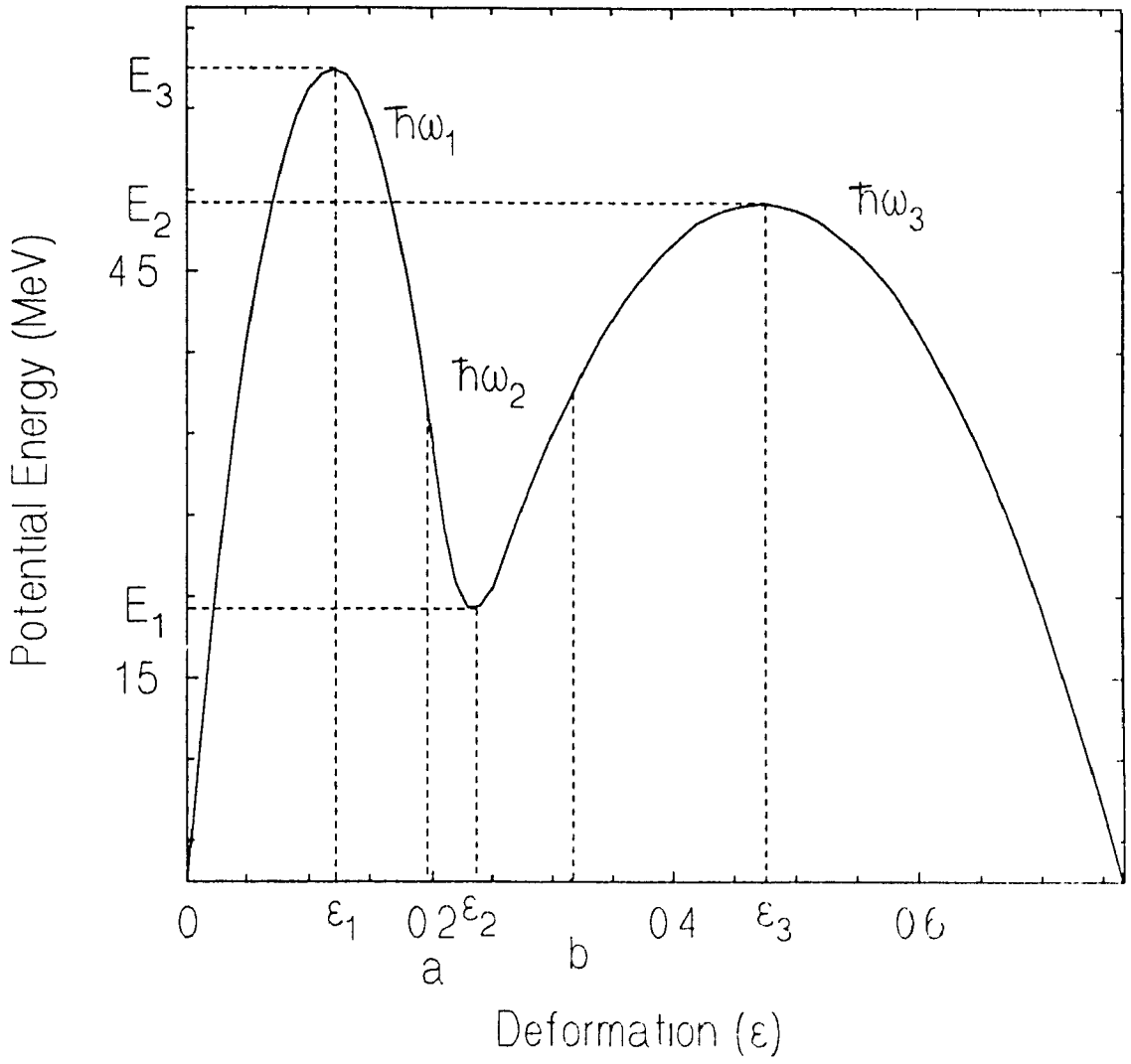

FIG. 10. The Strutinsky barrier approximated by three smoothly joined parabolas

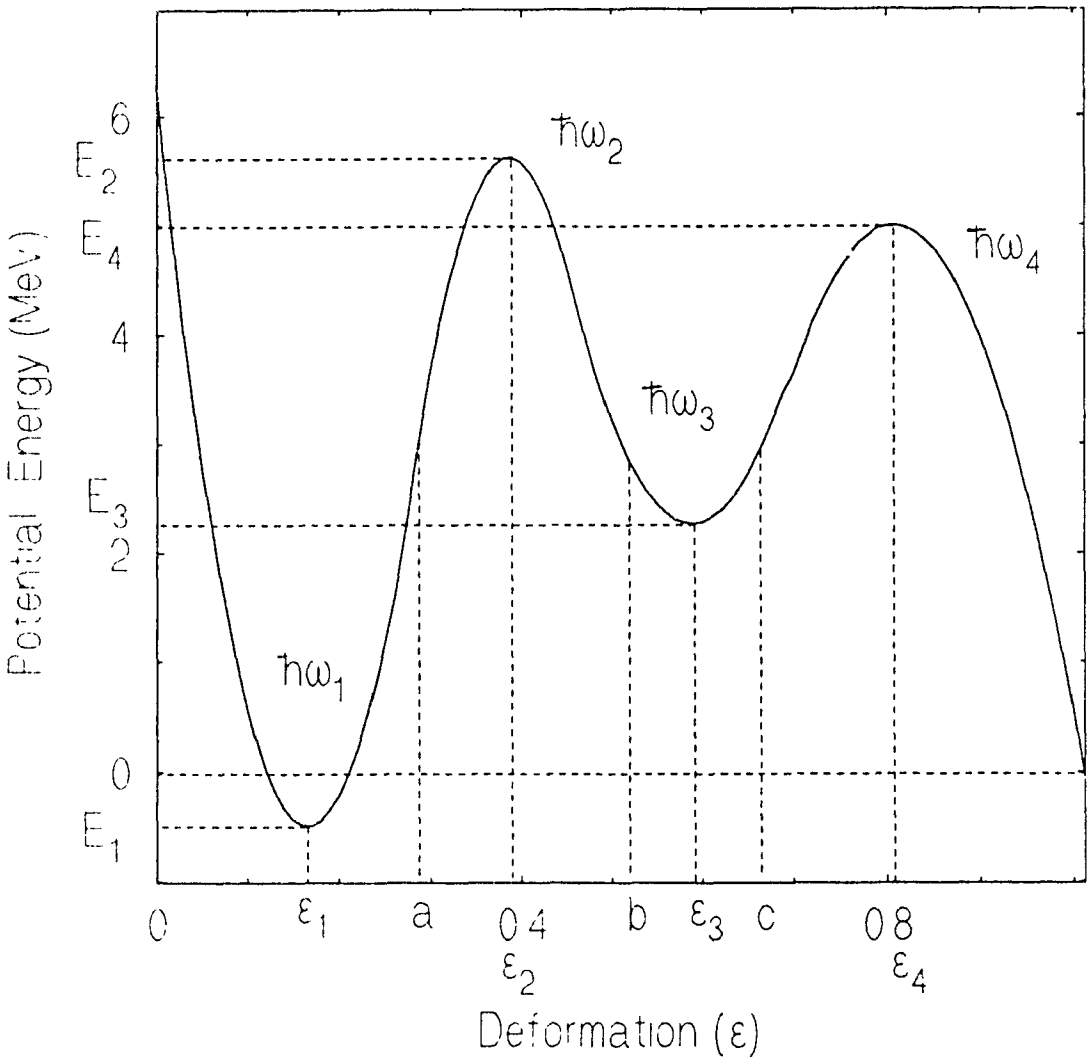

FIG. 11. The Strutinsky barrier including the first well

CHAPTER 3

JWKB

The JWKB approximation method provides a connection between classical and quantum mechanics, and is accredited to among others, B.S Jeffreys [1923][31], Wentzel, Kramers [1926][32], and Brillouin. In the usual JWKB approximation, the solution of the Schrödinger equation is expressed in terms of an asymptotic series from which the first order JWKB solutions are obtained. There are different mathematical variations of this leading to the same result. In 1965, Fröman[14] published a book in which he points out that the former works on this subject were unclear, and lacked mathematical rigour. He strongly criticises the methods used in developing connection formulas, and their bidirectional nature.

In barrier penetration problems, the wave function $\psi(x)$ in various regions, diverges on both sides of a classical turning point (Fig. 12). It is therefore essential to describe a method by which one can smoothly join two wave functions in both regions, removing this discontinuity. The connection formulas make use of a direction denoted by $(\rightharpoonup, \rightharpoonup, \rightharpoonup)$,describing the replacement of one term by another. For example, in the connection formula,

$$A\cos(f(r)) + Bg(r) \rightarrow (A+B)\exp(f(r)) \qquad (3.00)$$

the wavefunction on the left hand side connects smoothly with the function on the right at the turning point. Fröman pointed out that the bidirectional connection formulas developed by Bohm and others omit certain terms which would otherwise reveal their unidirectional nature. In Eq. (3.00), if A and B are known, one can get the term (A+B). On the other hand, there is no way of knowing A and B individually from the sum (A+B). Clearly, if B=0 in Eq. (3.00), the connection formula becomes bidirectional

$$A\cos(f(r)) \rightleftharpoons A\exp(f(r)) \qquad (3.01)$$

But this is not true in general .

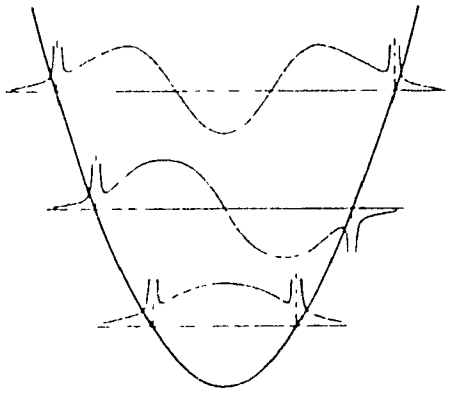

FIG. 12. JWKB approximation wave functions for the first three states for states in a potential well. Taken from D Rapp , H Rinehart

3.1 The JWKB Asymptotic Approximation

It was suggested by B.S. Jeffreys[31] in 1961 that the JWKB method be called the asymptotic approximation because of the exclusive use of the asymptotic expansions in the development of the JWKB equations. This method is widely used to explain fission phenomena involving barrier penetration. Some of the authors who made notable contributions are David Bohm[11], Kemble[13], Morse and Feshbach[33], and D.S. Onley[34]. This method involves solving the Schrödinger equation

$$\frac{d^2}{dx^2}\psi+\left(\frac{Q(x)}{\lambda}\right)^2\psi=0 \qquad \lambda<1 \tag{3.10}$$

by expanding $\psi(x)$ as

$$\psi(x)=\exp\left[\frac{1}{\lambda}\int_{x_0}^{x}dx\sum_{i=0}^{\infty}y_i(x)\lambda^i\right] \tag{3.11}$$

Reinserting $\psi(x)$ into Eq. (3.10) and putting $\lambda^{i=1,2,\ldots}=0$ yields

$$y_0=\pm iQ(x) \tag{3.12}$$

$$\frac{d}{dx}y_{i-1}=-\sum_{u=0}^{i}y_u y_{i-u} \qquad i=1,2,3,\ldots \tag{3.13}$$

This equation is in general not convergent, but asymptotic. Retaining the first three terms in the exponent, gives the second order JWKB solution.

$$\psi(x) = \left(\frac{Q}{\lambda}\right)^{-1/2} \exp\left[\pm i \int_{x_o}^{x} (1+\frac{1}{2}\epsilon_o)\,\frac{Q}{\lambda}\,dx\right] \qquad (3.14)$$

The first order JWKB-approximation is

$$\psi(x) = \left(\frac{Q}{\lambda}\right)^{-1/2} \exp\left[\pm i \int_{x_o}^{x} \frac{Q}{\lambda}\,dx\right] \qquad (3.15)$$

The connection formulas developed using the first order JWKB solution can be found in publications by R.E Langer[35], E.C Kemble[13] and D. Bohm[11]. The bidirectional formula connecting the classically allowed region to the forbidden one is

$$\frac{1}{\sqrt{k_1}} \exp\left(-\int_{x}^{a} k_1 \frac{dx}{\hbar}\right) \rightarrow \frac{2}{\sqrt{k_2}} \cos\left(\int_{a}^{x} k_2 \frac{dx}{\hbar} - \frac{\Pi}{4}\right) \qquad (3.16)$$

and a similar formula to connect the classically forbidden region to the allowed one is given by,

$$\frac{1}{\sqrt{k_2}} \sin\left(-\int_{a}^{x} k_2 \frac{dx}{\hbar} - \frac{\Pi}{4}\right) \rightarrow -\frac{1}{\sqrt{k_1}} \exp\left(\int_{x}^{a} k_1 \frac{dx}{\hbar}\right) \qquad (3.17)$$

$$k_1 = \sqrt{2m(V-E)} \qquad k_2 = \sqrt{2m(E-V)} \qquad (3.18)$$

3.2 Froman's JWKB Equations

Fröman started . h the one-dimensional time-independent Schrödinger equation Eq. (3.20).

$$\frac{d^2}{dz^2}\psi + Q^2(z)\psi = 0 \qquad (3.20)$$

Here , z is a complex variable and $Q^2(z)$ is an analytic function single valued in a certain region of the complex z plane. This equation is transformed by introducing new variables (w, φ) defined by

$$\psi = [q(z)]^{-1/2}\varphi(z) \qquad (3.21)$$

$$w(z) = \int^z q(\xi)\, d\xi \qquad (3.22)$$

Eq. (3.20) can be rewritten as

$$\frac{d^2}{dw^2}\varphi + (1+\varepsilon)\varphi = 0 \qquad (3.23)$$

$$\varepsilon = \frac{Q^2 - q^2}{q^2} - q^{-1/2}\frac{d^2}{dw^2}(q^{1/2}) \qquad (3.24)$$

3.21 The Function $\varepsilon(z)$

If we put $\varepsilon = 0$ in Eq. (3.24), the exact solutions to Eq. (3.23) are $\varphi = e^{iw}, e^{-iw}$, and the resulting wave function is ,

$$\Psi = q^{-1/2}\exp\left[\pm\int^z q(\xi)\, d\xi\right] \qquad (3.210)$$

If we choose $q^2(z)$ equal to $Q^2(z)$, the resulting function $\varepsilon(z)$ is not equal to zero but is small. In this case

Eq. 3.210 will give the usual form of the asymptotic JWKB approximation Eq. (3.15).

3.22 The Function q(z)

The solutions to Eq. (3.23), when $\varepsilon=0$,have been studied by Charles E. Hecht and Joseph E. Mayer [1957][36], where they give a solution that can be derived to any degree of accuracy specified. They also demonstrate the limit at which the usual asymptotic JWKB solutions are derived. The zeroth order solution is given as,

$$\frac{d\nu_i}{dx}=\left[\frac{Q^2(x)}{1-\frac{1}{4\nu_i^2}}\right]^{1/2}, \quad \nu_i=\int q(x)\,dx \tag{3.220}$$

This equation has asymptotic solutions,

$$\nu(x)=c+\int Q(x)\,dx \quad classicalregion \tag{3.221}$$

$$\nu(x)=\frac{1}{2}\exp\left[-2\int -Q(x)\,dx\right] \quad non\ classical \tag{3.222}$$

Hecht and Mayer derived the JWKB solutions

$$\psi(x) = \left(\frac{dv_1}{dx}\right)^{1/2} \sin(v_1) \qquad (3.223)$$

which lead to the usual JWKB solutions,

$$\psi(x) = \frac{1}{Q(x)} \sin\int Q(x)\,dx \qquad (3.224)$$

$$\psi(x) = \frac{1}{-Q(x)} \exp-\int -Q(x)\,dx \qquad (3.225)$$

In his method, Hecht finds q(x) in the first order approximation to be,

$$q^{(1)}(x)^2 = Q^2(x)\left[1 - \frac{1}{4}\frac{(Q^2)''}{Q^4} - \frac{5}{16}\frac{[(Q^2)'']^2}{Q^6} - \frac{1}{4}\xi^2 \ldots\ldots\right], \qquad (3.226)$$

$$\xi = \int Q(x)\,dx + \frac{\pi}{4} \quad classical$$

$$q^{(1)}(x)^2 = Q'(x)\left[1 - \frac{1}{4}\frac{(Q')''}{Q^4} + \frac{5}{16}\frac{[Q'']'}{Q^6} - 16e^{-2\Omega} + 240e^{-4\Omega} \ldots\right], \qquad (3.227)$$

$$\Omega = \int -Q(x)\,dx + 1 \quad non\ classical$$

A JWKB approximation based on the choice of q(x) is useful when Q(x) has a singular behaviour in the neighbourhood of the

breakdown of the usual JWKB approximation. Requiring ϵ to be small in the singular region, leads to the function q(x) differing from Q(x) in the neighbourhood of the singularity. The function q(x) is approximated everywhere else by Q(x). Fröman has studied the cases of Barrier Transmission and Bound states, and has found that for parabolic barriers the exact solutions require Q(x) equal to q(x).

3.23 F Matrix

Fröman developed an exact solution to Eq. (3.23) by expressing φ in the form

$$\varphi = a_1(w)\exp(iw) + a_2(w)\exp(-iw) \qquad (3.230)$$

from which he obtains

$$\frac{d}{dw}\varphi = ia_1\exp(iw) - ia_2\exp(-iw) \qquad (3.231)$$

By imposing a condition which allows $a_1(w)$ and $a_2(w)$ in Eq.(3.231) to be treated as constants,

$$\frac{da_1}{dw}\exp(iw) + \frac{da_2}{dw}\exp(-iw) = 0 \qquad (3.232)$$

he gets a new form of Eq.(3.23) in terms of two first order differential equations

$$\frac{d}{dw}a_1=\frac{1}{2}i\varepsilon[a_1+a_2\exp(-2iw)] \tag{3.233}$$

$$\frac{d}{dw}a_2=-\frac{1}{2}i\varepsilon[a_2+a_1\exp(2iw)] \tag{3.234}$$

These two equations can be replaced by one equation in matrix form

$$\frac{d}{dw}\bar{a}=\bar{M}(w)\,\bar{a}(w) \tag{3.235}$$

Integration of this equation yields

$$\bar{a}(w)=\bar{F}(w,w_o)\,\bar{a}(w_o) \tag{3.236}$$

which is a general solution to Eq. (3.235). Using this result, Fröman derives a general solution to Eq. (3.20) as,

$$\psi(x)=\overline{\zeta}(z)\,\bar{F}(z,z_o)\,\bar{a}(z_o) \tag{3.237}$$

All the F-matrices are defined in Appendix B.

Using these results, and the estimates of the function $\bar{F}$ known as the F matrix, Fröman derived the unidirectional connection formulas (3.238), (3.239), and (3.2310), which can only be used if the classical turning points of the applicable region are well separated and there is at most one turning point between regions. The unidirectional connection formulas from Fröman's F-matrix formulation are given as,

from allowed → to forbidden

(3.238)

$$Aq^{-1/2}\exp\left(i|w|+\frac{\pi}{4}\right)+Bq^{-1/2}\exp\left(-i\left(|w|+\frac{\pi}{4}\right)\right)\rightarrow(A+B)\,|q|^{-1/2}\exp\left(|w|\right)$$

$$|q|^{-1/2}\cos\left(|w|+\gamma-\frac{\pi}{4}\right)\rightarrow\sin\gamma\,|q|^{-1/2}\exp\left(|w|\right) \qquad (3.239)$$

and from forbidden → to allowed

$$|q|^{-1/2}\exp\left(-|w|\right)\rightarrow 2|q|^{-1/2}\cos\left(|w|-\frac{\pi}{4}\right) \qquad (3.2310)$$

CHAPTER 4

Penetrability Calculations using JWKB

4.1 Asymptotic JWBK Approximation

Ignatyuk[15] was the first to derive an expression for the penetrability through a double-humped barrier using the asymptotic form of the JWKB method. The penetrability is defined as ,

$$P(E) = \left| \frac{\psi_{trans}\sqrt{k_{trans}}}{\psi_{inc}\sqrt{k_{inc}}} \right|^2 \qquad (4.10)$$

Ignatyuk's derivation can be represented by using the following notations (Bhandari[16]),

$$a_1(x_1) = \frac{1}{\sqrt{k(x)}} \exp\left(\pm \int_{x}^{x_1} k(x)\, dx \right) \qquad (4.11)$$

$$f_1(x_1) = \frac{1}{\sqrt{k(x)}} \exp\left(\pm \int_{x_1}^{x} k(x)\, dx \right) \qquad (4.12)$$

$$k(x) = \left(\frac{2\mu}{\hbar^2} \right)^{1/2} (E - V(x))^{1/2} \qquad (4.13)$$

$$\hat{k}(x) = \left(\frac{2\mu}{\hbar^2}\right)^{1/2} (V(x) - E)^{1/2} \tag{4.14}$$

$$\nu_1 = \int_{t_1}^{t_2} \hat{k}dx, \nu_2 = \int_{t_2}^{t_3} kdx, \nu_3 = \int_{t_3}^{t_4} \hat{k}dx \tag{4.15}$$

The turning points are denoted as t_i; μ is the effective mass of the nuclei obtained from semiempirical results; and V(x) is the double-humped potential. With Eqs. (4.11) to (4.15), the connection formulas in Eqs. (3.16) and (3.17) can be rewritten as

(allowed → to forbidden)

$$a_+ \rightarrow e^{-i\pi/4}\left(f_+ + \frac{1}{2}if_-\right) \tag{4.17}$$

$$a_- \rightarrow e^{i\pi/4}\left(f_+ - \frac{1}{2}if_-\right) \tag{4.18}$$

(forbidden → to allowed)

$$f_+ \rightarrow \frac{1}{2}\left(e^{i\pi/4}a_+ + e^{-i\pi/4}a_-\right) \tag{4.19}$$

$$f_- \rightarrow \left(e^{-i\pi/4}a_+ + e^{i\pi/4}a_-\right) \tag{4.110}$$

It can be shown from these equations that the following relations are satisfied,

$$a_i(x_i) = e^{\pm i\nu_{i-1}} a_i(x_{i-1}) \tag{4.111}$$

$$f_i(x_i) = e^{\pm i\nu_{i-1}} f_i(x_{i-1}) \tag{4.112}$$

From Fig. 13, in region V it is assumed that we have only a transmitted wave. The wavefunction in this region can be written as

$$\psi_V(\varepsilon) = a_+(\varepsilon) \tag{4.113}$$

Region V is a classically allowed region. The wavefunction in region IV , a classically forbidden region, can be obtaining by connecting it at turning point t_4 with $\psi_V(\varepsilon)$ by using Eq. (4.17). Therefore,

$$\psi_{IV}(\varepsilon) = e^{-i\pi/4}\left(f_+(t_4) + \frac{1}{2} i f_-(t_4)\right) \tag{4.114}$$

Substituting from Eq. (4.112) gives,

$$\psi_{IV}(\varepsilon) = e^{-i\pi/4}\left(e^{\nu_1} f_-(t_3) + \frac{1}{2} i e^{-\nu_1} f_+(t_3)\right) \tag{4.115}$$

Similarly, the wavefunction in region III is

$$\psi_{III}(\varepsilon) = i e^{i\nu_2}\left(\frac{1}{4} e^{-\nu_1} - e^{\nu_1}\right) a_-(t_2) + e^{-i\nu_2}\left(e^{\nu_1} + \frac{1}{4} e^{-\nu_1}\right) a_+(t_2) \tag{4.116}$$

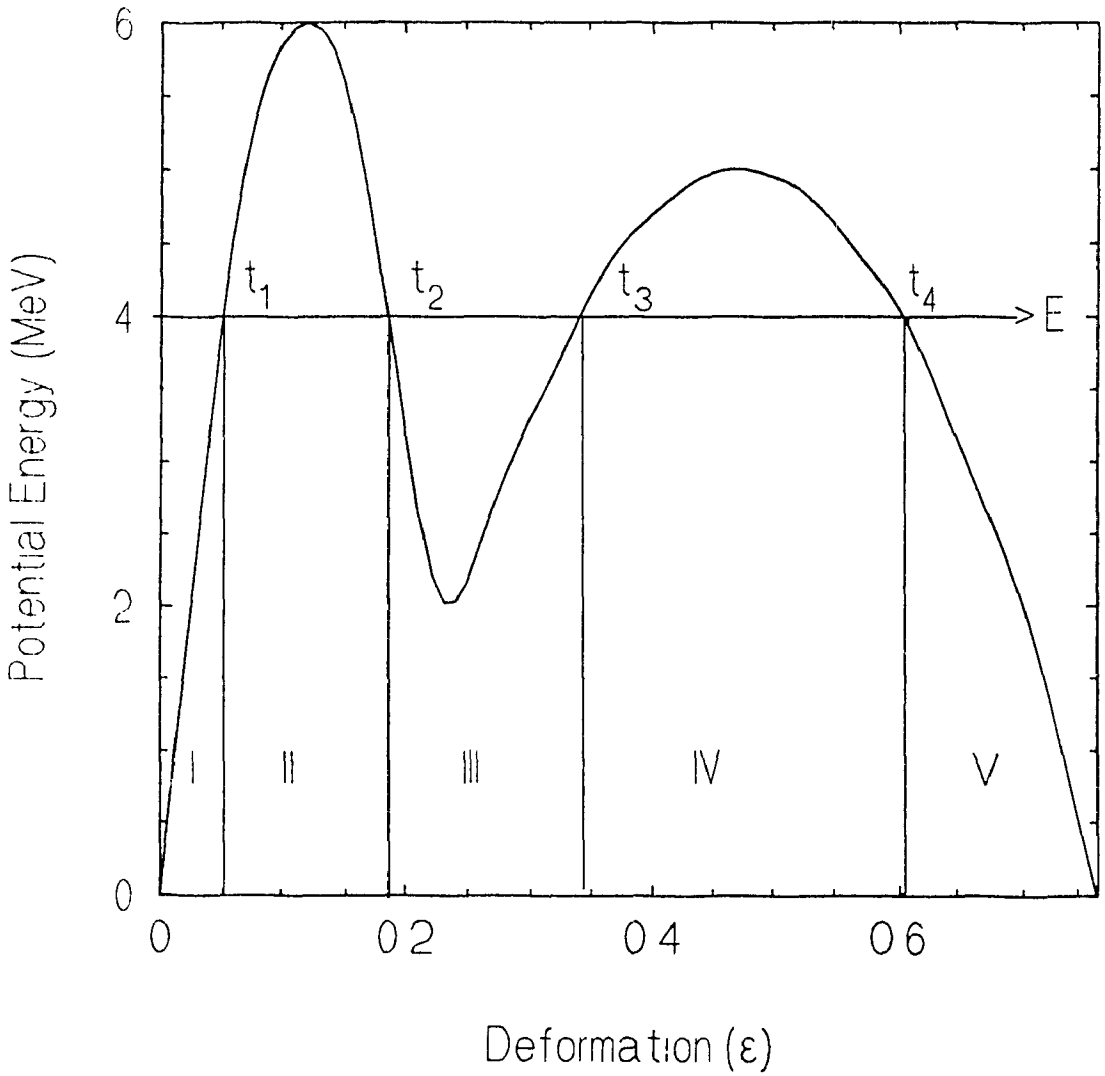

FIG. 13. Regions used in the JWKB asymptotic approximation for Ignatyuk's results

and in region II

(4.117)

$$\psi_{II}(\varepsilon) = \left[ie^{iv_2}\left(\frac{1}{4}e^{-v_3}-e^{v_3}\right)e^{i\pi/4}+e^{-iv_2}\left(e^{v_3}+\frac{1}{4}e^{v_3}\right)e^{-i\pi/4}\right]f_-(t_1) + \left[\frac{1}{2}ie^{-iv_2}\left(e^{v_3}+\frac{1}{4}e^{-v_3}\right)e^{-i\pi/4}+\frac{1}{2}e^{iv_2}\left(\frac{1}{4}e^{-v_3}-e^{v_3}\right)e^{i\pi/4}\right]f_+(t_1)$$

and finally in region I

(4.118)

$$\psi_I(\varepsilon) = \left[i\left(e^{iv_3}+\frac{1}{4}e^{-v_3}\right)\left(\frac{1}{4}e^{-v_2}-e^{iv_2}\right)e^{v_2}+\left(\frac{1}{4}e^{-v_2}-e^{v_2}\right)\left(e^{v_2}+\frac{1}{4}e^{-v_2}\right)e^{iv_1}\right]a_+(t_1) + \left[\left(\frac{1}{4}e^{-iv_3}-e^{v_3}\right)\left(\frac{1}{4}e^{-v_2}-e^{v_2}\right)e^{iv_2}+\left(e^{v_2}+\frac{1}{4}e^{-v_2}\right)\left(e^{v_2}+\frac{1}{4}e^{-v_2}\right)e^{-iv_2}\right]a_-(t_1)$$

The incident part of $\psi_I(\varepsilon)$ is the term involving $a_-(t_1)$. In region V we have only a transmitted wave. Using Eq. (4.10) and noting that k(trans)=k(inc), the penetrability is

(4.119)

$$P(E) = \left|\frac{1}{\left(\frac{1}{4}e^{-iv_3}-e^{v_3}\right)\left(\frac{1}{4}e^{-v_2}-e^{v_2}\right)e^{iv_2}+\left(e^{v_2}+\frac{1}{4}e^{-v_2}\right)\left(e^{v_3}+\frac{1}{4}e^{-v_3}\right)e^{-iv_2}}\right|$$

The transmission coefficient for barrier B alone from Ψ_{III} is

$$P_B = \left|\frac{1}{\left(e^{v_3}+\frac{1}{4}e^{-v_3}\right)}\right|^2 \qquad (4.120)$$

Similarly, for barrier A we have

$$P_A = \left| \frac{1}{(e^{\nu_2} + \frac{1}{4} e^{-\nu_1})} \right|^2 \qquad (4.121)$$

From Eq. (4.120) and (4.121)

$$(e^{\nu_3} + \frac{1}{4} e^{-\nu_3}) = |1/P_B|^{1/2} \qquad (4.122)$$

$$(e^{\nu_2} + \frac{1}{4} e^{-\nu_1}) = |1/P_A|^{1/2} \qquad (4.123)$$

P(E) can be expressed in terms of P_A and P_B (Bhandhari[16-18]),

(4.124)

$$P(E) = \frac{P_A P_B}{[1+[(1-P_A)(1-P_B)]^{1/2}]^2 \cos^2 \nu_2 + [1-[(1-P_A)(1-P_B)]^{1/2}]^2 \sin^2 \nu_2}$$

Using the approximations $P_A \sim e^{-2\nu_1}, P_B \sim e^{-2\nu_3}$, gives us Ignatyuk's[15] expression,

$$P(E) = \frac{64 P_A P_B}{[(P_A P_B + 16)^2 \cos^2 \nu_2 + 16 (P_A + P_B)^2 \sin^2 \nu_2]} \qquad (4.125)$$

4.2 Penetrability From Fröman's F Matrix Formalism

When the classical turning points are well separated, the unidirectional connection formulas (3.238), (3.239), and (3.2310) are valid. Using these formulas, Lebeouf[20] obtained the wave functions for regions I and V (Eqs. (4.20) and (4.21)).

$$\psi_V = -Aq^{-1/2}\exp\left(i\left(\int_{t_4}^{z} q(z)\,dz + \frac{\pi}{4}\right)\right) \tag{4.20}$$

(4.21)

$$\psi_I = 4Aq^{-1/2}\exp\left(\int_{t_1}^{t_4} q(z)\,dz\right)\exp\left(\int_{t_2}^{t_3} q(z)\,dz\right)\cos(\nu_2)\cos\left(\int_{t_2}^{z} q(z)\,dz + \frac{\pi}{4}\right)$$

From these wave functions the penetrability obtained is

$$P(E) = \frac{P_A P_B}{4\cos^2\nu_2} \tag{4.22}$$

$$\nu_2 = \int_{t_2}^{t_3} q(z)\,dz \tag{4.23}$$

$$P_A=\exp(-2\nu_1), \quad P_B=\exp(-2\nu_3) \tag{4.24}$$

When the classical turning points are close together, Lebeouf uses Froman's F matrix formalism to obtain solutions for the wave functions in regions III and V. From ψ_{III}, ψ_V the other wave functions $\psi_I, \psi_{II}, \psi_{IV}$ are obtained with the help of the unidirectional connection formulas (3.238), (3.239), and (3.2310). He obtained the following penetrability equation,

$$P(E)=\frac{P_A P_B}{(2-P_B)+4\cos(\nu_2)\sin(\nu_2)(1-P_B)^{1/2}} \tag{4.25}$$

$$P_A=e^{-2\nu_1}, \quad P_B=\frac{1}{1+e^{2\nu_3}} \tag{4.26}$$

Eq. (4.25) requires that the classical turning points be close together. This occurs near the top of the barrier.

CHAPTER 5

Exact Methods

A more successful approach to barrier tunnelling calculations is that of penetrability through a two-peaked barrier using exact solutions. This technique, initiated by Wong and Bang[1969][10], has been employed more systematically by Cramer and Nix[1970][19] and Sharma and Lebeouf[1975][20-22].

5.1 Cramer and Nix Double-Humped Penetrability

Cramer and Nix calculated the exact penetrability through a two-peaked fission barrier consisting of two parabolic peaks connected smoothly with a third parabola forming the intermediate well (Eq. (5.11)). Such a double-humped barrier can be described in terms of six parameters; peak maximum energies E1 and E3 , well depth energy E2 and frequencies $\hbar\omega_1, \hbar\omega_2, \hbar\omega_3$ (Fig. 10). For an incident wave of unit amplitude, the amplitude of the transmitted wave is

determined by smoothly matching the wave functions and their derivatives at the points where the parabolas are joined. The penetrability is then obtained from the amplitude of the transmitted wave.

To find the wave functions in different regions, we solve the Schrödinger's equation

$$\frac{d^2}{d\epsilon^2}\psi(\epsilon)+\frac{2\mu}{\hbar^2}[E-V(\epsilon)]\psi(\epsilon)=0 \qquad (5.10)$$

The potential energy and each region (I,II,III) considered are shown in Fig. 14. The potential energy is defined as

$$V(\epsilon)=E_i\pm\frac{1}{2}\mu\omega_i^2(\epsilon-\epsilon_i)^2 \quad , i=1,2,3 \qquad (5.11)$$

$$V(\epsilon)=0 \qquad \epsilon=0 \qquad (5.12)$$

The solution to the Schrodinger equation are of the form

$$\psi_I=A\psi(\rightarrow)+B\varphi(\leftarrow) \qquad \epsilon\leq a \qquad (5.13a)$$

$$\psi_{II}=C\sigma_2+D\eta_2 \qquad a\leq\epsilon\leq b \qquad (5.13b)$$

$$\psi_I=T\psi_3(\rightarrow) \qquad b\leq\epsilon \qquad (5.13c)$$

In region I, wave packet phase velocities move left and right. In region II, the functions are chosen with a mixture of waves travelling in both directions, since C and D are not contained in the final expression explicitly. Substituting,

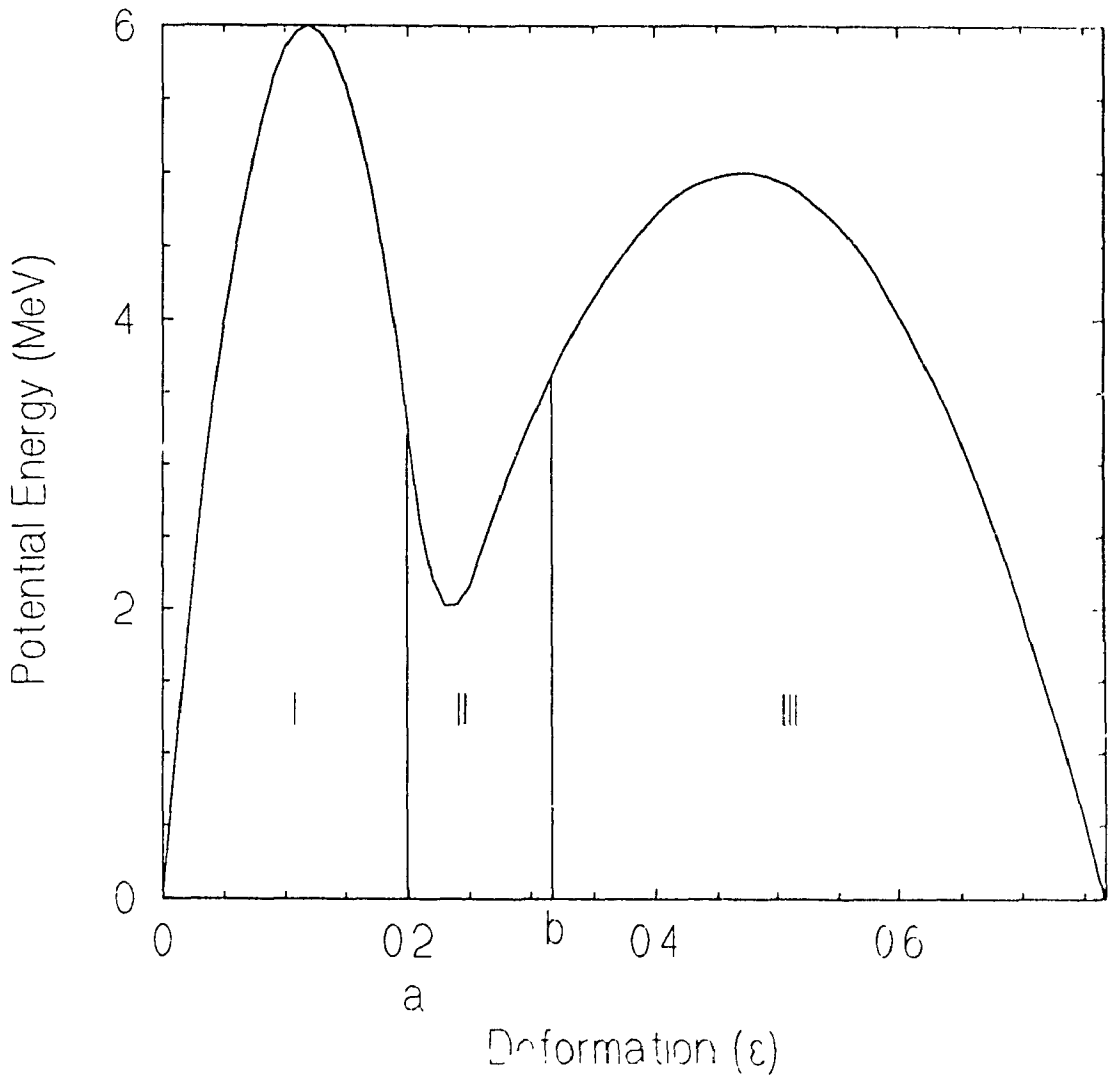

FIG. 14. Regions used by Cramer and Nix

$$u(\epsilon) = \sqrt{2\hbar\omega_1}\,(\epsilon-\epsilon_1)\,(\sqrt{\mu}/\hbar) \tag{5.14a}$$

$$v(\epsilon) = \sqrt{2\hbar\omega_2}\,(\epsilon-\epsilon_2)\,(\sqrt{\mu}/\hbar) \tag{5.14b}$$

$$w(\epsilon) = \sqrt{2\hbar\omega_3}\,(\epsilon-\epsilon_3)\,(\sqrt{\mu}/\hbar) \tag{5.14c}$$

Eq. (5.10) can be transformed into the well known Weber's differential equations,

$$d^2y/du^2 + (\frac{1}{4}u^2-\alpha)\,y=0 \tag{5.15a}$$

$$d^2y/dv^2 - (\frac{1}{4}v^2+\alpha)\,y=0 \tag{5.15b}$$

Whose solutions are the Weber Cylinder Parabolic functions given by,

$$\psi_I(\rightarrow) = E^*(\alpha_1, -u) \tag{5.16a}$$

$$\varphi_1(\leftarrow) = E(\alpha_1, -u) \tag{5.16b}$$

$$\psi_3(\rightarrow) = E(\alpha_3, w) \tag{5.16c}$$

$$\delta_2 = U(\alpha_2, v) \tag{5.16d}$$

$$\eta_2 = V(\alpha_2, v) \tag{5.16e}$$

The wave functions in the various regions are therefore,

$$\psi_I = AE^*(\alpha_1, -u) + BE(\alpha_1, -u) \tag{5.17a}$$

$$\psi_{II} = CU(\alpha_2, v) + DV(\alpha_2, v) \tag{5.17b}$$

$$\psi_{III} = TE(\alpha_3, w) \tag{5.17c}$$

Requiring these wave functions and their derivatives to be continuous at connecting points a and b, the transmission

coefficient as the ratio of the transmitted amplitude T to the incident amplitude A can be shown to be (see Appendix A),

(5.18)

$$\frac{T}{A}=\frac{v'u'W[E^*(\alpha_1,-u),E(\alpha_1,-u)]\,W[U(\alpha_2,v),V(\alpha_2,v)]}{\begin{vmatrix} E_a(\alpha_1,-u) & -V_a(\alpha_2,v) & -U_a(\alpha_2,v) & 0 \\ -u'E_a^{(-u)}(\alpha_1,-u) & -v'V_a^{(v)}(\alpha_2,v) & v'U_a^{(v)}(\alpha_2,v) & 0 \\ 0 & V_b(\alpha_2,v) & U_b(\alpha_2,v) & -E_b(\alpha_3,w) \\ 0 & v'V_b^{(v)}(\alpha_2,v) & v'U_b^{(v)}(\alpha_2,v) & -w'E_b^{(w)}(\alpha_3,w) \end{vmatrix}}$$

And the probability of tunnelling through the barrier is ,

$$P=(\omega_3/\omega_1)^{1/2}|T/A|^2 \tag{5.19}$$

The deformation parameters at energy maxima and minima, Wronskians, and α_i are given by,

$$\epsilon_1=\left[\sqrt{\frac{2E_1}{(\hbar\omega_1)^2}}\right]\left[\frac{\hbar}{\sqrt{\mu}}\right] \tag{5.110a}$$

$$a=\epsilon_1+\left[\sqrt{\frac{2(E_1-E_2)}{(\hbar\omega_1)^2}}\right]\left[1+\left(\frac{\hbar\omega_1}{\hbar\omega_2}\right)^2\right]^{-\frac{1}{2}}\left[\frac{\hbar}{\sqrt{\mu}}\right] \tag{5.110b}$$

$$\epsilon_2=a+\left[\sqrt{\frac{2(E_1-E_2)}{(\hbar\omega_2)^2}}\right]\left[1+\left(\frac{\hbar\omega_2}{\hbar\omega_1}\right)^2\right]^{-\frac{1}{2}}\left[\frac{\hbar}{\sqrt{\mu}}\right] \tag{5.110c}$$

$$b=\epsilon_2+\left[\sqrt{\frac{2(E_3-E_2)}{(\hbar\omega_2)^2}}\right]\left[1+\left(\frac{\hbar\omega_2}{\hbar\omega_3}\right)^2\right]^{-\frac{1}{2}}\left[\frac{\hbar}{\sqrt{\mu}}\right] \tag{5.110d}$$

$$\epsilon_3=b+\left[\sqrt{\frac{2(E_3-E_2)}{(\hbar\omega_3)^2}}\right]\left[1+\left(\frac{\hbar\omega_3}{\hbar\omega_2}\right)^2\right]^{-\frac{1}{2}}\left[\frac{\hbar}{\sqrt{\mu}}\right] \tag{5.110e}$$

$$W[E^*(\alpha_1,-u),E(\alpha_1,-w)]=2i \tag{5.111}$$

$$W[U(\alpha_2,-v),V(\alpha_2,v)]=\sqrt{\frac{2}{\pi}} \tag{5.112}$$

$$\alpha_i=\frac{(E_i-E)}{\hbar\omega_i} \qquad i=1,2,3$$

5.2 Triple-Humped Barrier Penetrability

Using the ingredient in the work of Cramer and Nix, Sharma and Lebeouf[12] extended the calculations to triple-humped barriers. Triple-humped barriers had been suggested by Möller and Nix[9] to explain anomalies in Thorium experimental data.

In a three-humped barrier, the solutions of the Schrödinger equations in the five regions are (Fig. 15),

$$\psi_1=AE(\alpha_1,-x_1), \tag{5.22}$$

$$\varphi_2=BU(\alpha_2,x_2)+CV(\alpha_2,x_2), \tag{5.23}$$

$$\varphi_3=DW(\alpha_3,x_3)+FW(\alpha_3,-x_3), \tag{5.24}$$

$$\varphi_4=GU(\alpha_4,x_4)+HV(\alpha_4,x_4), \tag{5.25}$$

$$\varphi_5=TE(\alpha_5,x_5), \tag{5.26}$$

with

$$\alpha_i=(E_i-E)/\hbar\omega_i \qquad i=1,2,3,4,5 \tag{5.27}$$

$$x_i=(2\mu\omega_i/\hbar)^{1/2}(\epsilon-\epsilon_i) \qquad i=1,2,3,4,5 \tag{5.28}$$

the penetrability is given by,

$$P=(\omega_3/\omega_1)^{1/2}|T/A|^2 \tag{5.29}$$

where

$$\frac{T}{A}=\frac{I}{\det D}, \tag{5.210}$$

and

$$I=\begin{array}{c} x_1' x_2' x_3' x_4 Wr\left[E^*(\alpha_1,-x_1),E(\alpha_1,-x_1)\right] \\ Wr\left[U(\alpha_2,x_2),V(\alpha_2,x_2)\right] Wr\left[W(\alpha_3,x_3)\,W(\alpha_3,-x_3)\right] \\ Wr\left[U(\alpha_4,x_4)\,V(\alpha_4,x_4)\right] \end{array} \tag{5.211}$$

The determinant D is ,

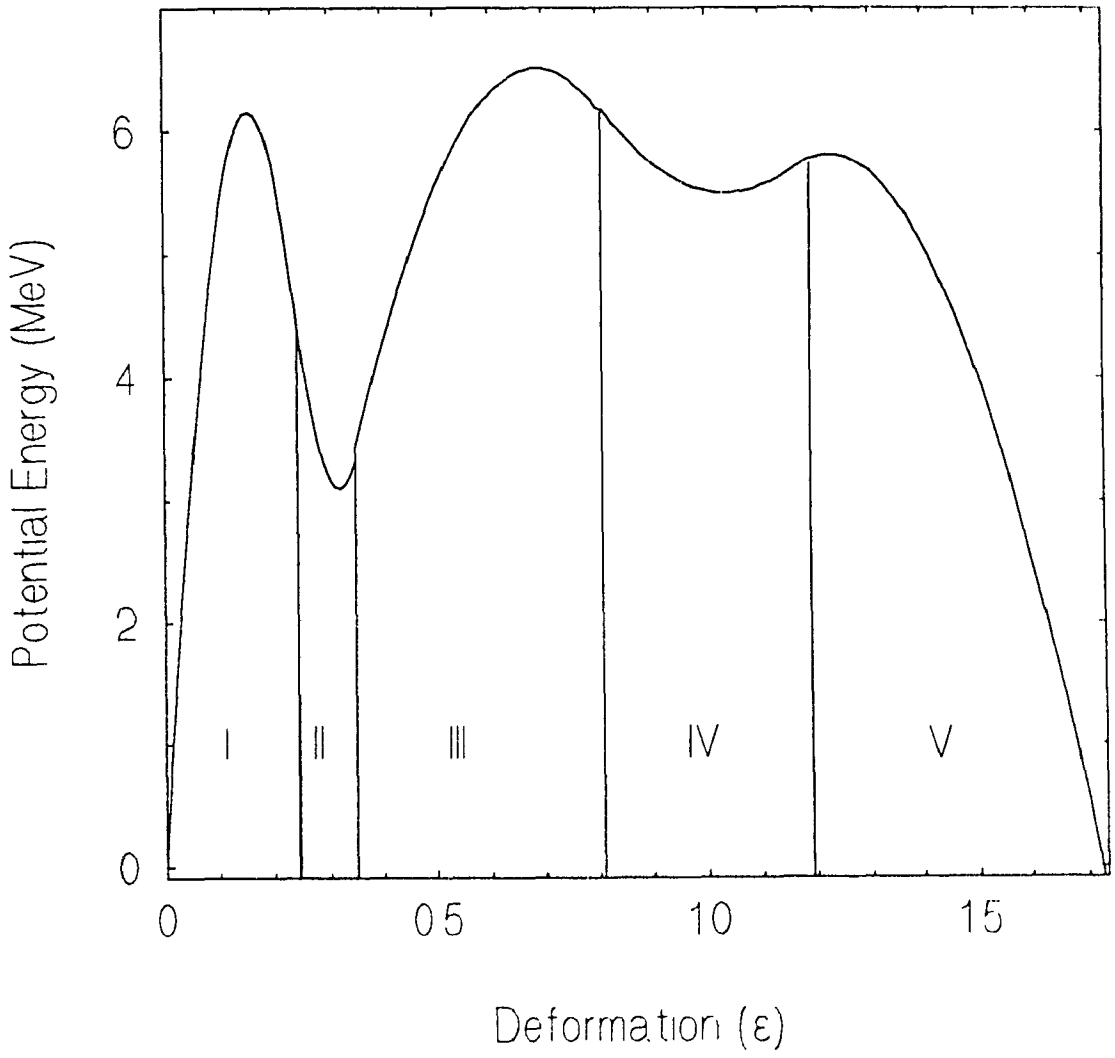

FIG. 15. Regions used by Sharma and Lebeouf in Triple-Humped calculations

(5.212)

$$D=\begin{bmatrix}
E_a(\alpha_1,-x_1) & -U(\alpha_2,x_2) & -V_a(\alpha_2,x_2) & 0 & 0 & 0 & 0 & 0\\
-x'_1E_a^{-x_1}(\alpha_1,-x_1) & -x'_2U_a^{x_2}(\alpha_2,x_2) & -x'_2V_a^{x_2}(\alpha_2,x_2) & 0 & 0 & 0 & 0 & 0\\
0 & U_b(\alpha_2,x_2) & V_b(\alpha_2,x_2) & -W_b(\alpha_3,x_3) & -W_b(\alpha_3,-x_3) & 0 & 0 & 0\\
0 & x'_2U_b^{x_2}(\alpha_2,x_2) & x'_2V_b^{x_2}(\alpha_2,x_2) & -x'_3W_b^{x_3}(\alpha_3,x_3) & x'_3W_b^{-x_3}(\alpha_3,-x_3) & 0 & 0 & 0\\
0 & 0 & 0 & W_c(\alpha_3,x_3) & W_c(\alpha_3,-x_3) & -U_c(\alpha_4,x_4) & -V_c(\alpha_4,x_4) & 0\\
0 & 0 & 0 & x'_3W_c^{x_3}(\alpha_3,x_3) & -x'_3W_c^{-x_3}(\alpha_3,-x_3) & -x'_3U_c^{x_4}(\alpha_4,x_4) & x'_4V_c^{x_4}(\alpha_4,x_4) & 0\\
0 & 0 & 0 & 0 & 0 & U_d(\alpha_4,x_4) & V_d(\alpha_4,x_4) & -E_d(\alpha_5,x_5)\\
0 & 0 & 0 & 0 & 0 & x'_4U_d^{x_4}(\alpha_4,x_4) & x'_4V_d^{x_4}(\alpha_4,x_4) & -x'_5E_d^{x_5}(\alpha_5,x_5)
\end{bmatrix}$$

5.3 Enhanced Double-Humped Methods

The Cramer and Nix expression obtained in section 5.1 assumes zero reflection in region III (Eq. 5.13c). Leboeuf and Sharma have discarded this assumption to extend the exact double-humped penetrability expressions to include reflection in region III. The actual Strutinsky barrier includes a first well. All methods mentioned so far assume the nuclei to be initially in its ground state. Leboeuf and Sharma also developed an expression for the penetrability with the inclusion of the first well.

5.31 Sharp Drop Approximation

Sharma and Lebeouf[20] have included reflection in the third region of Fig. 14 by redefining the barrier regions (Fig. 16). This involves the addition of an extra region to the Cramer and Nix barrier region III by approximating the left part of the third parabola by a step. This method called "The Sharp Drop Approximation" yield four wavefunctions,

$$\psi_I = AE^*(\alpha_1, -u) + BE(\alpha_1, -u) \qquad 0 \le \epsilon \le a \qquad (5.310)$$

$$\psi_{II} = CU(\alpha_2, v) + DV(\alpha_2, v) \qquad a \le \epsilon \le b \qquad (5.311)$$

$$\psi_{III} = FW(\alpha_3, w) + GW(\alpha_3, -w) \qquad b \le \epsilon \le \epsilon_2 \qquad (5.312)$$

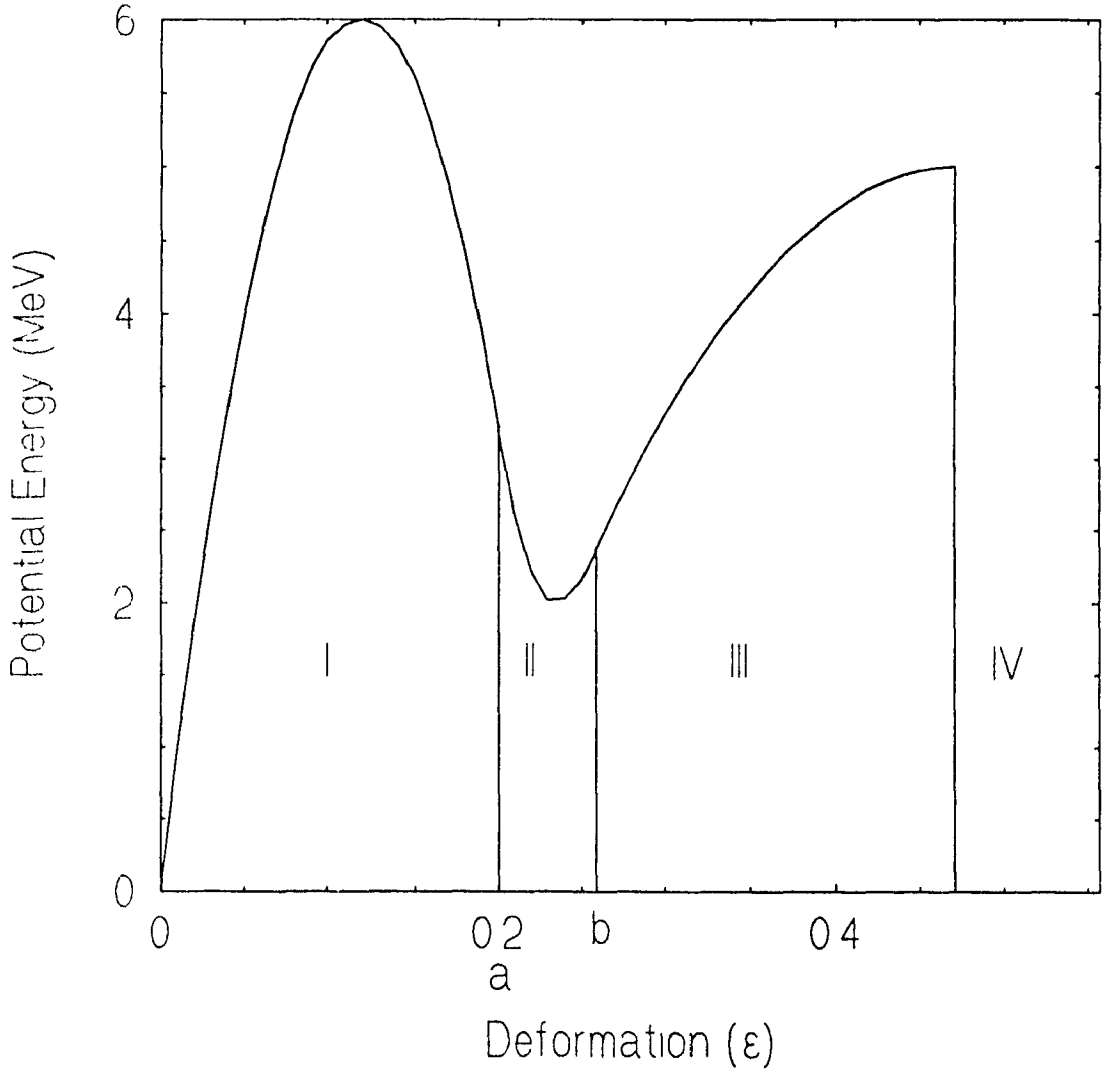

FIG. 16. Regions used by Sharma and Leboeuf in the Sharp Drop Approximation method

$$\psi_I = T\exp(ik\epsilon) \qquad \epsilon \geq \epsilon_3 \tag{5.313}$$

The method is similar to that of the previous section. Leboeuf derives the penetrability to be

$$P(E) = \left(\frac{E}{\hbar\omega_1}\right)^{1/2} \left|\frac{T}{A}\right|^2 \tag{5.314}$$

$$\frac{T}{A} = \frac{2\sqrt{2/\pi}u'v'w'i}{\begin{vmatrix} E_a(\alpha_1,-u) & -U_a(\alpha_2,v) & -V_a(\alpha_2,v) & 0 & 0 & 0 \\ -u'E_a^{-u}(\alpha_1,-u) & -v'V_a^{v}(\alpha_2,v) & -v'V_a^{v}(\alpha_2,v) & 0 & 0 & 0 \\ 0 & U_b(\alpha_2,v) & V_b(\alpha_2,v) & -W_b(\alpha_3,w) & -W_b(\alpha_3,-w) & 0 \\ 0 & v'U_b^{v}(\alpha_2,v) & v'V_b(\alpha_2,v) & -w'W_b^{-w}(\alpha_3,w) & w'W_b^{-w}(\alpha_3,-w) & 0 \\ 0 & 0 & 0 & W_{\epsilon_3}(\alpha_3,w) & W_{\epsilon_3}(\alpha_3,-w) & e^{ik\epsilon_3} \\ 0 & 0 & 0 & w'W_{\epsilon_3}^{w}(\alpha_3,w) & -w'W_{\epsilon_3}^{-w}(\alpha_3,-w) & -ik\epsilon^{ik\epsilon_3} \end{vmatrix}} \tag{5.315}$$

5.32 Initial Nuclear State

Another improvement explored by Lebeouf and Sharma[21] involves the original Strutinsky's barrier which includes a primary well (Fig. 17). All the methods already mentioned assume that the nuclide is in its ground state. As well, this method does not limit the outgoing wavefunction to zero reflection. It is of interest therefore, to investigate the effects of initial nuclear state on penetrability calculations. We hence have five wave functions.

$$\psi_I = AV(-\alpha_1, ix_1) + BU(-\alpha_1, -ix_1) \tag{5.320}$$

$$\psi_{II} = BW(\alpha_2, x_2) + DW(\alpha_2, -x_2) \tag{5.321}$$

$$\psi_{III} = FU(\alpha_3, x_3) + GV(\alpha_3, x_3) \tag{5.322}$$

$$\psi_{IV} = HW(\alpha_4, x_4) + KW(\alpha_4, -x_4) \tag{5.323}$$

$$\psi_V = T\exp[i(2\mu E/\hbar^2)^{1/2}\epsilon] \tag{5.324}$$

$$P(E) = (E/\hbar\omega_1)^{1/2} I \tag{5.325}$$

$$D=\frac{1}{\left|W_r\left[V(-\alpha_1, ix_1), V^*(-\alpha_1, ix_1)\right]\right|}\left|\frac{T}{A}\right|^2 \qquad (5.326)$$

It can be shown that

$$\frac{\left|W_r\left[U(-\alpha_1, ix_1), V(-\alpha_1, ix_1)\right]\right|^2}{\left|W_r\left[V(-\alpha_1, ix_1), V^*(-\alpha_1, ix_1)\right]\right|}=\sqrt{(2/\pi)}\sec(\pi\alpha_1)\Gamma(\alpha_1+\frac{1}{2}) \qquad (5.327)$$

The determinant T/A is given in Eq. (5.328)

(5.328)

$$\frac{T}{A} = \frac{}{\sqrt{2\pi}x_1'x_2'x_3'x_4'i}$$

$$\begin{vmatrix}
U_{a_2}(-\alpha_1, ix_1) & -W_{a_2}(\alpha_2, x_2) & -W_{a_2}(-\alpha_2, -x_2) & 0 & 0 & 0 & 0 & 0 \\
ix_1'U_{a_2}^{\lambda_1}(-\alpha_1, ix_1) & x_2'W_{a_2}^{x_2}(\alpha_2, x_2) & x_2'W_{a_2}^{x_2}(\alpha_2, -x_2) & 0 & 0 & 0 & 0 & 0 \\
0 & W_{a_3}(\alpha_2, x_2) & W_{a_3}(\alpha_2, -x_2) & -U_{a_3}(\alpha_3, x_3) & -V_{a_3}(\alpha_3, x_3) & 0 & 0 & 0 \\
0 & x_2'W_{a_3}^{\lambda_2}(\alpha_2, x_2) & -x_2'W_{a_3}^{x_2}(\alpha_2, x_2) & -x_3'W_{a_3}^{\lambda_3}(\alpha_3, x_3) & -x_3'V_{a_3}^{\lambda_3}(\alpha_3, x_3) & 0 & 0 & 0 \\
0 & 0 & 0 & V_{a_4}(\alpha_3, x_3) & V_{a_4}(\alpha_3, x_3) & -W_{a_4}(\alpha_4, x_4) & -W_{a_4}(\alpha_4, -x_4) & 0 \\
0 & 0 & 0 & x_3'U_{a_4}^{\lambda_3}(\alpha_3, x_3) & x_3'V_{a_4}^{x_3}(\alpha_3, x_3) & -x_4'W_{a_4}^{a_4}(\alpha_4, x_4) & x_4'W_{a_4}^{x_4}(\alpha_4, -x_4) & 0 \\
0 & 0 & 0 & 0 & 0 & W_{\epsilon_4}(\alpha_4, x_4) & W_{\epsilon_4}(\alpha_4, -x_4) & -e^{ikc_4} \\
0 & 0 & 0 & 0 & 0 & x_4'W_{\epsilon_4}^{x_4}(\alpha_4, x_4) & -x_4'W_{\epsilon_4}^{x_4}(\alpha_4, -x_4) & -ike^{ikc_4}
\end{vmatrix}$$

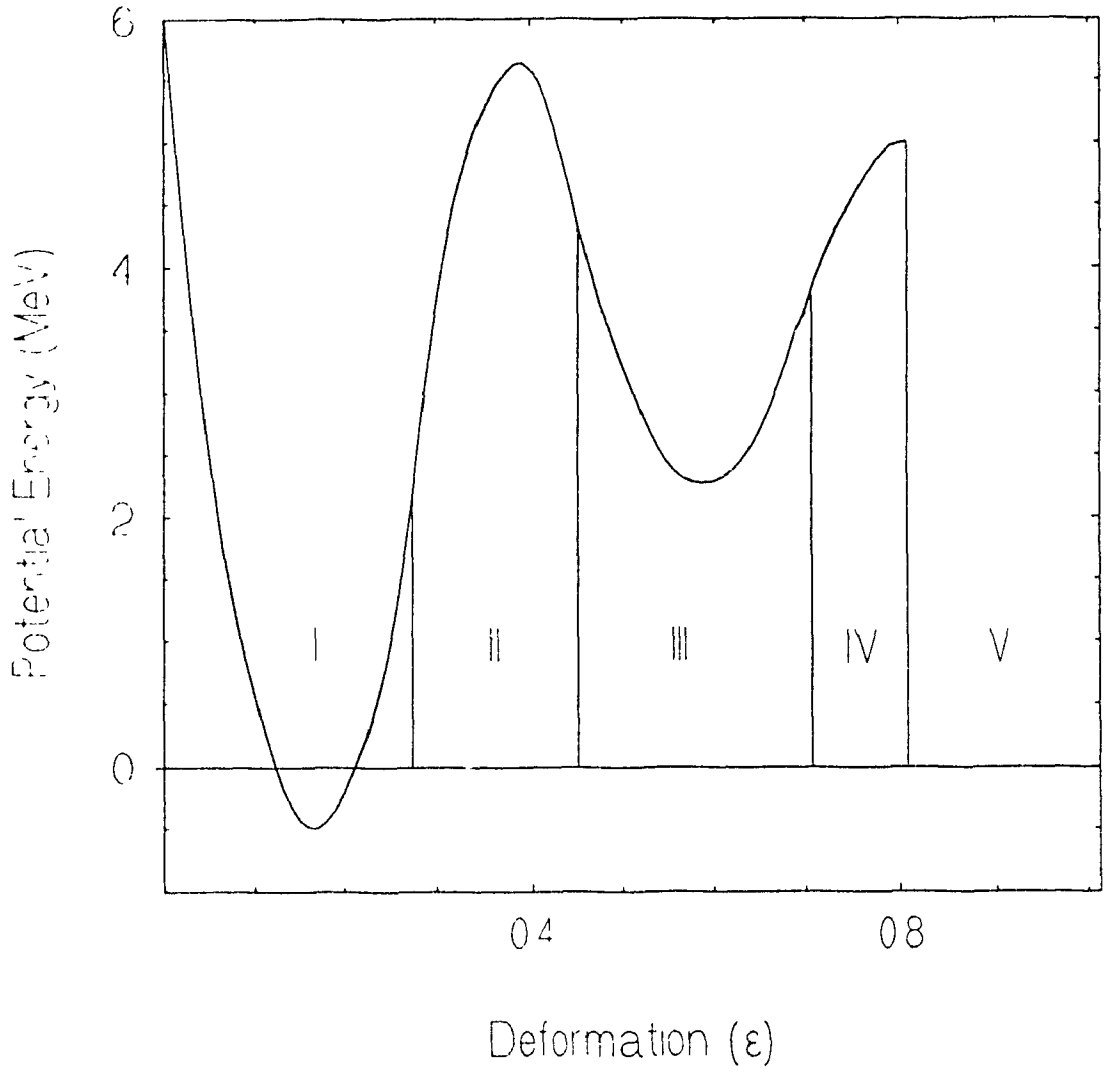

FIG. 17. Regions used by Sharma and Leboeuf for the Initial Nuclear State method.

CHAPTER 6

Fission

According to LDM , a point of instability between coulomb and surface effects is reached for elements close to the limiting value of $(Z^2/A)=14MeV(10r_o/3e_2)$. The probability of tunnelling through a barrier of a given width exhibit an exponential. The main successes of Strutinsky's barrier lies in explaining the experimentally observed resonance and intermediate structure in fission cross sections as well as isomeric fission.

6.1 Spontaneous Fission

It has been shown by Nix and Walker[1969][37] that the spontaneous fission half life can be written as

$$\tau^{s.f}=(\ln 2)\left(2\frac{\pi}{\omega_s}\right)\frac{1}{P(E_o)} \qquad (6.10)$$

where $P(E_o)$ is the penetrability at energy E_o and $2\pi/\omega_s$ is the time

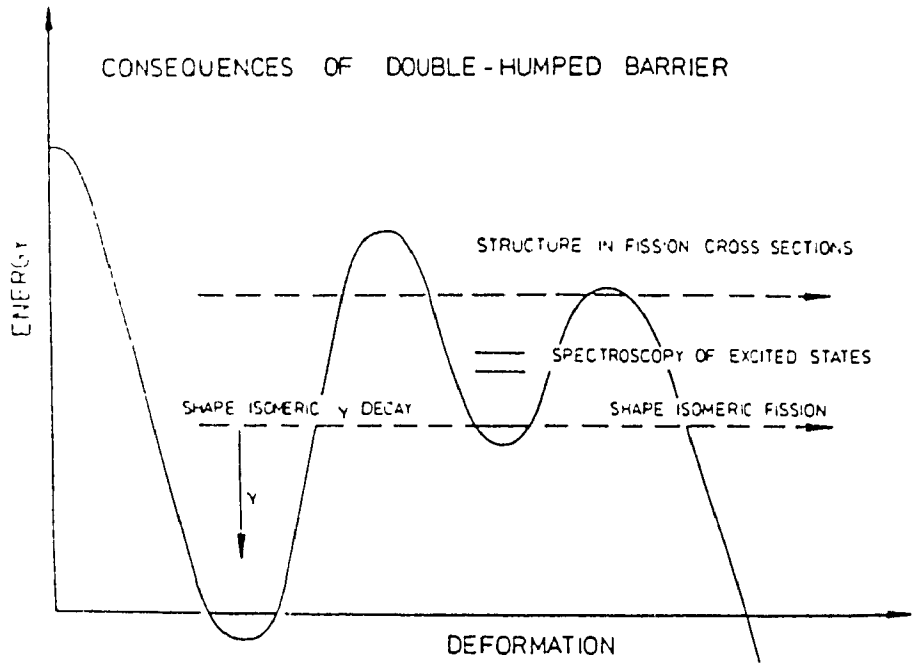

FIG. 18. Schematic demonstrating the model for Isomeric fission and gamma decay competition Taken from H J Specht

required for a single assault on the barrier. If we take an estimate of the frequency $\omega_s = 1 MeV/\hbar$, Eq. (6.10) becomes

$$\tau^{sf} = 10^{-28.0} [P(E_o)]^{-1} yr \tag{6.11}$$

In the asymptotic JWKB approximation , $P(E_o)$ is given by Eq. (4.120).

$$P(E_o) = \left| \frac{1}{e^{\nu_T} + \frac{1}{4} e^{-\nu_T}} \right|^2 \tag{6.12}$$

For a single-humped barrier

$$\nu_T = \int_{a_1}^{a_2} k(x)\, dx \tag{6.13}$$

For a double-humped barrier

$$\nu_T = \nu_1 + \nu_2 + \nu_3 \tag{6.14}$$

Since the ground state energy E_o is always lower than E_2 (well), a resonance structure is not expected in the ground state fission half-lives.

6.2 Isomeric Fission

Polikanov et al [1962][38], reported the discovery of a nuclide exhibiting an unusually short spontaneous fission half-life ($\tau_{1/2}$~0.02sec). The nuclide was identified as Am^{242} whose spontaneous fission life time was actually 5×10^{11}yr. It was expected that such a relatively short half-life would decay preferably by gamma emission. In 1962 Polikanov hypothesized that the spontaneously fissioning isomer might be a ground state in the second well. The short spontaneous fission lifetime is then attributed to the fact that the barrier is narrower and only approximately one half as high for the isomer as for the ground state. Since the nuclide has available different means of decay such as gamma, beta and alpha emission, the total half-life is given by,

$$\frac{1}{\tau_i} = \frac{1}{\tau_i^{sf}} + \frac{1}{\tau_i^{\gamma}} + \frac{1}{\tau_i^{\beta}} + \frac{1}{\tau_i^{\alpha}} + \cdots\cdots \qquad (6.20)$$

It is expected that beta and alpha decay modes will be sufficiently long, and that they can be neglected in Eq. (6.20). Gamma emission from an isomeric state can in certain circumstances compete favourably with spontaneous fission. The half-life for gamma emission is

$$\tau_1^{\gamma} = \frac{\tau^{\gamma}}{P_A(E_1)} \qquad (6.21)$$

In Eq. (6.21), τ^{γ} is the half-life for gamma decay from a state of Energy E_i in the first well, know experimentally to be 10^{-14} sec = $10^{-21.5}$ yr. The partial spontaneous fission half-life from state E_i depends on the penetrability through barrier B. Using Eq. (6.10)

$$\tau_i^{sf} = \ln(2)\ (2\pi/\omega_2)\ [P_B(E_1)]^{-1} \quad \text{sec} \qquad (6.22)$$

The total isomeric half life is therefore

$$\tau_i(E_1) = \left[\frac{P_A(E_1)}{10^{-14.0}} + \frac{P_B(E_1)\,\omega_2}{\ln(2)\sqrt{2\pi}} \right]^{-1} \qquad (6.23)$$

The energy values at resonances can be approximated by the well-known results of a harmonic well extended to infinity, as

$$E_n = E_2 + \left(n + \frac{1}{2}\right)\hbar\omega_2 \qquad (6.24)$$

The parameters E_2 and $\hbar\omega_2$ can hence be determined approximately by knowing the ground state isomeric energy and the isomeric spontaneous fission half life.

$$\omega_2 = \left(\frac{1}{\tau_1} - \frac{P_A(E_1)}{10^{-14.0}} \right) \left(\frac{\ln 2\,(2\pi)}{P_B(E_1)} \right) \qquad (6.25)$$

$$E_2 = E_1 - \frac{1}{2}\hbar\left[\frac{1}{\tau_1} - \frac{P_A(E_1)\ln(2)2\pi}{P_B(E_1)10^{-14.0}}\right] \qquad (6.26)$$

Bjornholm and Lynn[39] have listed a set of barrier parameters for the first and second barriers (TABLE I). The barrier parameters for the well can be deduced using Eqs. (6.25) and (6.26).

TABLE I. Experimental Values for double-humped barrier parameters for nuclei of the actinide region (Ac^{89}-Lr^{103}) . Taken from S Bjornholm and J E Lynn 1980

	E_1	E_3	$\hbar\omega_1$	$\hbar\omega_2$
Ra228	8.0 ±0.5	8.5 ±0.5		
Ac226	6.0 ±0.6	7.7 ±0.3		
Th227	5.9 ±0.3	6.6 ±0.3		
Th234	6.1 ±0.2	6.5 ±0.3	1.0	0.75
U236	5.6 ±0.2	5.5 ±0.2	1.04	0.60
U238	5.70±0.2	5.7 ±0.2	1.04	0.60
Np237	5.7 ±0.2	5.4 ±0.2	0.80	0.52
Pu235	5.8	5.1 ±0.4	0.80	0.52
Pu237	5.90	5.20	0.80	0.52
Pu238	5.5 ±0.2	5.0 ±0.2	1.04	0.60
Pu239	6.2 ±0.2	5.5 ±0.2	0.80	0.52
Pu240	5.6 ±0.2	5.1 ±0.2	1.04	0.60
Pu241	6.1 ±0.2	5.4 ±0.2	0.80	0.52
Pu242	5.6 ±0.2	5.1 ±0.2	1.04	0.60
Pu243	5.9 ±0.2	5.2 ±0.2	0.80	0.52
Pu244	5.4 ±0.2	5.0 ±0.2	1.04	0.60
Pu245	5.6 ±0.2	5.0 ±0.2	0.80	0.52
Am239	6.2 ±0.3	5.6	0.80	0.52
Am240	6.5 ±0.2	5.2 ±0.3	0.65	0.45
Am241	6.0 ±0.2	5.1 ±0.3	0.80	0.52
Am242	6.5 ±0.2	5.4 ±0.3	0.65	0.45
Am243	5.9 ±0.2	5.4 ±0.3	0.80	0.52
Am244	6.3 ±0.2	5.4 ±0.3	0.65	0.45
Am245	5.9 ±0.2	5.2 ±0.3	0.80	0.52
Cm241	6.3 ±0.3	4.3 ±0.5	0.80	0.52
Cm242	5.8 ±0.4	4.0 ±0.5	1.04	0.60
Cm243	6.4 ±0.3	4.3	0.80	0.52
Cm244	5.8 ±0.2	4.3 ±0.3	1.04	0.60
Cm245	6.2 ±0.2	5.0	0.80	0.52
Cm250	5.3	3.9	1.04	0.60
Bk250	6.1	4.1	0.65	0.45
Cf253	5.4	3.6	0.8	0.52

CHAPTER 7

Computational Considerations

The numerical analysis for the host of penetrability expressions requires the knowledge of ν_1, ν_2, ν_3 for the JWKB methods, and the Weber Functions U(a,x), V(a,x), W(a,x), and E(a,x) and their derivatives, for the exact methods. As well, it is important to limit the investigation of these expressions to physically tenable limits. These limits are obtained from TABLE I.

7.1 JWKB Variables ν_i

The problem of solving the asymptotic JWKB method numerically is reduced to finding expressions for ν_1, ν_2, ν_3 in their corresponding regions. To simplify matters, the potential energy and consequently Q(x) are rewritten using the following relations.

$$Q^2(x) = \frac{2\mu}{\hbar^2}[E \mp V(x)] \tag{7.10}$$

$$V(x) = E_1 \pm \frac{1}{2}\mu\omega_1^2(x-x_1)^2 \tag{7.11}$$

$$\mu = 0.540A^{5/3}\hbar^2 MeV \tag{7.13}$$

$$\mu' = \mu/\hbar^2 = 0.540A^{5/3} \tag{7.14}$$

$$a^2 = 2\frac{|E-E_1|}{\mu'(\hbar\omega_1)^2} \tag{7.15}$$

$$A = \mu'\hbar\omega_1 \tag{7.16}$$

$$v = (x-x_1), \quad dv = dx \tag{7.17}$$

The function Q(x) is therefore,

$$Q^2(x) = \frac{2\mu}{\hbar^2}\left[E \mp \left(E_1 \pm \frac{1}{2}\mu\omega_1^2(x-x_1)^2\right)\right] \tag{7.18}$$

$$Q^2(x) = \frac{2\mu}{\hbar^2}\left[\pm|E-E_1| \mp \frac{1}{2}\mu\omega_1^2(x-x_1)^2\right] \tag{7.19}$$

$$Q^2(x) = (\mu\hbar\omega_1)^2\left[\pm\frac{2|E-E_1|}{\mu'[\hbar\omega_1]^2} \mp (x-x_1)^2\right] \tag{7.110}$$

The final expression is,

$$Q^2(x) = A^2[\pm a^2 \mp v^2] \tag{7.111}$$

$$Q(x) = A\sqrt{\pm a^2 \mp v^2} \tag{7.112}$$

When integrating in the three regions, four different possible integration schemes are found.

Case I

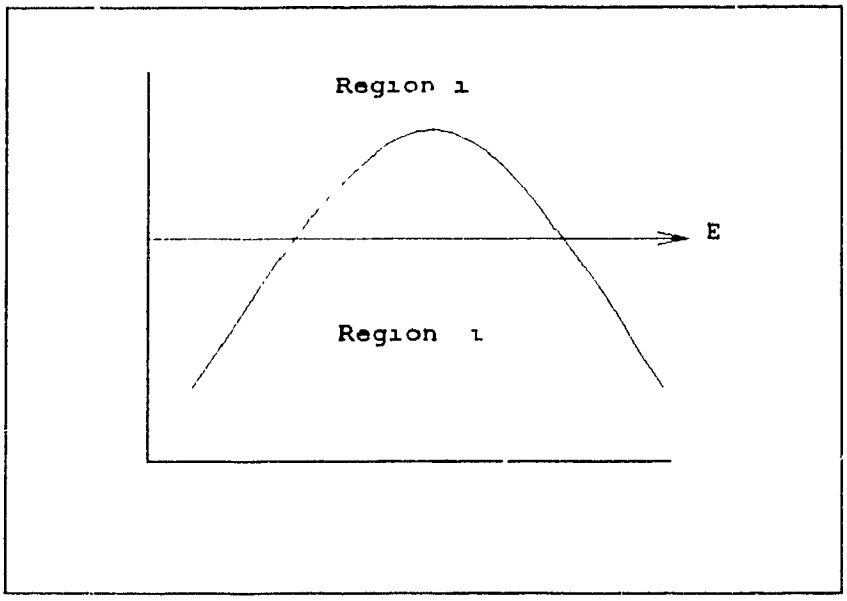

For region i, the integral is,

$$\int Q(x)\,dx = \int \sqrt{V(x) - E}\,dx = \int_{t_1}^{t_{1+}} A\sqrt{a^2 - v^2}\,dx \tag{7.113}$$

$$= \frac{A}{2}\left(v\sqrt{a^2-v^2}+a^2\sin^{-1}\left(\frac{v}{a}\right)\right) \qquad (7.114)$$

For region ii,

$$\int Q(x)\,dx = \int \sqrt{E-V(x)}\,dx = \int_{t_1}^{t_{11}} A\sqrt{v^2-a^2}\,dx \qquad (7.115)$$

$$= \frac{A}{2}\left(v\sqrt{v^2-a^2}+a^2\ln\left|v-\sqrt{v^2-a^2}\right|\right) \qquad (7.116)$$

Case II

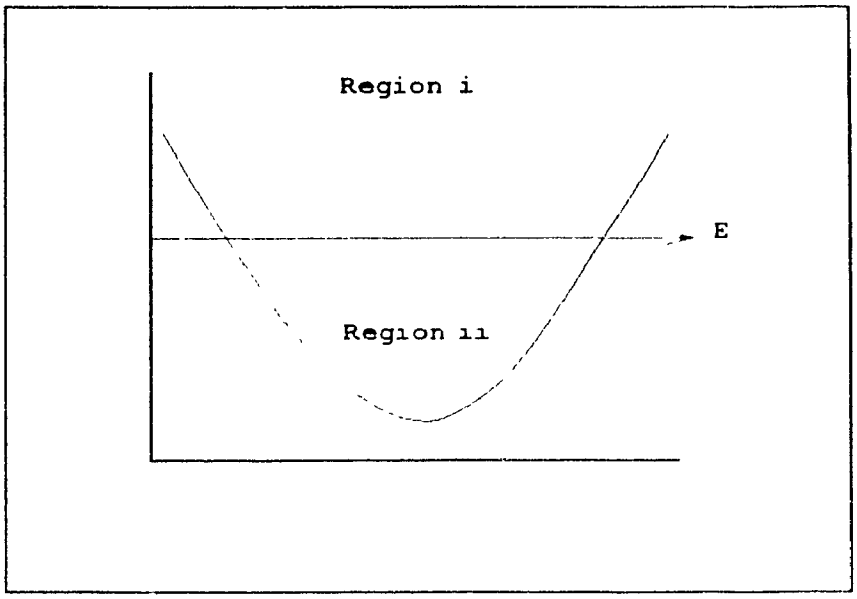

For region i, the integral is,

$$\int Q(x)\,dx=\int\sqrt{V(x)-E}\,dx=\int_{t_i}^{t_{i+1}} A\sqrt{v^2-a^2}\,dx \tag{7.117}$$

$$=\frac{A}{2}\left(v\sqrt{v^2-a^2}+a^2\ln\left|v-\sqrt{v^2-a^2}\right|\right) \tag{7.118}$$

For region ii,

$$\int Q(x)\,dx=\int\sqrt{E-V(x)}\,dx=\int_{t_i}^{t_{i+1}} A\sqrt{a^2-v^2}\,dx \tag{7.119}$$

$$=\frac{A}{2}\left(v\sqrt{a^2-v^2}+a^2\sin^{-1}\left(\frac{v}{a}\right)\right) \tag{7.120}$$

Denoting Eqs. (7.114) and (7.120) as $I_1(x_1,x_2,i)$ and Eqs. (7.116) and (7.118) as $I_2(x_1,x_2,i)$, then the total integral from one connecting point to the next in crossing from one parabola to an adjacent one is,

$$v_i=I_2(c_{i-1},t_i,i-1)+I_1(c_i,c_{i-1},i)+I_2(t_{i+1},c_i,i+1) \qquad where(t_i\le C_{i-1}\ \wedge\ t_{i+1}>c_i) \tag{7.121}$$

$$=I_2(c_{i-1},t_i,i-1)+I_1(t_{i+1},c_{i-1},i) \qquad where(t_i<C_{i-1}\ \wedge\ t_{i+1}\le c_i) \tag{7.122}$$

$$=I_1(c_i,t_i,i)+I_2(t_{i+1},c_i,i+1) \qquad where(t_i>C_{i-1}\ \wedge\ t_{i+1}>c_i) \tag{7.123}$$

$$= I_1(t_{i-1}, t_i, i)$$

$$\text{where}(t_i \geq C_{i-1} \ \wedge \ t_{i-1} \geq C_i) \tag{7.124}$$

The first two terms of the integral $I(x_1, x_2, i)$ are the limits of integration. The third term i denotes the region of integration. The turning point are indicated by the symbol t_1 and the connecting points a and b as c_2 and c_3 respectively.

7.2 Weber Functions

The exact methods of Cramer and Nix, and Sharma and Leboeuf, require the Weber Cylindrical Parabolic Functions for computational results. The general equations for Weber functions[40] U, V, W, and E and their derivatives are given as series expansions.

(7.20)

$$U(a,x) = \frac{\cos\left(\pi\left(\frac{1}{4}+\frac{1}{2}a\right)\right)\Gamma\left(\frac{1}{4}-\frac{1}{2}a\right)}{\sqrt{\pi}2^{\left(\frac{1}{2}a+\frac{1}{4}\right)}} y_1 + \frac{\sin\left(\pi\left(\frac{1}{4}+\frac{1}{2}a\right)\right)\Gamma\left(\frac{3}{4}-\frac{1}{2}a\right)}{\sqrt{\pi}2^{\left(\frac{1}{2}a-\frac{1}{4}\right)}} y_2$$

(7.21)

$$V(a,x) = \frac{1}{\Gamma\left(\frac{1}{2}-a\right)}\left[\frac{\sin\left(\pi\left(\frac{1}{4}+\frac{1}{2}a\right)\right)\Gamma\left(\frac{1}{4}-\frac{1}{2}a\right)}{\sqrt{\pi}2^{\left(\frac{1}{2}a+\frac{1}{4}\right)}} y_1 + \frac{\cos\left(\pi\left(\frac{1}{4}+\frac{1}{2}a\right)\right)\Gamma\left(\frac{3}{4}-\frac{1}{2}a\right)}{\sqrt{\pi}2^{\left(\frac{1}{2}a-\frac{1}{4}\right)}} y_2\right]$$

$$W(a,\pm x)=\frac{\sqrt{\cosh(\pi a)}}{2\sqrt{\pi}}\left(\left|\Gamma\left(\frac{1}{4}+\frac{1}{2}ia\right)\right|y_1\mp\sqrt{2}\Gamma\left(\frac{3}{4}+\frac{1}{2}ia\right)y_2\right) \quad (7.22)$$

$$E(a,x)=k^{-1/2}W(a,x)+ik^{1/2}W(a,-x) \quad (7.23)$$

$$k=\sqrt{1+e^{2\pi a}}-e^{\pi a} \quad (7.24)$$

The terms y_1 and y_2 are series expansions of the confluent hypergeometric functions ${}_1F_1$.

$$y_1=e^{-\frac{1}{4}\gamma x^2}\,{}_1F_1\left(\frac{1}{4}-\frac{1}{2}\gamma a;\frac{1}{2};\frac{1}{2}\gamma x^2\right) \quad (7.25)$$

$$y_2=xe^{-\frac{1}{4}\gamma x^2}\,{}_1F_1\left(\frac{3}{4}-\frac{1}{2}\gamma a;\frac{3}{2};\frac{1}{2}\gamma\right.$$

$$\gamma=1 \quad for \quad U,V \quad (7.26)$$

$$\gamma=-1 \quad for \quad W$$

When the variable a is negative, the function U(a,x) has an oscillatory region $-2\sqrt{|a|}<x<2\sqrt{|a|}$ on one side to positive infinity and negative infinity on the other side. When a is

positive, there are no oscillatory regions, only exponential regions which extend from negative infinity to positive infinity. In contrast, the function W(a,x) has an exponential region for $|x|<2\sqrt{a}$ separating two oscillatory region which extend to positive and negative infinity. When (a) is negative, the solutions are oscillatory throughout.

The values of U(a,x) and V(a,x) have been evaluated with the use of confluent hypergeometric functions for real arguments and for small to moderate a and x. The values have been checked against tables of Confluent Hypergeometric Functions[41]. For large a or x, U(a,x) is expressed as an expansion of Airy functions[42] (appendix C). When either a or x is negative or $x<2\sqrt{a}$, we use the confluent hypergeometric function defined as $H(m,a,x)=e^{-i\lambda}F(m+1-ia,2m+2;2ix)$ using computational methods described by Lowan and Horenstein[43]. Everywhere else, W(a,x) is resolved using Olver's Airy expansion method. Computational algorithms for Bessel, Airy, Hypergeometric, and Gamma functions are taken from "Methods and Programs for Mathematical Functions", by Stephen L. Moshier[44]. Fig. 19 demonstrates the function W(a,x) in the positive a and x quadrant.

Numerical results reveal that the Weber functions cannot be generally evaluated by series method. As well, interpolation methods yield precise resonance energy values but suffer in probability magnitude. TABLE II demonstrates the need for high precision when evaluating resonance peak maximum

due to very small peak widths. Instead, Cramer and Nix[19] have used a Lorenzian curve fitting method.

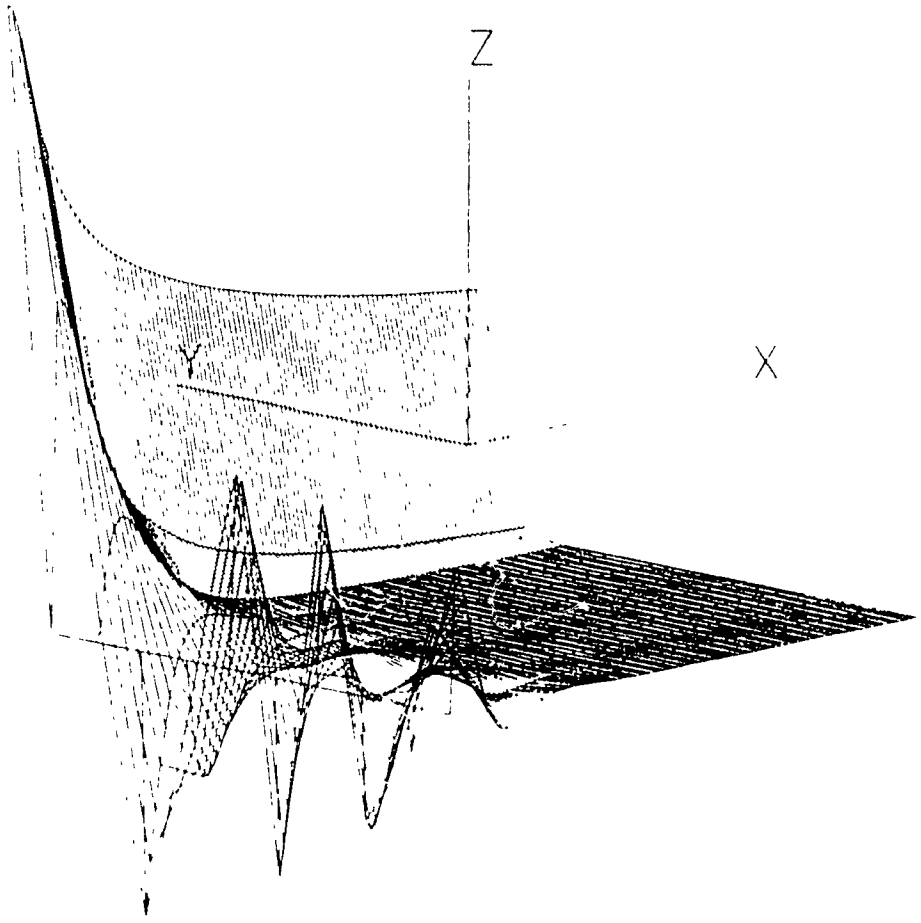

FIG. 19. Plot of the Weber Function W(a,x) for positive arguments

TABLE II. Iterations required to obtain the maximum penetrability at resonance (E = 2.39651359675713 and P_{max} = 4.51380e-002) Demonstrates the need for precision.

Energy	Penetrability	Energy	Penetrability
2.39600000000000	4.40779e-021	2.39651359500000	3.80336e-010
2.39610000000000	6.81007e-021	2.39651359600000	2.04844e-009
2.39620000000000	1.18687e-020	2.39651359610000	2.71931e-009
2.39630000000000	2.56330e-020	2.39651359620000	3.78306e-009
2.39640000000000	9.08024e-020	2.39651359630000	5.61916e-009
2.39641000000000	1.09200e-019	2.39651359640000	9.20638e-009
2.39642000000000	1.33806e-019	2.39651359650000	1.77590e-008
2.39643000000000	1.67765e-019	2.39651359660000	4.75519e-008
2.39644000000000	2.16495e-019	2.39651359670000	3.59570e-007
2.39645000000000	2.89988e-019	2.39651359671000	5.28275e-007
2.39646000000000	4.08373e-019	2.39651359672000	8.50970e-007
2.39647000000000	6.17319e-019	2.39651359673000	1.59332e-006
2.39648000000000	1.03970e-018	2.39651359674000	3.99335e-006
2.39649000000000	2.10805e-018	2.39651359675000	2.29738e-005
2.39650000000000	6.35038e-018	2.39651359675100	3.10510e-005
2.39650100000000	7.39880e-018	2.39651359675200	4.42765e-005
2.39650200000000	8.72999e-018	2.39651359675300	6.81662e-005
2.39650300000000	1.04556e-017	2.39651359675400	1.18248e-004
2.39650400000000	1.27484e-017	2.39651359675500	2.53276e-004
2.39650500000000	1.58870e-017	2.39651359675600	8.75231e-004
2.39650600000000	2.03453e-017	2.39651359675610	1.04620e-003
2.39650700000000	2.69816e-017	2.39651359675620	1.27216e-003
2.39650800000000	3.74856e-017	2.39651359675630	1.57847e-003
2.39650900000000	5.55703e-017	2.39651359675640	2.00898e-003
2.39651000000000	9.07678e-017	2.39651359675650	2.63832e-003
2.39651100000000	1.74141e-016	2.39651359675660	3.60474e-003
2.39651200000000	4.60568e-016	2.39651359675670	5.19137e-003
2.39651300000000	3.29750e-015	2.39651359675680	8.00070e-003
2.39651310000000	4.75874e-015	2.39651359675690	1.34550e-002
2.39651320000000	7.45988e-015	2.39651359675700	2.46101e-002
2.39651330000000	1.33346e-014	2.39651359675701	2.62104e-002
2.39651340000000	3.03334e-014	2.39651359675702	2.79133e-002
2.39651350000000	1.25435e-013	2.39651359675703	2.96686e-002
2.39651351000000	1.56017e-013	2.39651359675704	3.14951e-002
2.39651352000000	1.99318e-013	2.39651359675705	3.33742e-002
2.39651353000000	2.63505e-013	2.39651359675706	3.52367e-002
2.39651354000000	3.64538e-013	2.39651359675707	3.70881e-002
2.39651355000000	5.37141e-013	2.39651359675708	3.88758e-002
2.39651356000000	8.69162e-013	2.39651359675709	4.05651e-002
2.39651357000000	1.64023e-012	2.39651359675710	4.20779e-002
2.39651358000000	4.18200e-012	2.39651359675711	4.33589e-002
2.39651359000000	2.57192e-011	2.39651359675712	4.43740e-002
2.39651359100000	3.54299e-011	2.39651359675713	4.50930e-002
2.39651359200000	5.18909e-011	2.39651359675714	4.54499e-002
2.39651359300000	8.31894e-011	2.39651359675713	4.50930e-002
2.39651359400000	1.54477e-010	2.39651359675713	4.51380e-002

7.3 Barrier Parameters

The range of barrier parameters for nuclei in the actinide region of the periodic table is obtained from TABLE I in Chapter 6. For the actinide region , the values of the barrier parameters are found to be in the range detailed below.

DATA I

$236<A>245$	$A_{average}=240$
$5.40<E_1<6.50$	$E_{1_{average}}=5.95$
$1.50<E_2<2.40$	$E_{2_{average}}=1.95$
$4.00<E_3<5.70$	$E_{3_{average}}=4.85$
$0.50<\hbar\omega_1<1.05$	$\hbar\omega_{1_{average}}=0.78$
$0.70<\hbar\omega_2<1.00$	$\hbar\omega_{2_{average}}=0.85$
$0.45<\hbar\omega_3<0.60$	$\hbar\omega_{3_{average}}=0.53$

The Initial Nuclear State calculations require reasonable values for E_1 and $\hbar\omega_1$. Nix and Walker have remarked that the values of the energy minimum of the first well can be expected to lie approximately 0.5 MeV below the ground state. Hence, we take E_1 = -0.5 MeV. The barrier frequency is taken to be 1.0 MeV on the same basis.

To study the predictions of resonance peak energies, each one of the above six parameters are varied from its expected

actinide minimum to its expected maximum, while keeping the rest fixed at their average values.

Two other sets of data are used to study the behaviour above and below the maximum and minimum values, for asymmetric and symmetric barrier shapes.

DATA II (asymmetric)

$$E_1=6.00, E_2=2.00, E_3=5.00, \hbar\omega_1=1.30, \hbar\omega_2=2.00, \hbar\omega_3=0.48\ (MeV)$$

$$E_1=4.5\text{-}6.0, E_2=1.5\text{-}3.0, E_3=4.5\text{-}6.0,$$
$$\hbar\omega_1=0.5\text{-}1.6, \hbar\omega_2=1.30\text{-}3.5, \hbar\omega_3=0.3\text{-}1.4\ (MeV)$$

DATA III (symmetric)

$$E_1=6.00, E_2=2.00, E_3=6.00, \hbar\omega_1=1.00, \hbar\omega_2=0.5, \hbar\omega_3=1.00\ (MeV)$$

$$\hbar\omega_2=0.30\text{-}3.50\ (MeV)$$

As well , it can be shown from Eqs. (5.18), (5.315), and (5.327), that the effective mass parameter μ' cancels out of each probability equation. Therefore, the penetrability is independent of the choice of effective mass. We hence are not required to vary the atomic number. For DATA III, only $\hbar\omega_2$ is varied in order to maintain barrier symmetry.

CHAPTER 8

Results of Calculations

Energy levels or resonance peaks are demonstrated by abrupt peaks in the probability versus energy curve. The isomeric energy is the bound semi-stable ground state in the intermediate well. In contrast, spontaneous fission requires tunnelling through the complete barrier from it's ground state. The various methods mentioned, will deviate with respect to energy level values and maximum penetrabilities at resonance. This will have implications in predictions of isomeric and spontaneous fission half-lives. Bjornholm has accumulated tables of data from various authors. Each of the six parameters will be varied from it's expected minimum to expected maximum.

Abbreviations to the methods will be used as follows: JWKB, for Ignatyuk's expression; NIX, for Cramer and Nix method; FRO, for Lebeouf's use of unidirectional connection formulas; INS, for the Initial Nuclear State method; and SDA for the Sharp Drop Method. Energy levels are denoted as L_1.

8.1 Pure Vibrational Energy Levels

To demonstrate the characteristic probability graph, Figs. 20 to 26 are plots of the penetrability versus energy, with parameters taken from Sharma and Lebeouf[1975][21].

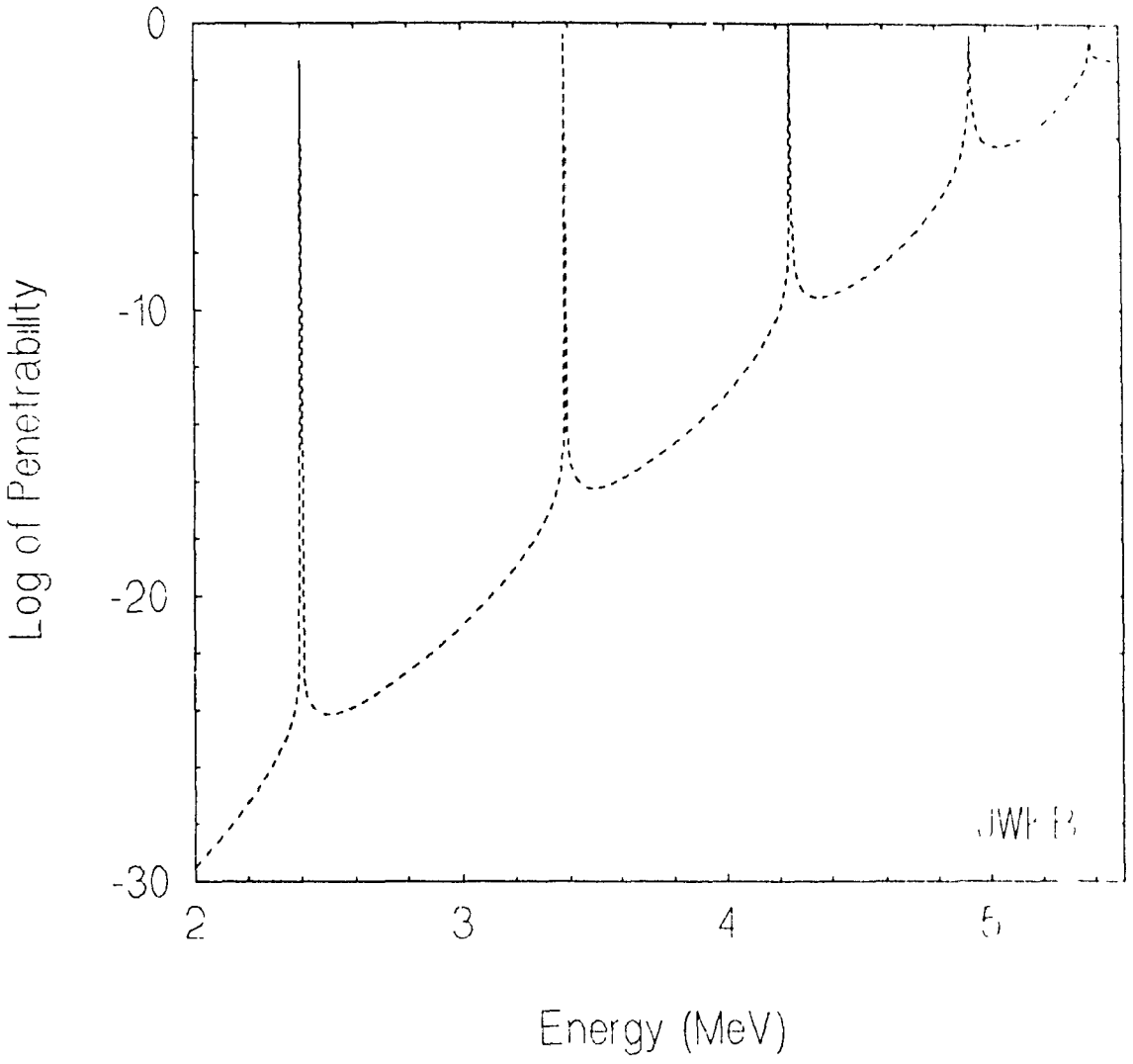

FIG. 20. Plot of log of Penetrability versus incident energy calculated in the JWKB method for barrier parameters E_1=5.8, E_2=1.9, E_3=5.4, $\hbar\omega_1$=0.8, $\hbar\omega_2$=1.0, $\hbar\omega_3$=0.6 MeV

The sharp spikes are resonance peaks characterized by a maximum peak height and a peak width. The probability of tunnelling through the barrier increases with increasing incident energy.

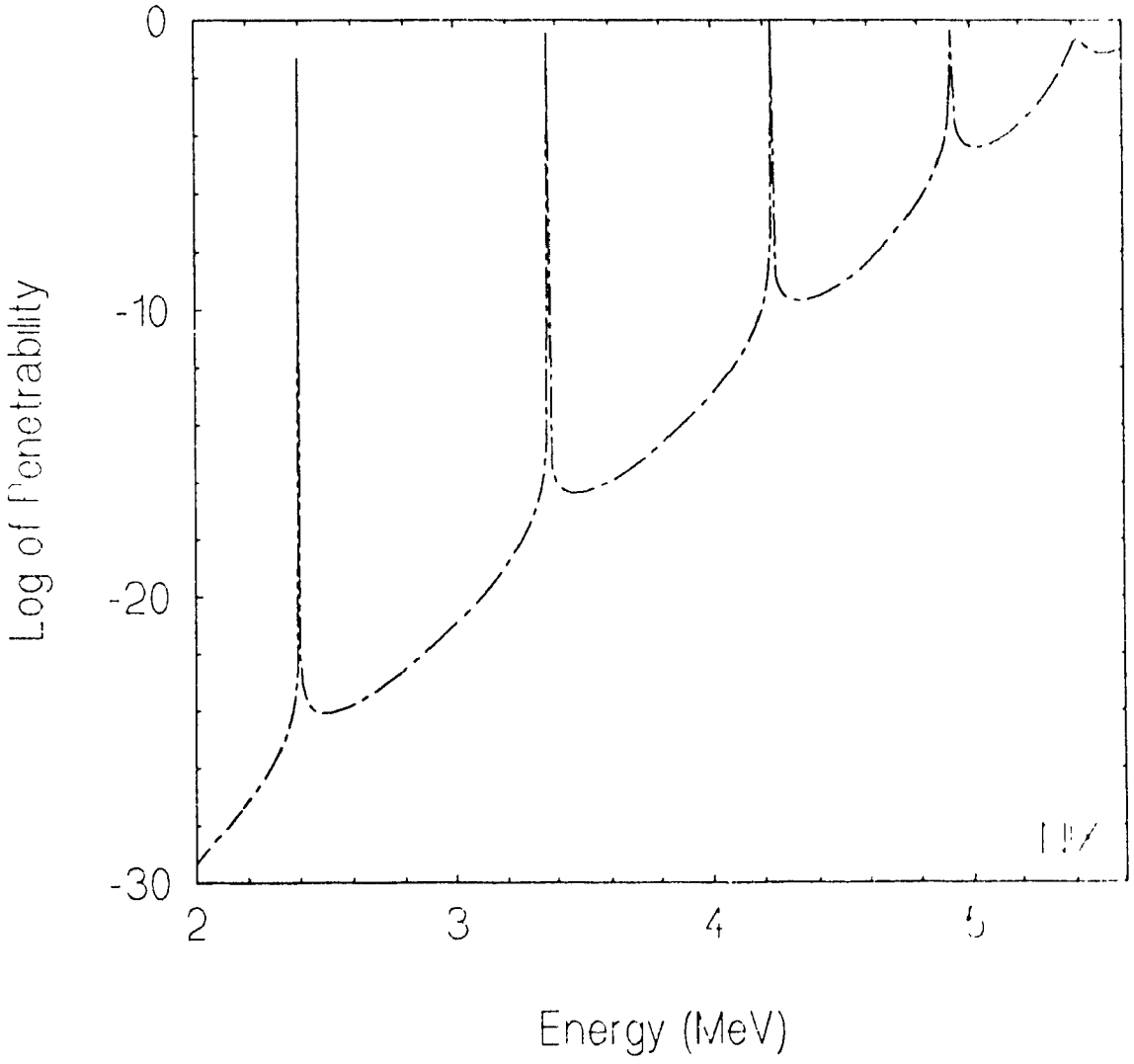

FIG. 21. Plot of log of Penetrability versus incident energy calculated in the NIX method for barrier parameters
E_1=5.8, E_2=1.9, E_3=5.4, $\hbar\omega_1$=0.8, $\hbar\omega_2$=1.0, $\hbar\omega_3$=0.6 *MeV*

The same number of energy levels are present for all methods, with similar level spacing and energy values.

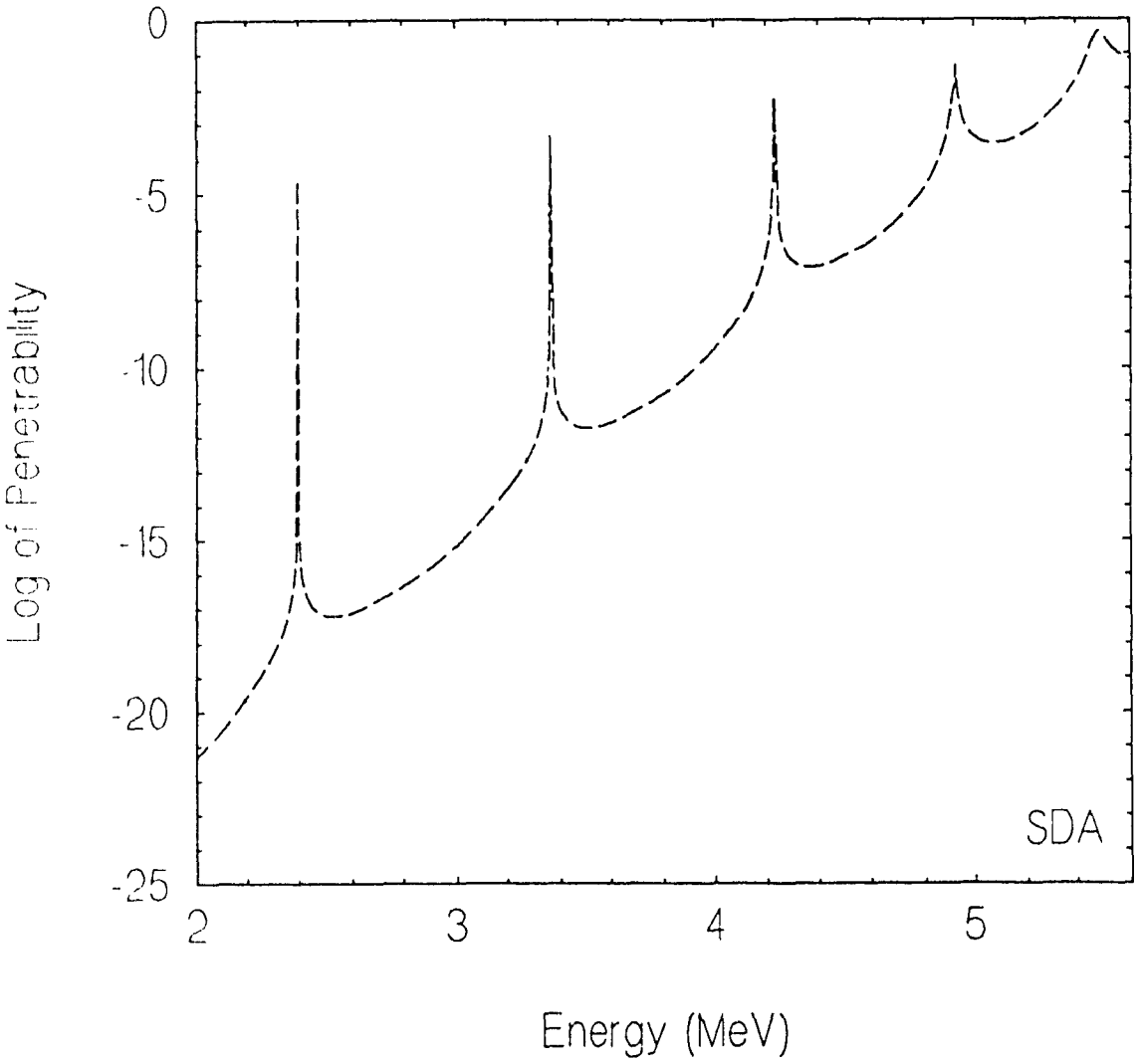

FIG. 22. Plot of log of Penetrability versus incident energy calculated in the SDA method for barrier parameters
E_1=5.8, E_2=1.9, E_3=5.4, $\hbar\omega_1$=0.8, $\hbar\omega_2$=1.0, $\hbar\omega_3$=0.6*MeV*

The INS produces more peaks. Remarkably, all the levels present in the JWKB, NIX, and SDA are present in the INS, along with additional ones.

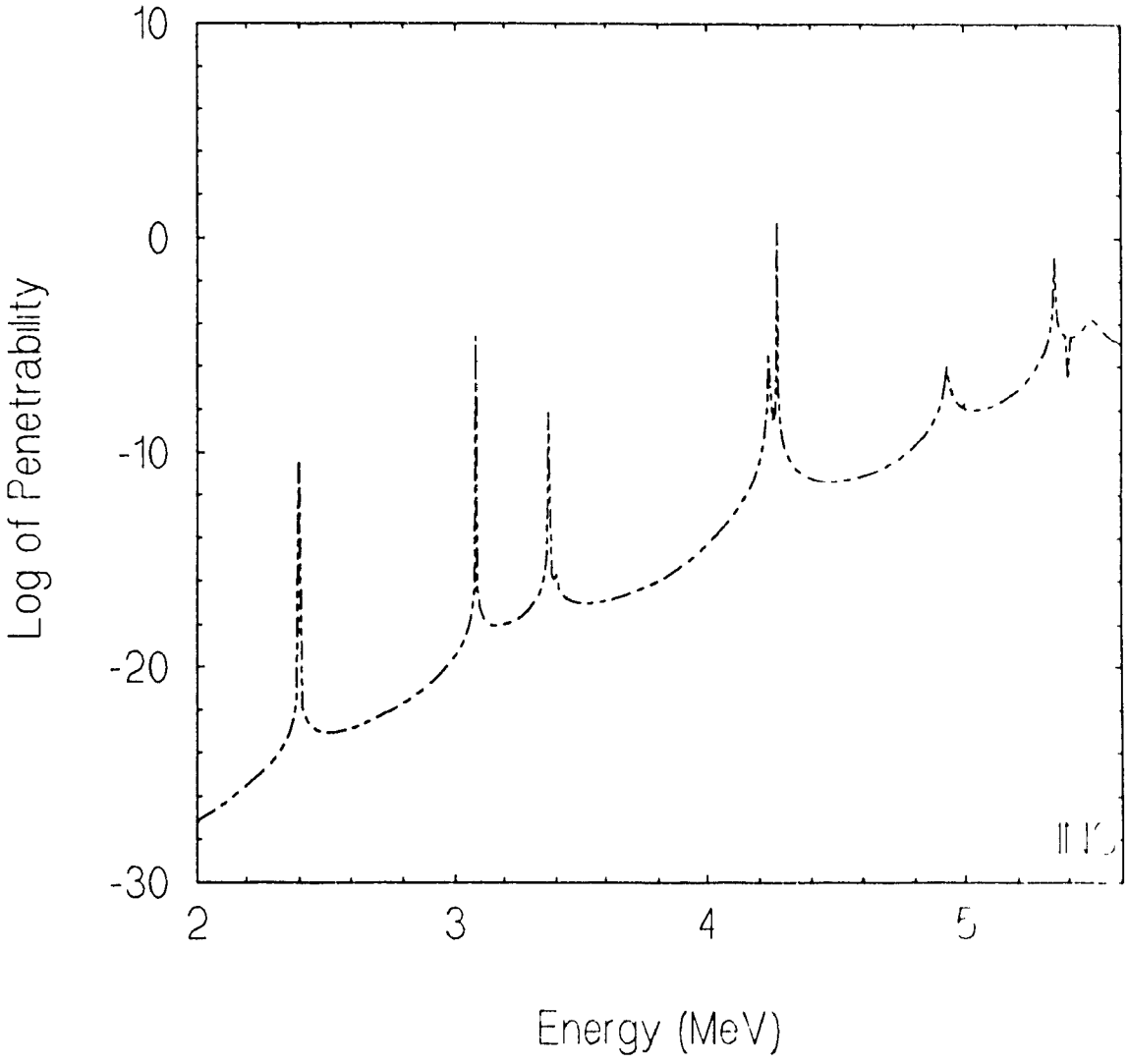

FIG. 23. Plot of log of Penetrability versus incident energy calculated in the INS method for barrier parameters E_1=5.8, E_2=1.9, E_3=5.4, $\hbar\omega_1$=0.8, $\hbar\omega_2$=1.0, $\hbar\omega_3$=0.6, V_0=6.2, E_1=-0.5MeV

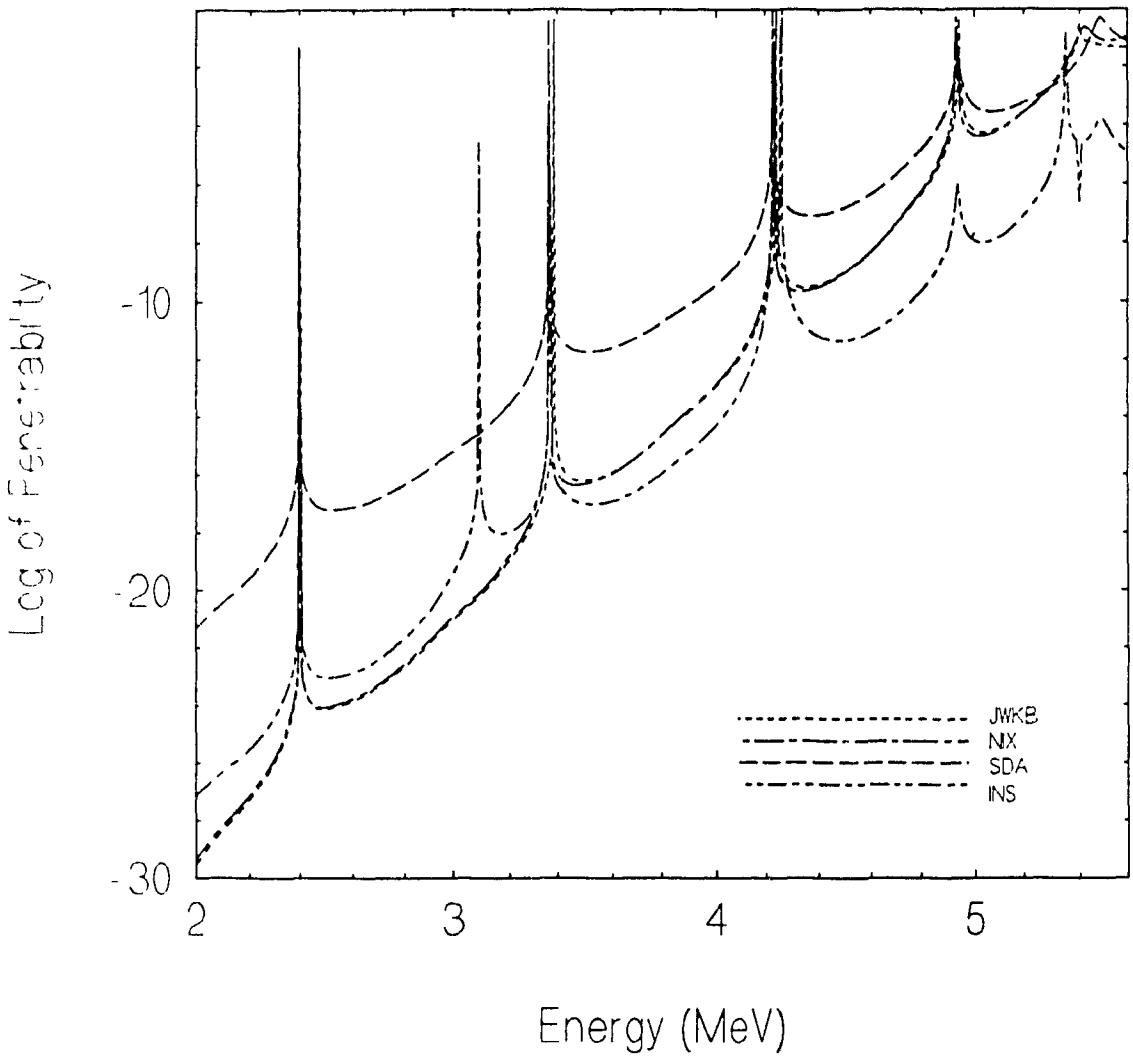

FIG. 24. Graphs 20-23 superimposed.

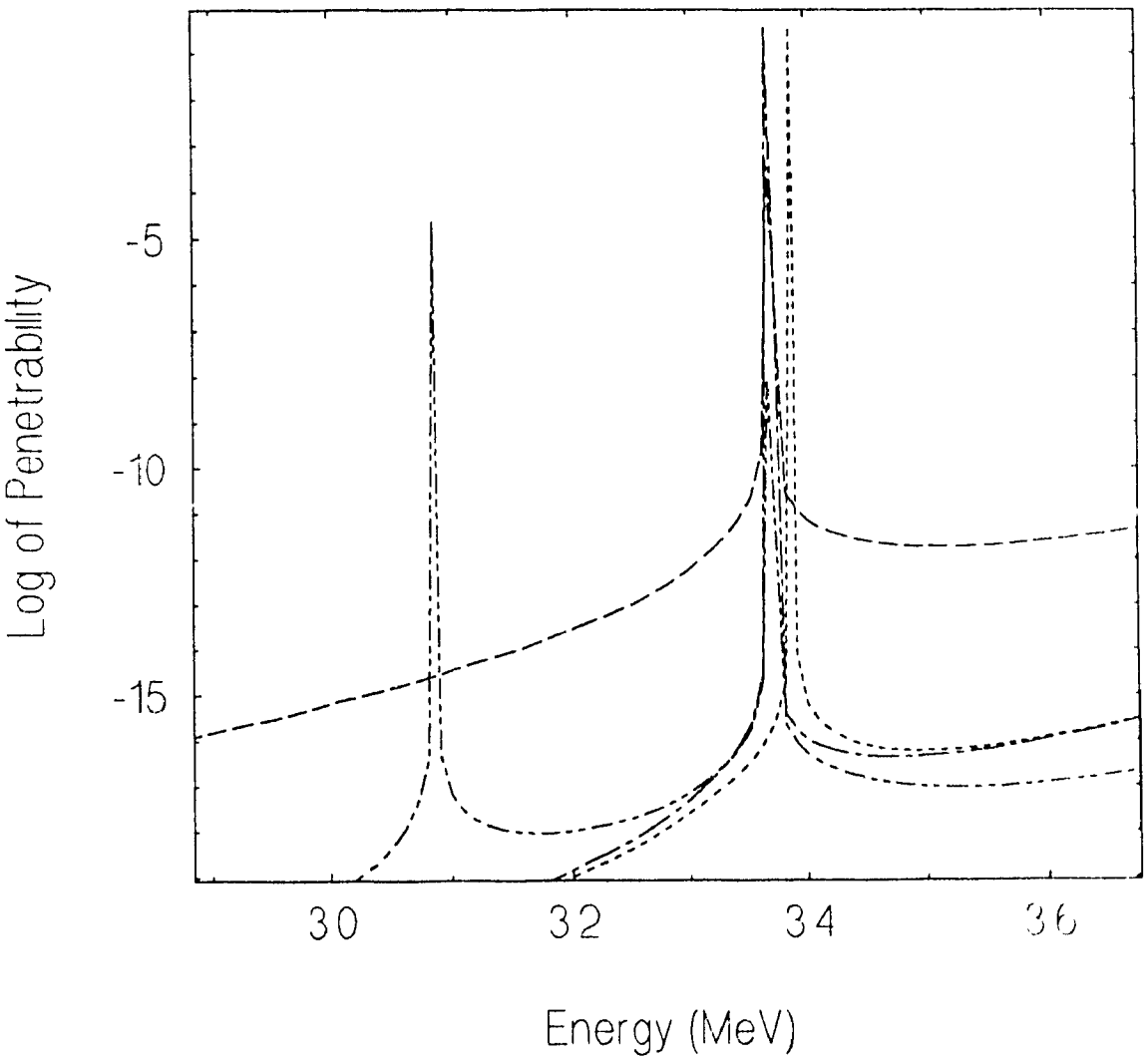

FIG. 25 Zoom of Graph 24 in the energy range 3 05-3 50MeV

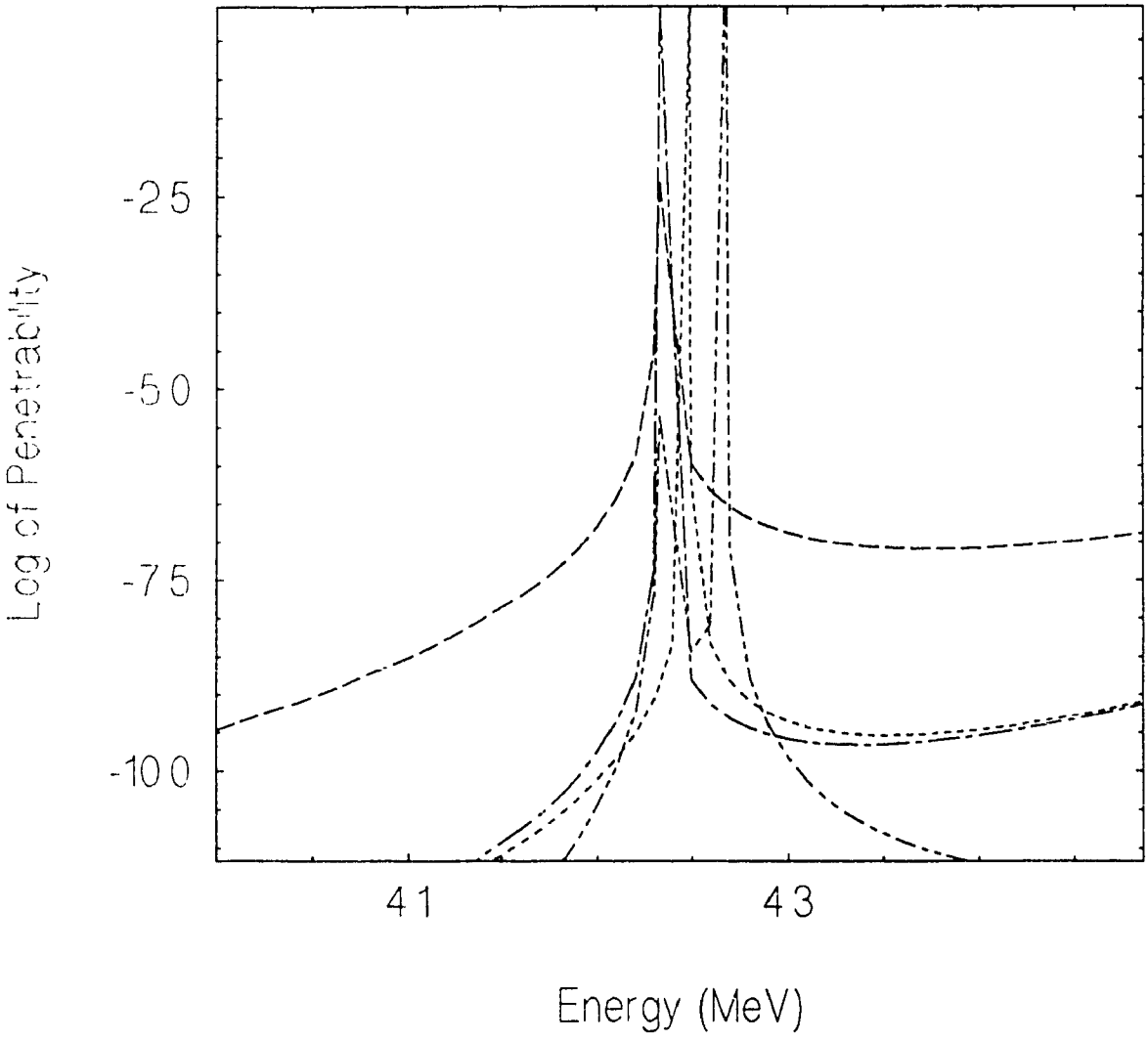

FIG. 26. Zoom of Graph 24 in the energy range 4.20-4 35MeV.

Figs. 20 to 26 demonstrate the general agreement among all methods with respect to resonance energy levels. The major difference among methods is the penetrability values at a specific energy. The JWKB and NIX results are very close with respect to penetrability values and resonance levels. From TABLES III, IV and V, for low incident energies, all exact methods reproduce the same peak energies. The peaks deviate slightly at high resonance levels. The maximum difference was found to be of the order of 1.5keV for Data I, 1.7keV for Data II, and 0keV for Data III. Therefore, one may conclude that for the actinide region and for heavier nuclei, all exact methods reproduce the isomeric energies exactly, and predict other energy levels with hardly any deviation. This is surprising in view of the fact that rather wide differences exist in the development of exact penetrability expressions. No noticeable difference has been found between JWKB and FRO for all energy levels using DATA I. Hence, like the exact methods, the JWKB approximation reproduces identical isomeric energies. We notice from TABLE II that the JWKB and FRO isomeric energy levels change only with changes in E_2 and $\hbar\omega_2$. However, for the Exact methods, the first energy level increases along with an increase in any of the barrier parameters. Therefore, the Exact and JWKB methods will become further apart at higher values of E_1, E_3, $\hbar\omega_1$, and $\hbar\omega_3$.

The JWKB results at low energies follow very well the spacing rule for an harmonic-oscillator potential well

extended to infinity. Cramer and Nix have remarked that the perturbation required to transform an intermediate parabolic well into a two-peaked barrier is negative. This is reflected at all peaks for the exact methods and begins to reveal itself for the JWKB , at higher vibrational states.

The figures 27 to 39 show the variations of the exact method from the JWKB. For the actinide region (Data I), the first energy level is the least deviated, with shifts usually under 10keV. Data II exhibit the opposite effects; level 1 shifts are wider than L2 and L3, and are for the most part above 50 keV; even reaching 80keV for low E_1 values. L_1 can differ as much as 150keV for the symmetric barriers of Data III. Particularly striking is the fact that peak shifts cross over one another. This is especially evident with changing $\hbar\omega_2$ for all data sets.

The greatest difference between the Exact and JWKB isomeric half-lives of DATA I have been found to be 10%. Yet, it is possible to adjust $\hbar\omega_2$ or E_2 in order to bring the JWKB and NIX results into agreement. Decreasing $\hbar\omega_2$ by 0.2 MeV will increase the isomeric half-live by approximately 55%. Isomeric half-lives range from 0.02ns to 0.1ms. Experimentally, the half-lives may differ by as high as 48% (ex. Am^{241} $(1.5\pm0.6)\times10^{-6}$ sec).

TABLE III. Energy values for the first energy level (L1) in the intermediate well for varied barrier parameters of Data I.

	JWKB	FRO	NIX	INS	SDA	
5.40	2.3750	2.3750	2.3725	2.3725	2.3725	
5.60	2.3750	2.3750	2.3725	2.3725	2.3725	
5.80	2.3750	2.3750	2.3726	2.3726	2.3726	E_1
6.00	2.3750	2.3750	2.3726	2.3726	2.3726	
6.20	2.3750	2.3750	2.3726	2.3726	2.3726	
6.40	2.3750	2.3750	2.3726	2.3726	2.3726	
1.60	2.0250	2.025	2.0233	2.0233	2.0233	
1.70	2.1250	2.1250	2.1231	2.1231	2.1231	
1.80	2.2250	2.2250	2.2229	2.2229	2.2229	
1.90	2.3250	2.3250	2.3227	2.3227	2.3227	
2.00	2.4250	2.4250	2.4225	2.4225	2.4225	E_2
2.10	2.5250	2.5250	2.5222	2.5222	2.5222	
2.20	2.6250	2.6250	2.6219	2.6219	2.6219	
2.30	2.7250	2.7250	2.7215	2.7215	2.7215	
2.40	2.8250	2.8250	2.8211	2.8211	2.8211	
2.50	2.9250	2.9250	2.9206	2.9206	2.9206	
4.00	2.3750	2.3750	2.3690	2.3690	2.3690	
4.40	2.3750	2.3750	2.3712	2.3712	2.3712	
4.80	2.3750	2.3750	2.3725	2.3725	2.3725	E_3
5.20	2.3750	2.3750	2.3733	2.3733	2.3733	
5.60	2.3750	2.3750	2.3738	2.3738	2.3738	
0.50	2.3750	2.3750	2.3717	2.3717	2.3717	
0.60	2.3750	2.3750	2.3723	2.3723	2.3723	
0.70	2.3750	2.3750	2.3725	2.3725	2.3725	$\hbar\omega_1$
0.80	2.3750	2.3750	2.3726	2.3726	2.3726	
0.90	2.3750	2.3750	2.3727	2.3727	2.3727	
1.00	2.3750	2.3750	2.3727	2.3727	2.3727	
0.60	2.2500	2.2500	2.2499	2.2499	2.2499	
0.80	2.3500	2.3500	2.3485	2.3485	2.3485	$\hbar\omega_2$
1.00	2.4500	2.4500	2.4423	2.4423	2.4423	
0.45	2.3750	2.3750	2.3708	2.3708	2.3708	
0.50	2.3750	2.3750	2.3721	2.3721	2.3721	
0.55	2.3750	2.3750	2.3729	2.3729	2.3729	$\hbar\omega_3$
0.60	2.3750	2.3750	2.3734	2.3734	2.3734	
0.65	2.3750	2.3750	2.3738	2.3738	2.3738	

TABLE IV. Energy values for the second energy level (L2) in the intermediate well for barrier parameters of Data I

	JWKB	FRO	NIX	INS	SDA	
5.40	3.2150	3.2150	3.1990	3.1990	3.1990	
5.60	3.2150	3.2150	3.1997	3.1997	3.1997	
5.80	3.2150	3.2150	3.2002	3.2002	3.2002	E_1
6.00	3.2150	3.2150	3.2006	3.2006	3.2006	
6.20	3.2150	3.2150	3.2009	3.2009	3.2009	
6.40	3.2150	3.2150	3.2011	3.2011	3.2011	
1.60	2.8701	2.8701	2.8573	2.8573	2.8573	
1.70	2.9689	2.9689	2.9556	2.9556	2.9556	
1.80	3.0675	3.0675	3.0537	3.0537	3.0537	
1.90	3.1659	3.1659	3.1516	3.1516	3.1516	
2.00	3.2640	3.2640	3.2493	3.2493	3.2493	E_2
2.10	3.3618	3.3618	3.3467	3.3467	3.3467	
2.20	3.4593	3.4593	3.4438	3.4438	3.4438	
2.30	3.5564	3.5564	3.5405	3.5405	3.5405	
2.40	3.6531	3.6531	3.6369	3.6369	3.6369	
2.50	3.7493	3.7493	3.7328	3.7328	3.7328	
4.00	3.1841	3.1841	3.1693	3.1693	3.1693	
4.40	3.2031	3.2031	3.1879	3.1879	3.1879	
4.80	3.2140	3.2140	3.1994	3.1994	3.1994	E_3
5.20	3.2201	3.2201	3.2068	3.2068	3.2068	
5.60	3.2233	3.2233	3.2117	3.2117	3.2117	
0.50	3.2137	3.2137	3.1920	3.1920	3.1920	
0.60	3.2150	3.2150	3.1973	3.1973	3.1973	
0.70	3.2150	3.2150	3.1996	3.1996	3.1996	
0.80	3.2150	3.2150	3.2006	3.2006	3.2006	$\hbar\omega_1$
0.90	3.2150	3.2150	3.2012	3.2012	3.2012	
1.00	3.2150	3.2150	3.2014	3.2014	3.2014	
0.60	2.8500	2.8500	2.8488	2.8488	2.8488	
0.80	3.1463	3.1463	3.1342	3.1342	3.1342	$\hbar\omega_2$
1.00	3.3997	3.3997	3.3810	3.3810	3.3810	
0.45	3.1991	3.1991	3.1860	3.1860	3.1860	
0.50	3.2103	3.2103	3.1960	3.1960	3.1960	
0.55	3.2175	3.2175	3.2030	3.2030	3.2030	$\hbar\omega_3$
0.60	3.2217	3.2217	3.2079	3.2079	3.2079	
0.65	3.2239	3.2239	3.2114	3.2114	3.2114	

TABLE V. Energy values for the third energy level (L3) in the intermediate well for varied barrier parameters of Data I

	JWKB	FRO	NIX	INS	SDA	
5.40	3.9624	3.9624	3.9478	3.9481	3.9481	
5.60	3.9644	3.9644	3.9509	3.9512	3.9512	
5.80	3.9655	3.9655	3.9533	3.9536	3.9536	E_1
6.00	3.9662	3.9662	3.9551	3.9554	3.9554	
6.20	3.9664	3.9664	3.9565	3.9569	3.9569	
6.40	3.9664	3.9664	3.9577	3.9580	3.9580	
1.50	3.5527	3.5527	3.5420	3.5420	3.5420	
1.60	3.6458	3.6458	3.6350	3.6351	3.6351	
1.70	3.7383	3.7383	3.7273	3.7274	3.7274	
1.80	3.8300	3.8300	3.8189	3.8191	3.8191	
1.90	3.9209	3.9209	3.9097	3.9099	3.9099	E_2
2.00	4.0109	4.0109	3.9994	3.9999	3.9999	
2.10	4.0999	4.0999	4.0881	4.0890	4.0890	
2.20	4.1877	4.1877	4.1756	4.1770	4.1770	
2.30	4.2742	4.2742	4.2616	4.2636	4.2640	
2.50	4.4423	4.4423	4.4282	4.4350	4.4350	
4.00	3.8310	3.8310	3.8161	3.8460	3.8457	
4.40	3.9108	3.9108	3.9001	3.9043	3.9043	
4.80	3.9611	3.9611	3.9499	3.9503	3.9503	E_3
5.20	3.9952	3.9952	3.9823	3.9823	3.9823	
5.60	4.0192	4.0192	4.0044	4.0044	4.0044	
0.50	3.9327	3.9327	3.9222	3.9225	3.9225	
0.60	3.9547	3.9547	3.9416	3.9419	3.9419	
0.70	3.9637	3.9637	3.9508	3.9511	3.9511	
0.80	3.9663	3.9663	3.9554	3.9557	3.9557	$\hbar\omega_1$
0.90	3.9664	3.9664	3.9578	3.9581	3.9581	
1.00	3.9664	3.9664	3.9591	3.9595	3.9595	
0.60	3.4487	3.4487	3.4416	3.4416	3.4416	
0.80	3.8782	3.8782	3.8676	3.8678	3.8678	$\hbar\omega_2$
1.00	4.1790	4.1790	4.1653	4.1667	4.1667	
0.45	3.9123	3.9123	3.9044	3.9045	3.9045	
0.50	3.9482	3.9482	3.9384	3.9386	3.9386	
0.55	3.9766	3.9766	3.9641	3.9646	3.9646	$\hbar\omega_3$
0.60	3.9989	3.9989	3.9844	3.9844	3.9844	
0.65	4.0165	4.0165	3.9984	3.9997	3.9997	

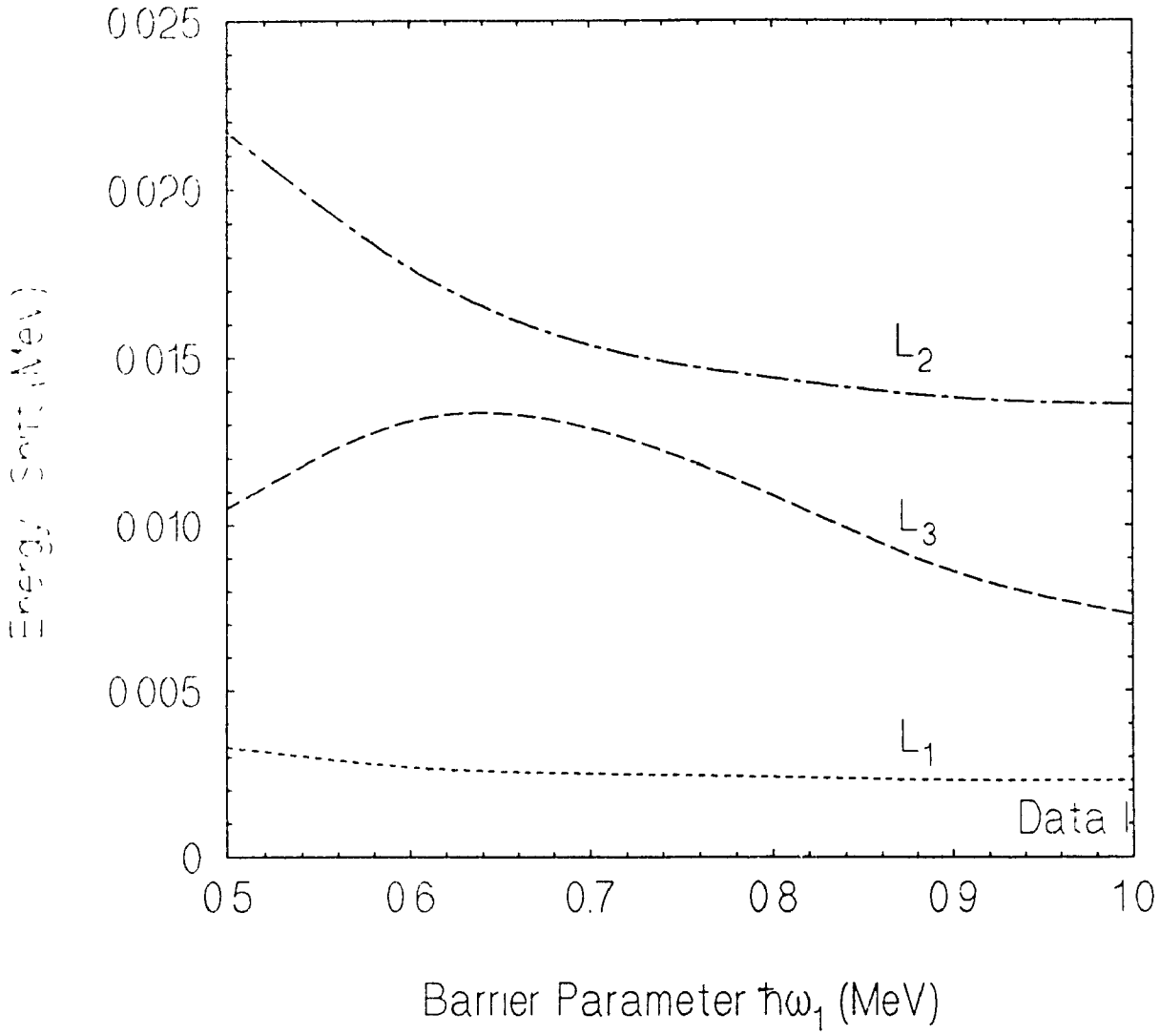

FIG. 27. Graph of energy shifts between exact and JWKB methods for Data I with varying barrier parameter $\hbar\omega_1$

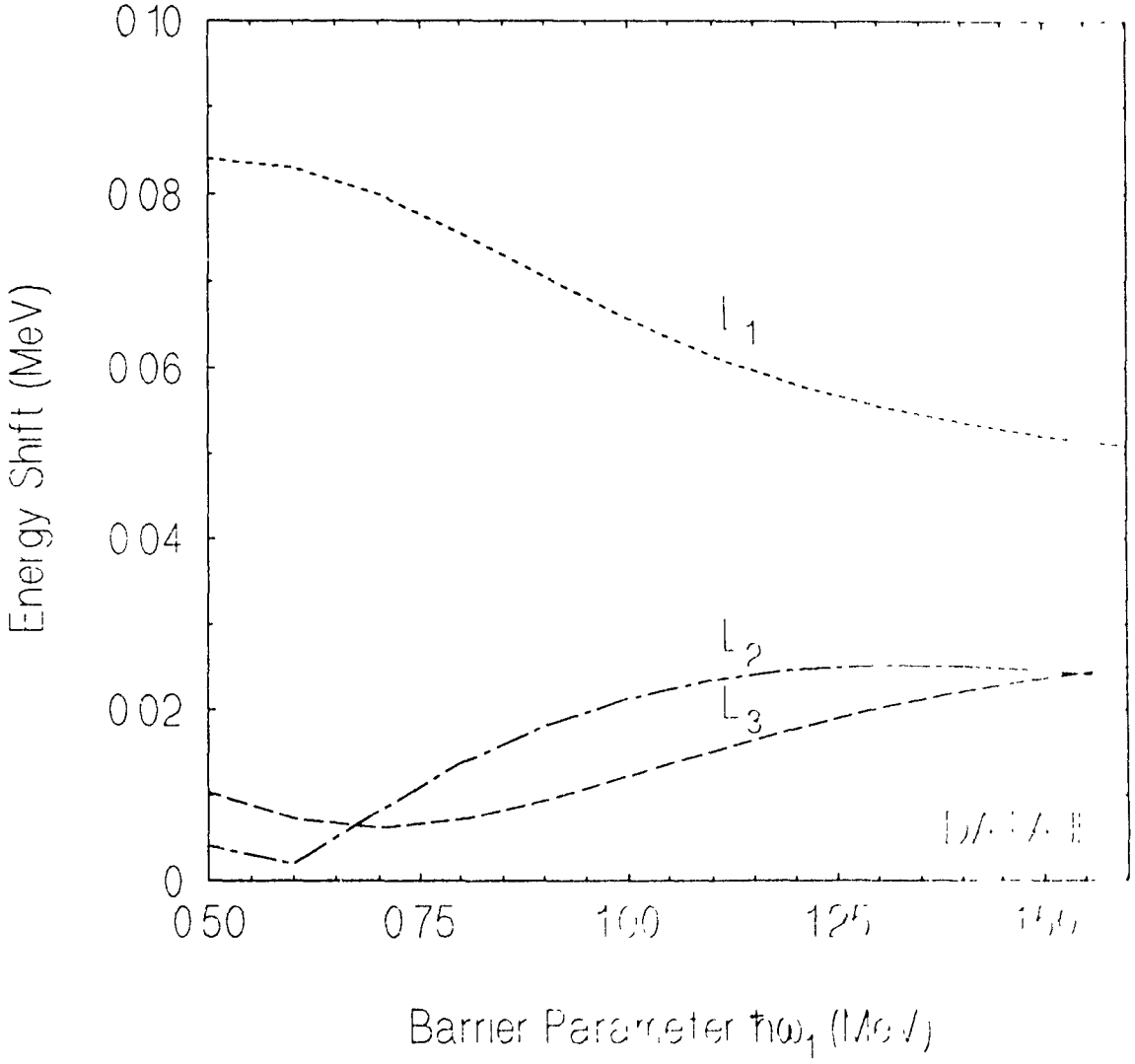

FIG. 28. Graph of energy shifts between exact and JWKB methods for Data II with varying barrier parameter $\hbar\omega_1$.

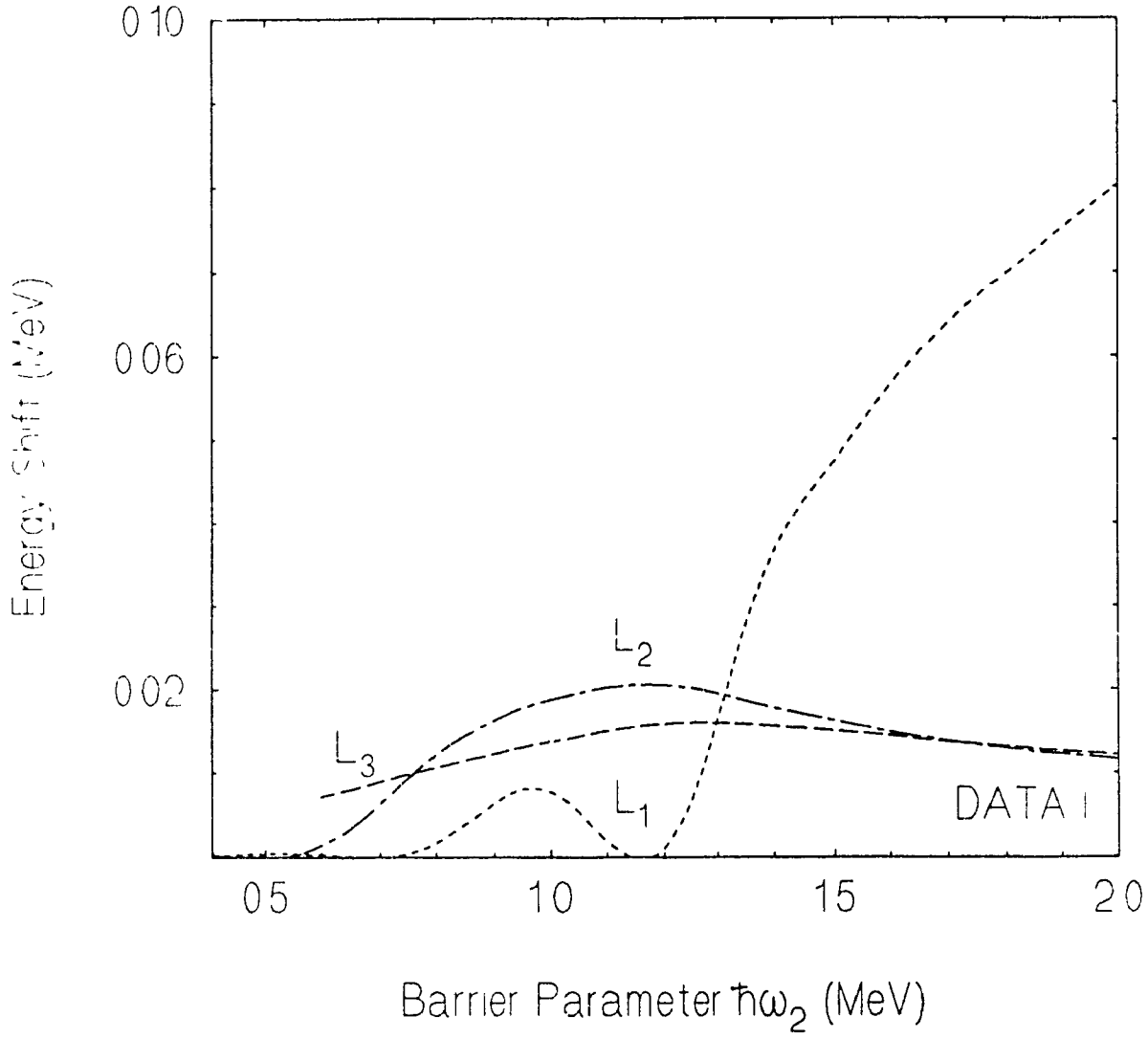

FIG. 29. Graph of energy shifts between exact and JWKB methods for Data I with varying barrier parameter $\hbar\omega_2$

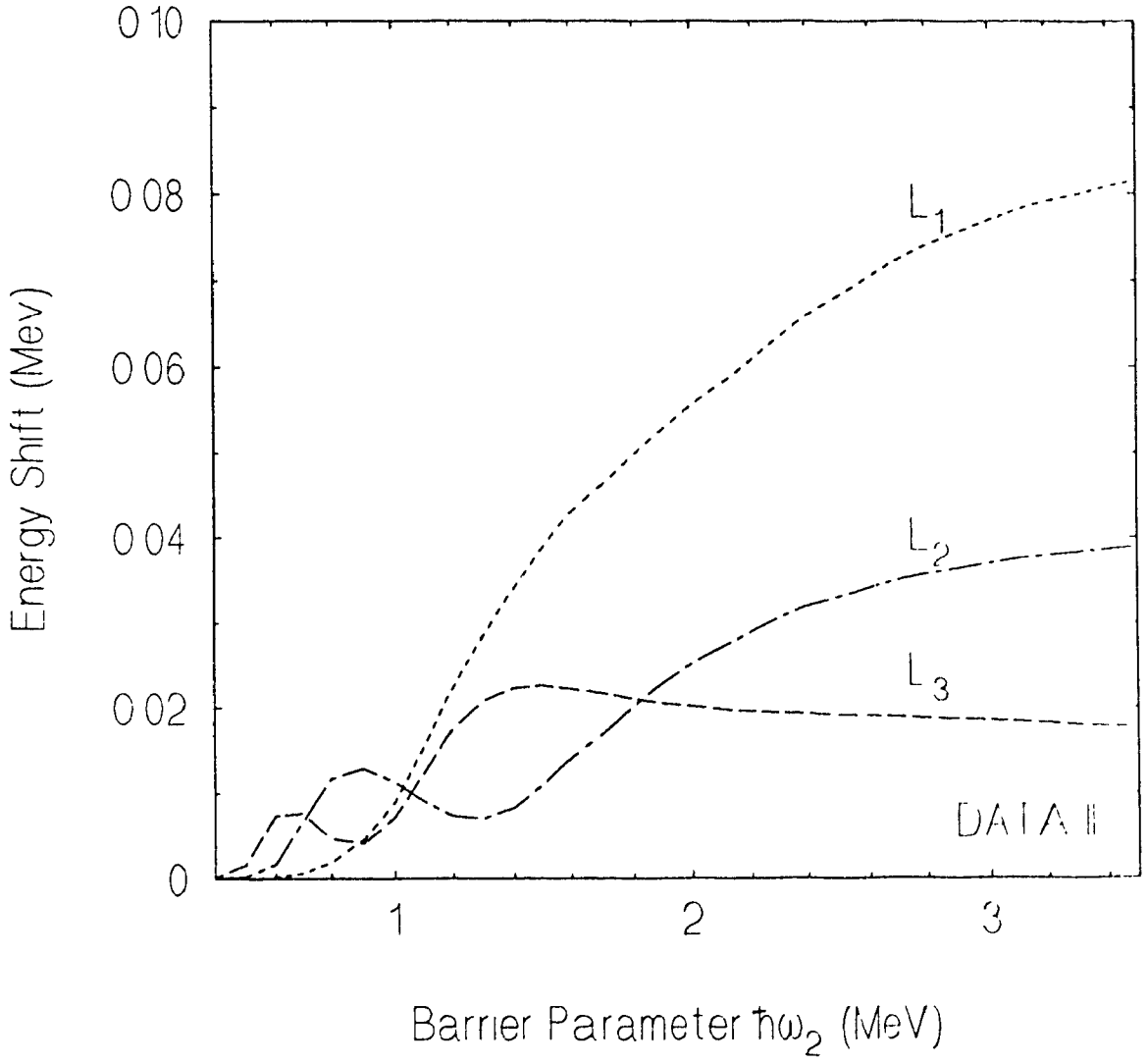

FIG. 30. Graph of energy shifts between exact and JWKB methods for Data II with varying barrier parameter $\hbar\omega_2$.

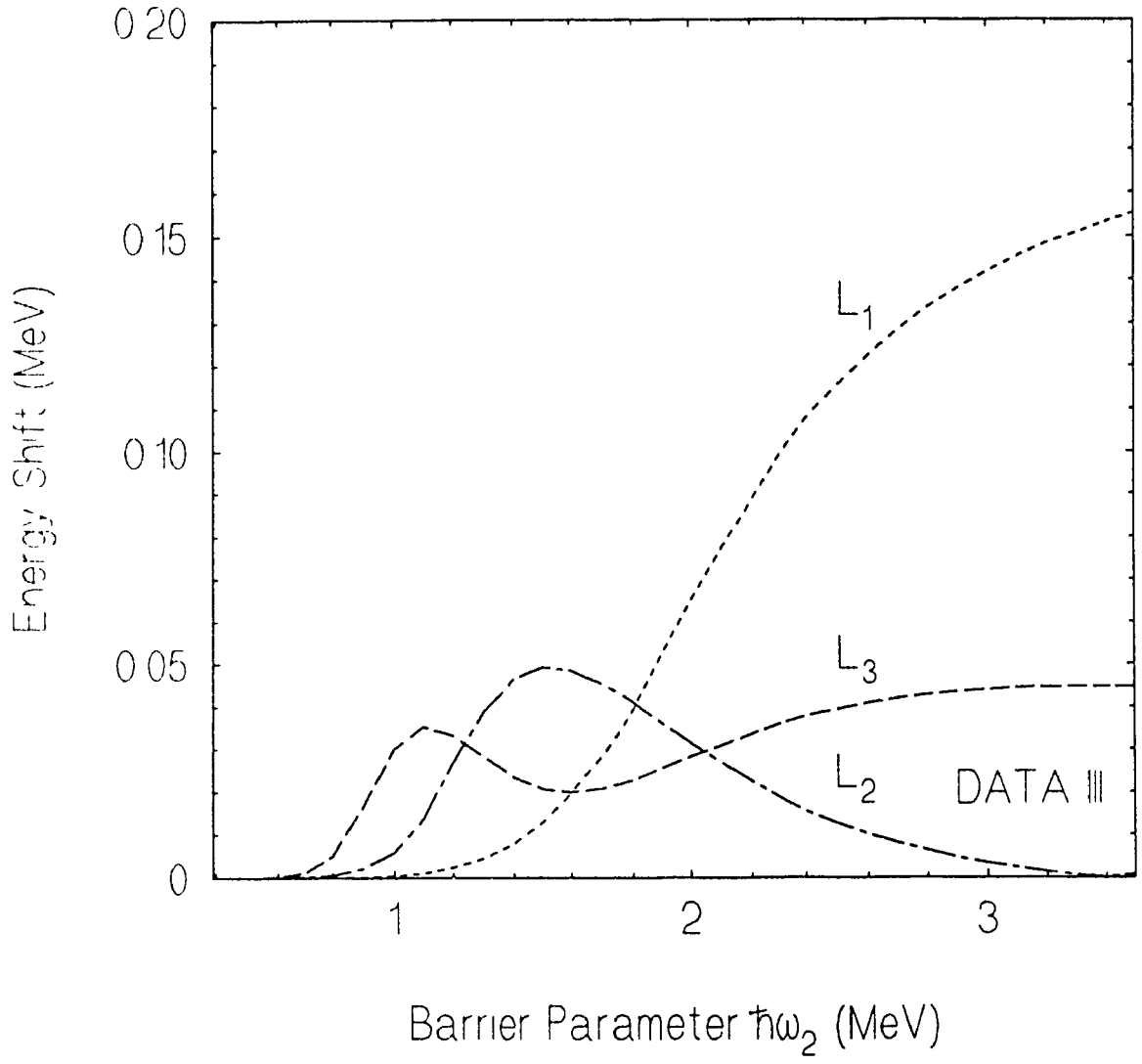

FIG. 31. Graph of energy shifts between exact and JWKB methods for Data III with varying barrier parameter $\hbar\omega_2$

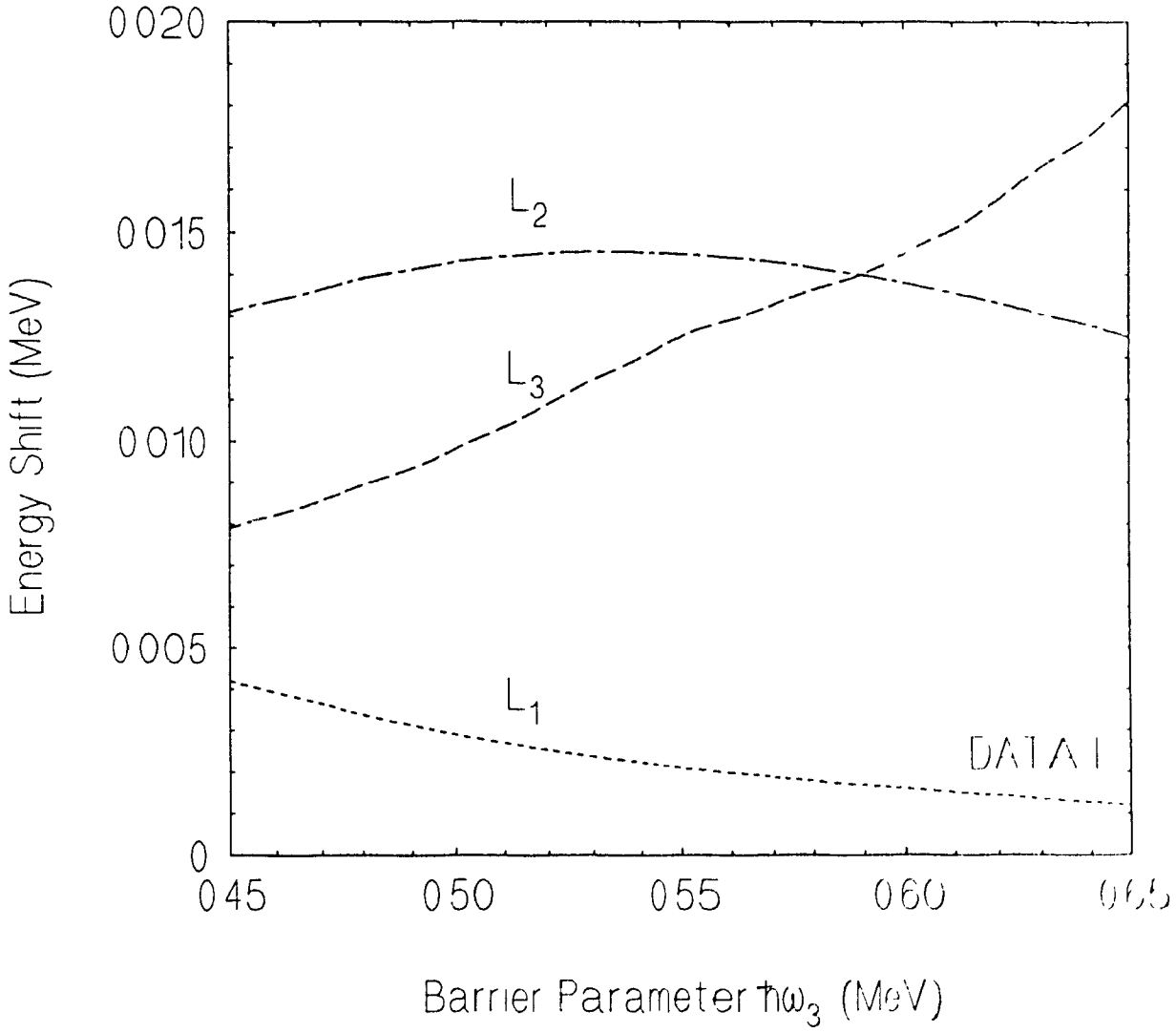

FIG. 32. Graph of energy shifts between exact and JWKB methods for Data I with varying barrier parameter $\hbar\omega_3$.

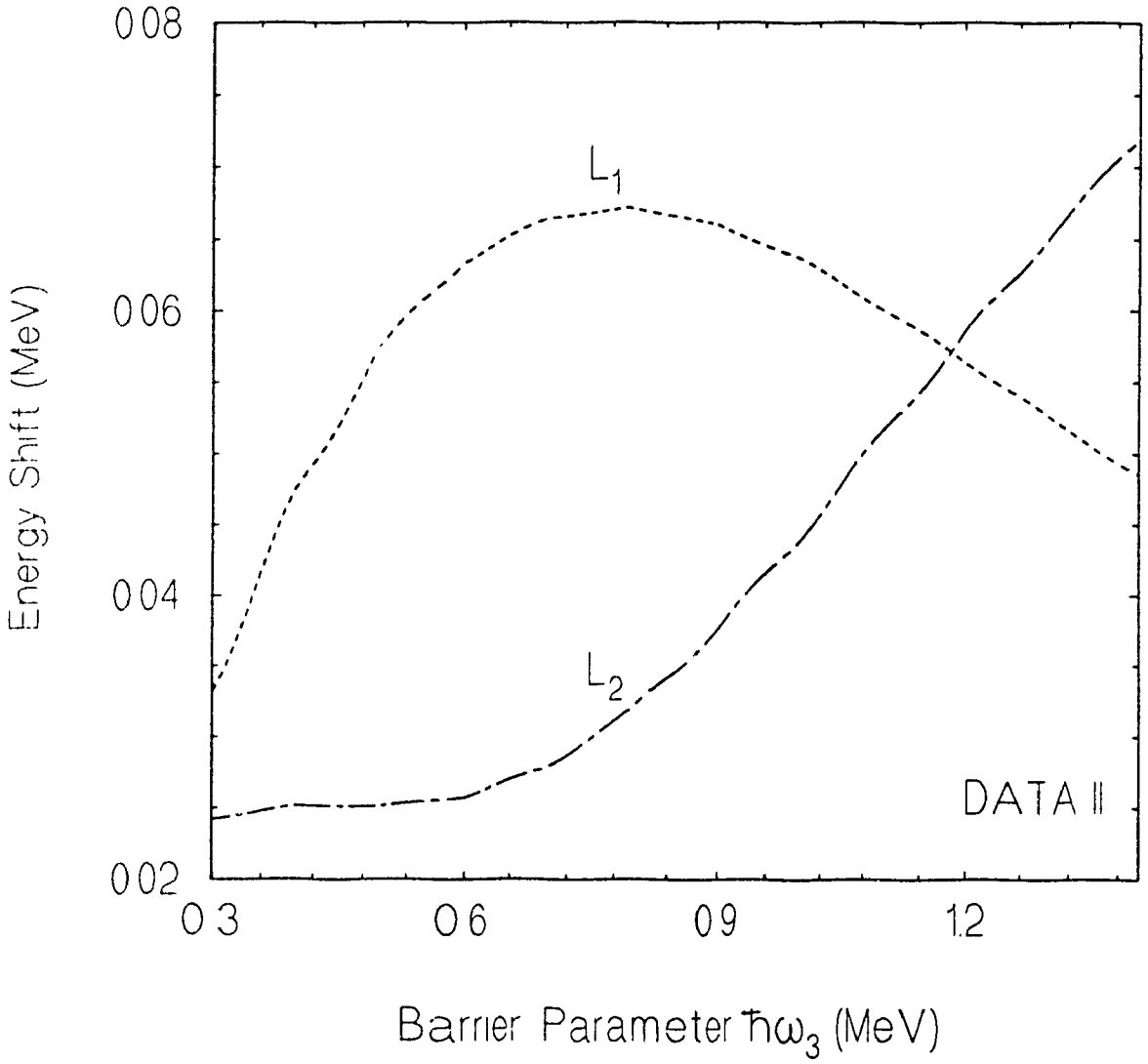

FIG. 33. Graph of energy shifts between exact and JWKB methods for Data II with varying barrier parameter $\hbar\omega_3$

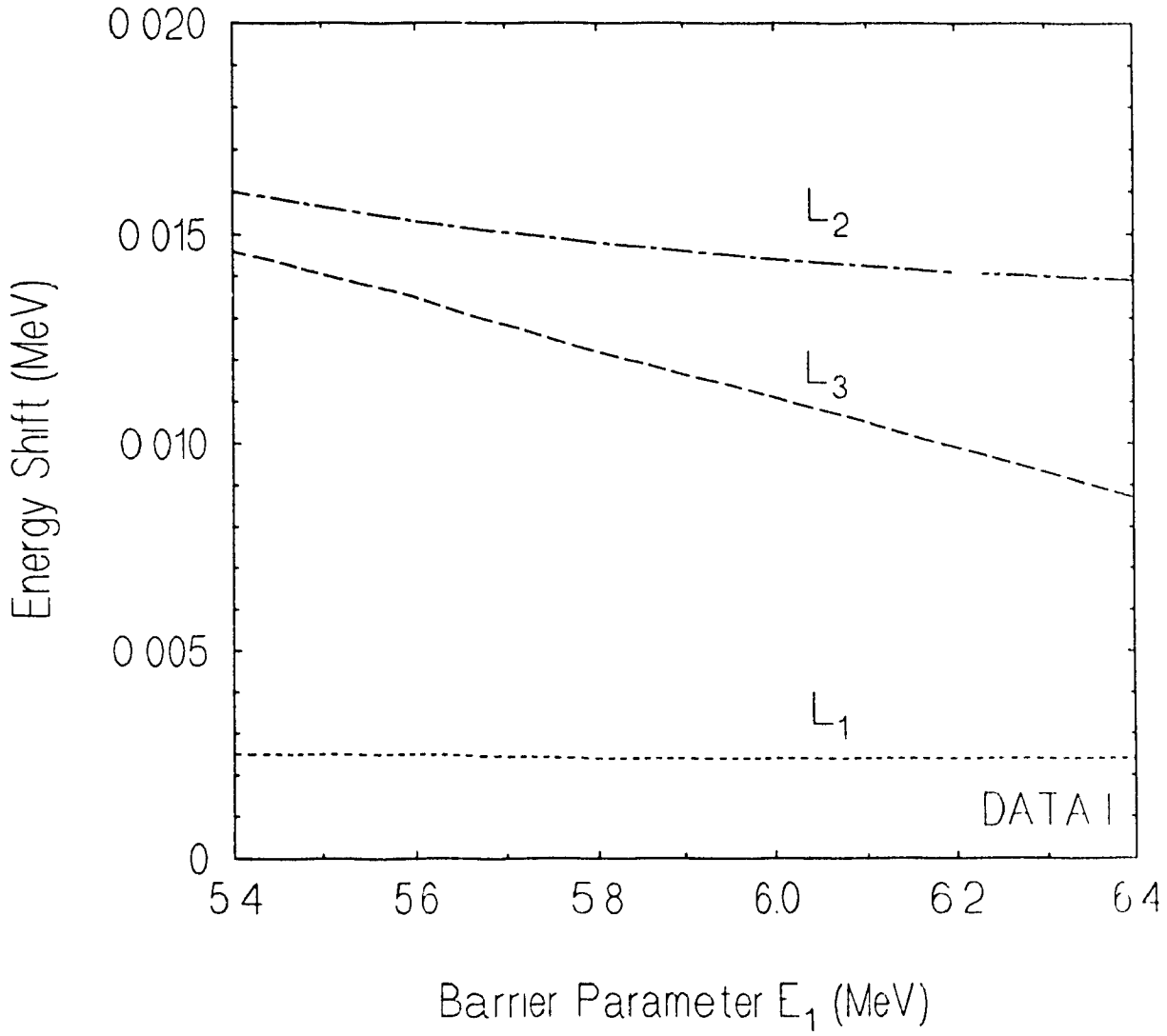

FIG. 34. Graph of energy shifts between exact and JWKB methods for Data I with varying barrier parameter E_1.

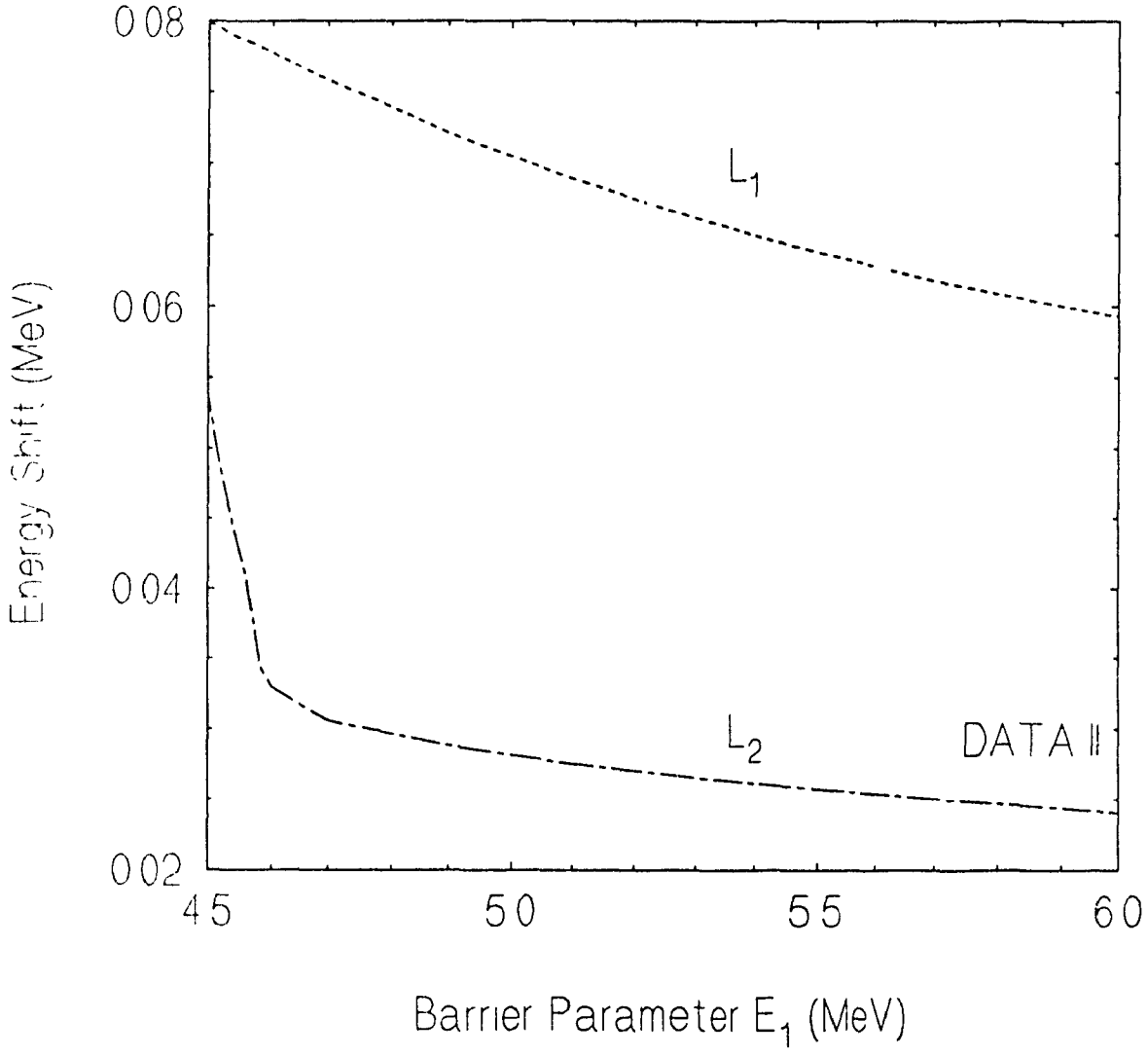

FIG. 35. Graph of energy shifts between exact and JWKB methods Data II with varying barrier parameter E_1

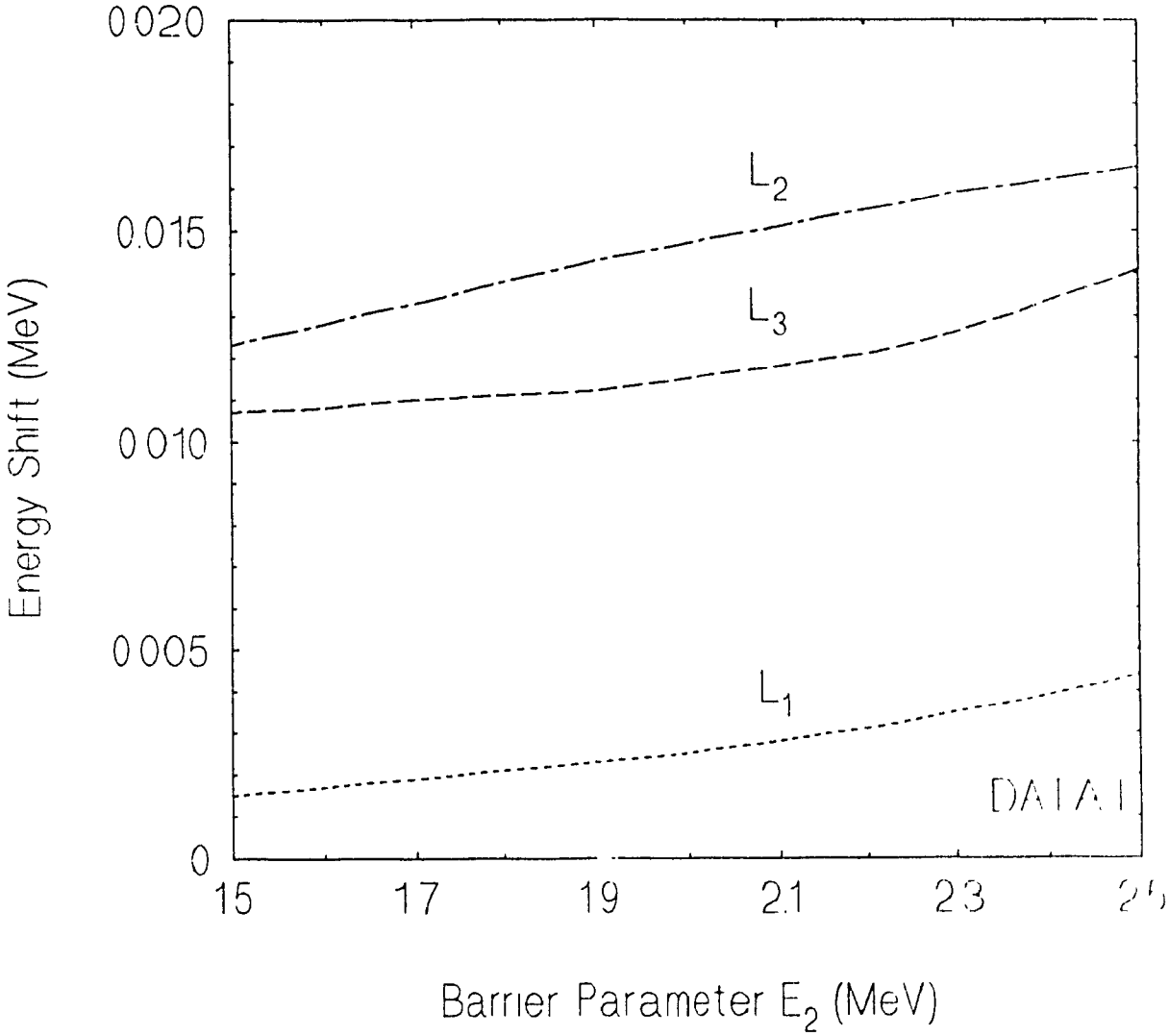

FIG. 36. Graph of energy shifts between exact and JWKB methods for Data I with varying barrier parameter E_2.

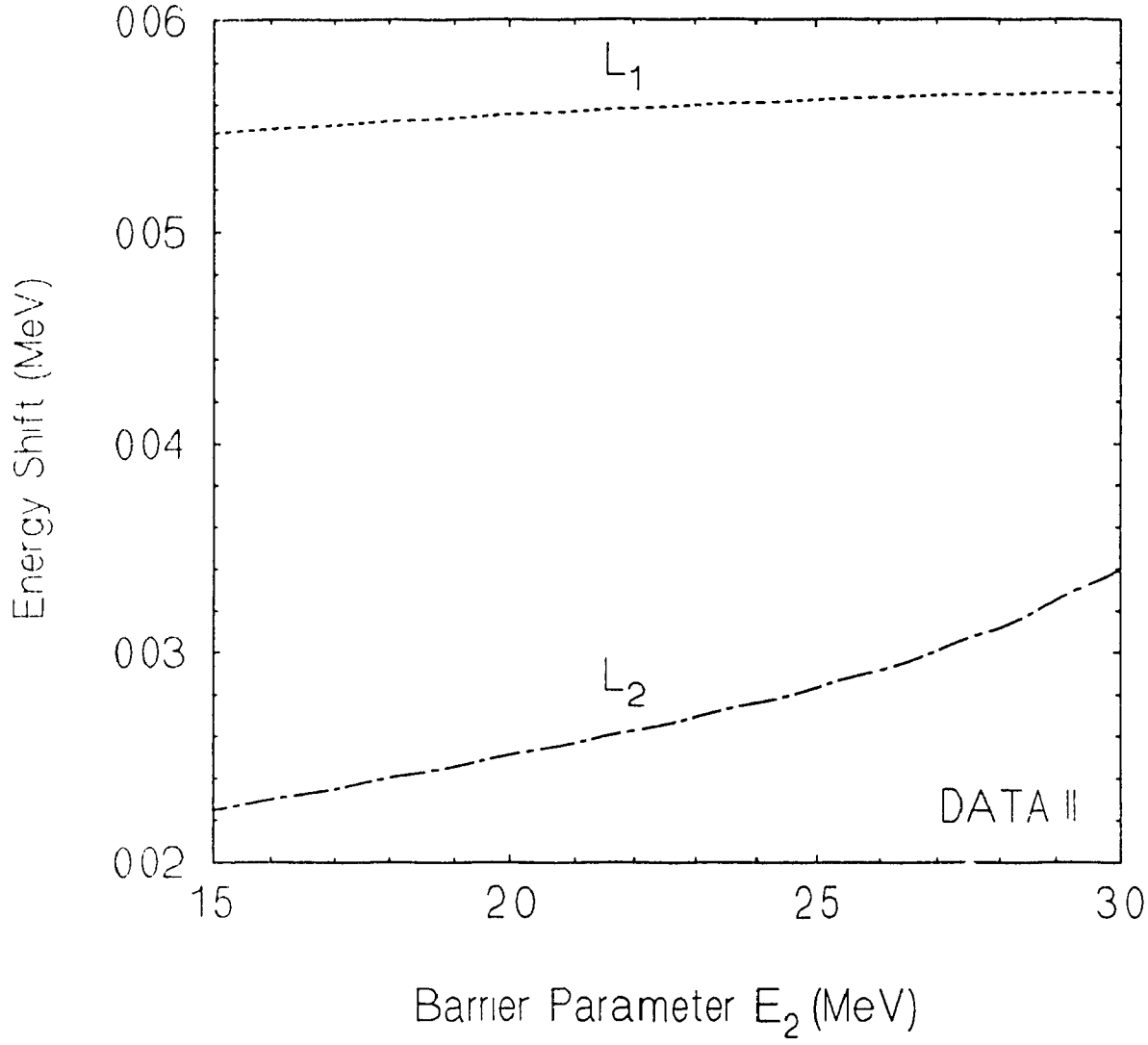

FIG. 37. Graph of energy shifts between exact and JWKB methods for Data II with varying barrier parameter E_2

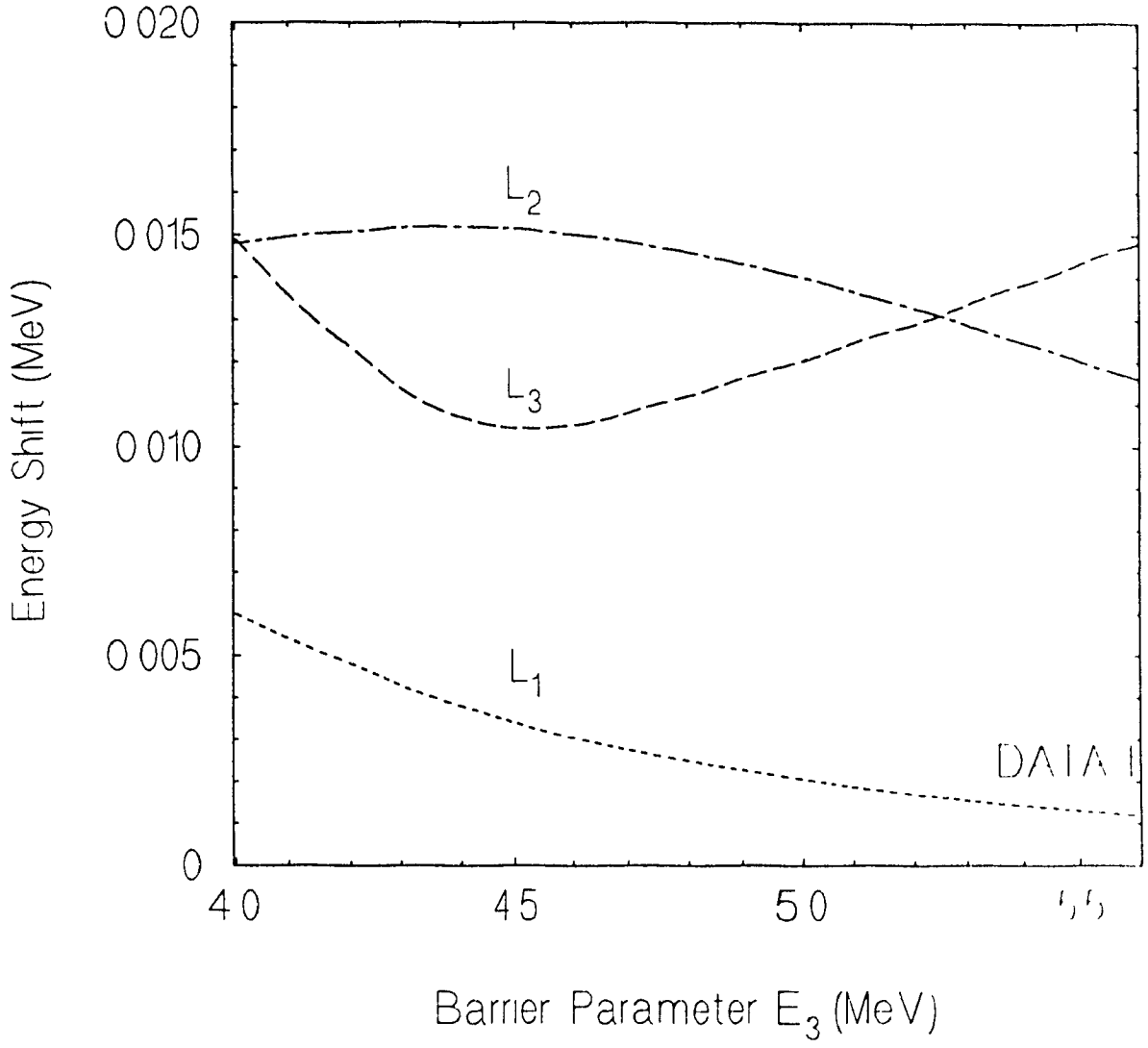

FIG. 38. Graph of energy shifts between exact and JWKB methods for Data I with varying barrier parameter E_3

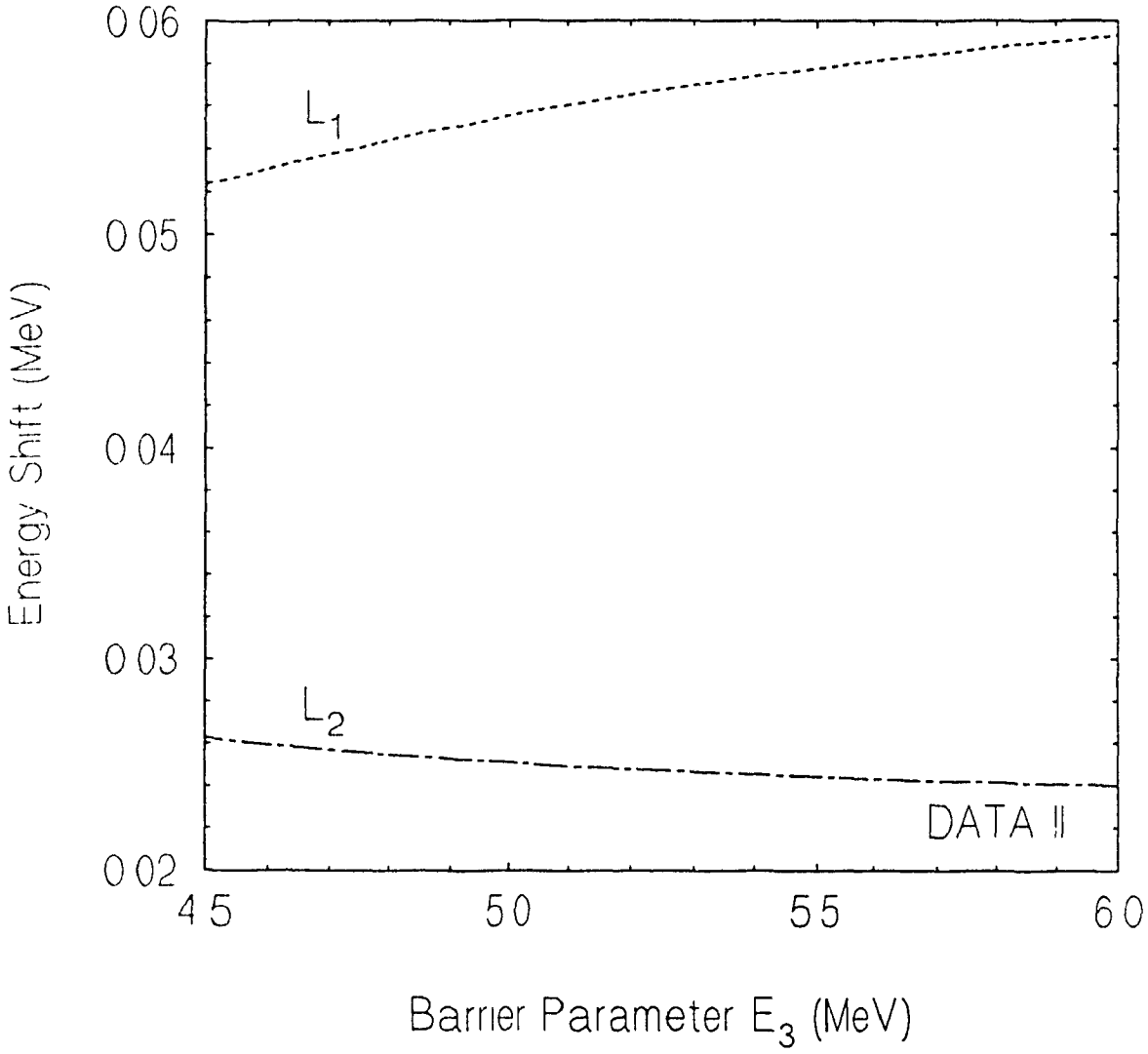

FIG. 39. Graph of energy shifts between exact and JWKB methods for Data II with varying barrier parameter E_3

8.2 Penetrability Peak Maximum

Numerically, the determination of P_{max} at resonance can be found by iteration whereas, Cramer and Nix have used a Lorenzian curve fitting method. The peak values for FRO are not considered since they are undetermined at resonance. The behaviour of maximum peak heights with changing barrier parameters are shown in Figs. 40 to 45.

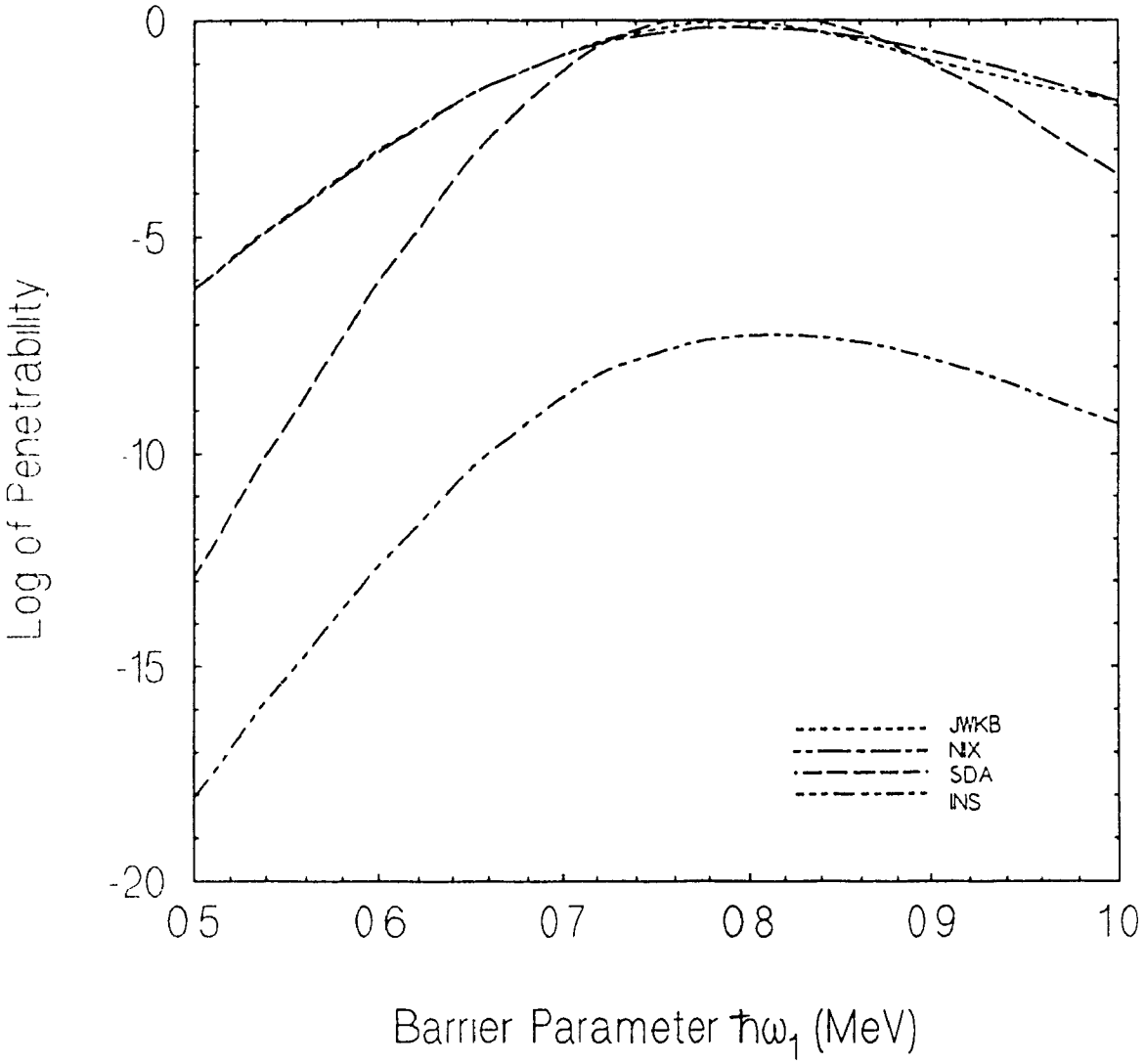

FIG. 40. Maximum Penetrability at resonance energy level L_1 for DATA I with changing barrier parameter $\hbar\omega_1$

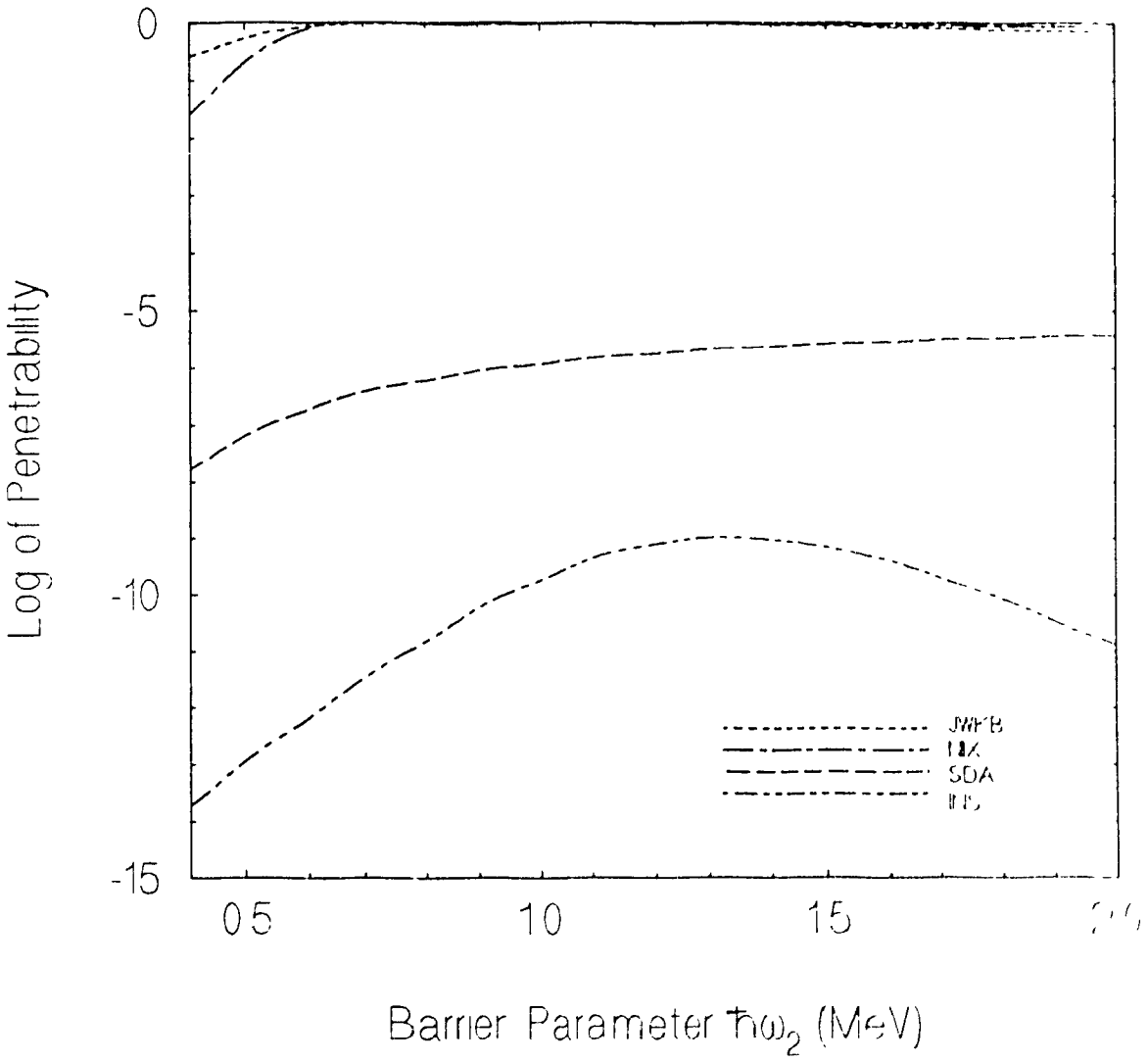

FIG. 41. Maximum Penetrability at resonance energy level L_1 for DATA I with changing barrier parameter $\hbar\omega_2$.

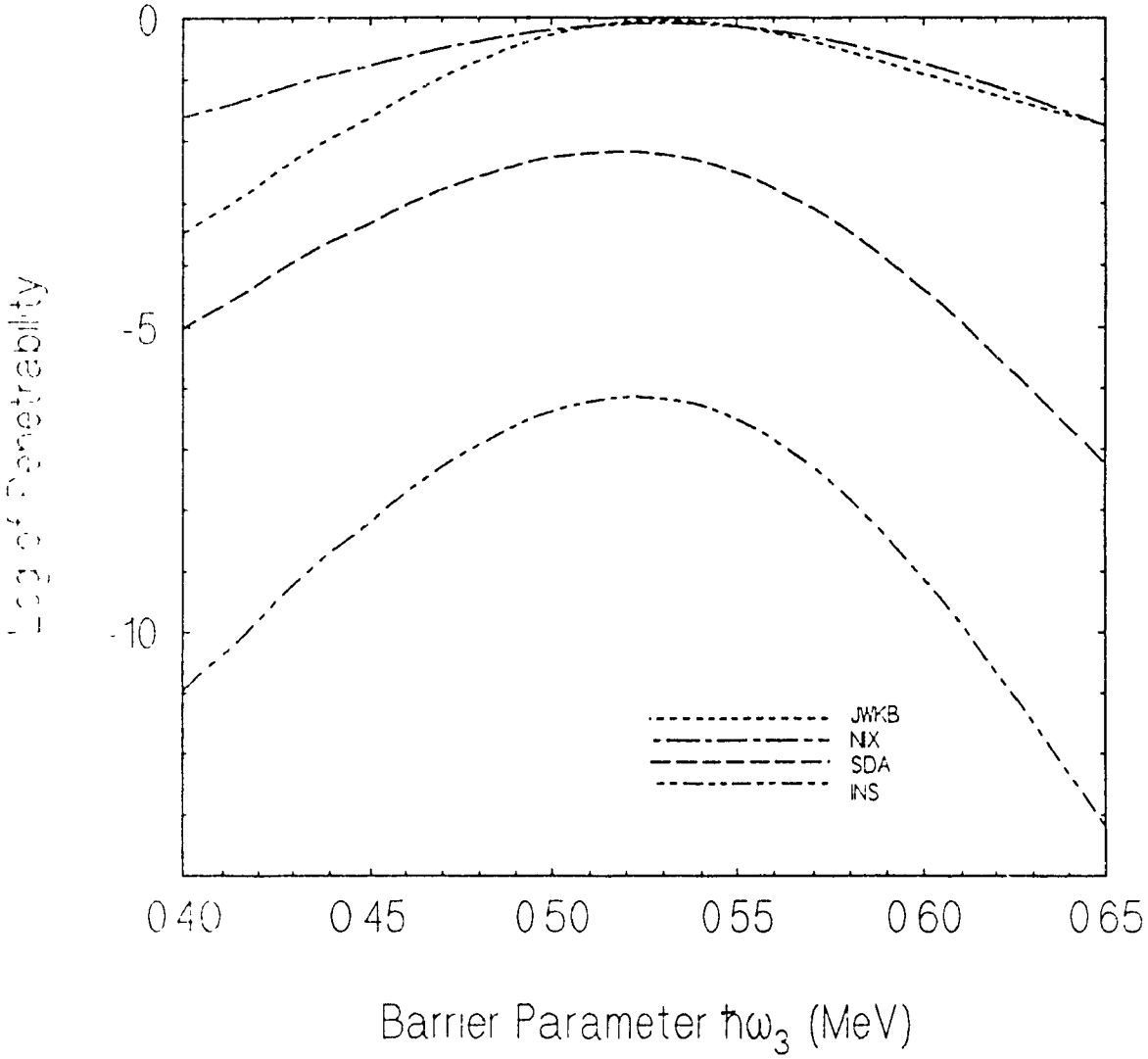

FIG. 42. Maximum Penetrability at resonance energy level L_i for DATA I with changing barrier parameter $\hbar\omega_3$

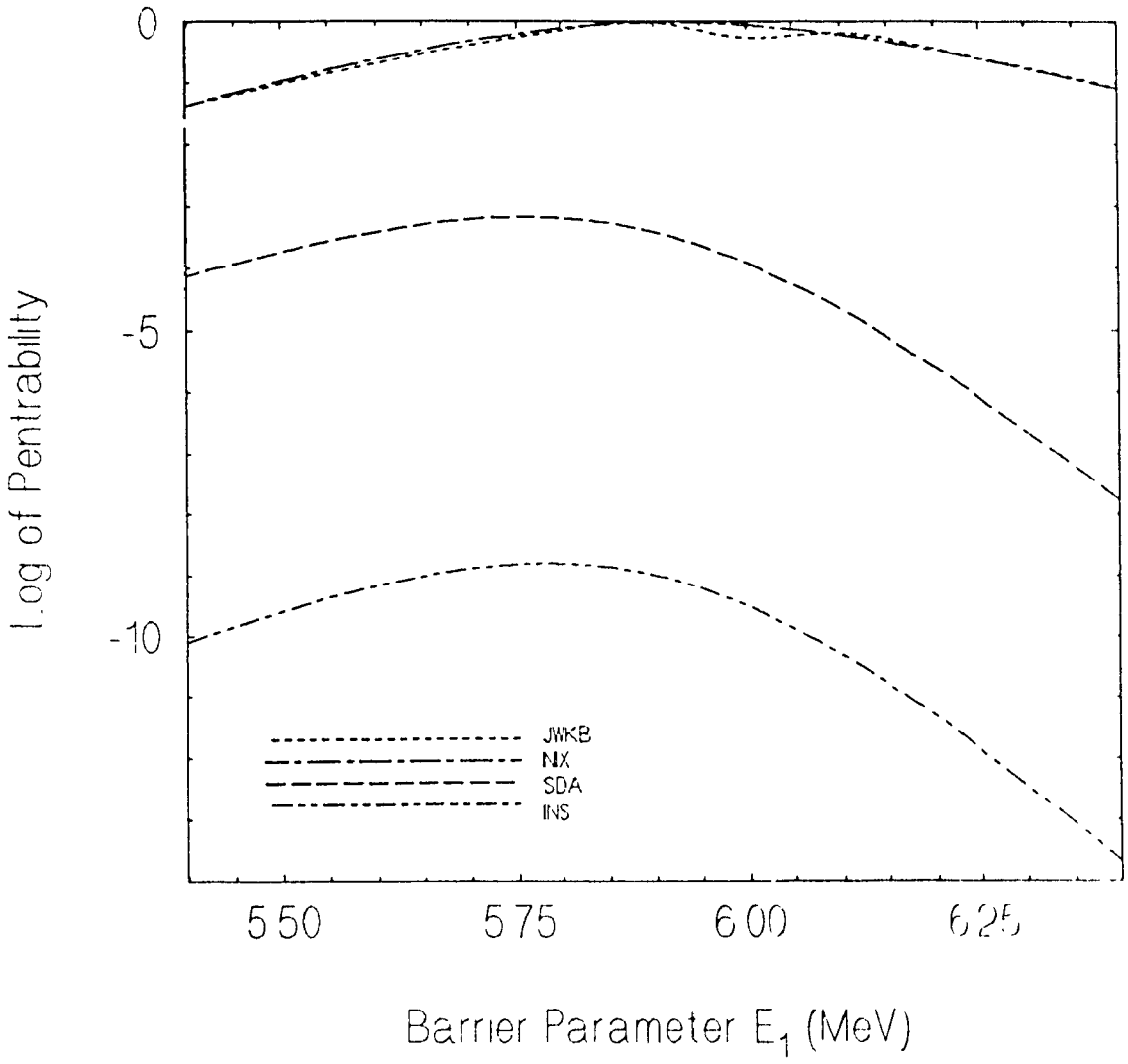

FIG. 43. Maximum Penetrability at resonance energy level L, for DATA I with changing barrier parameter E_1

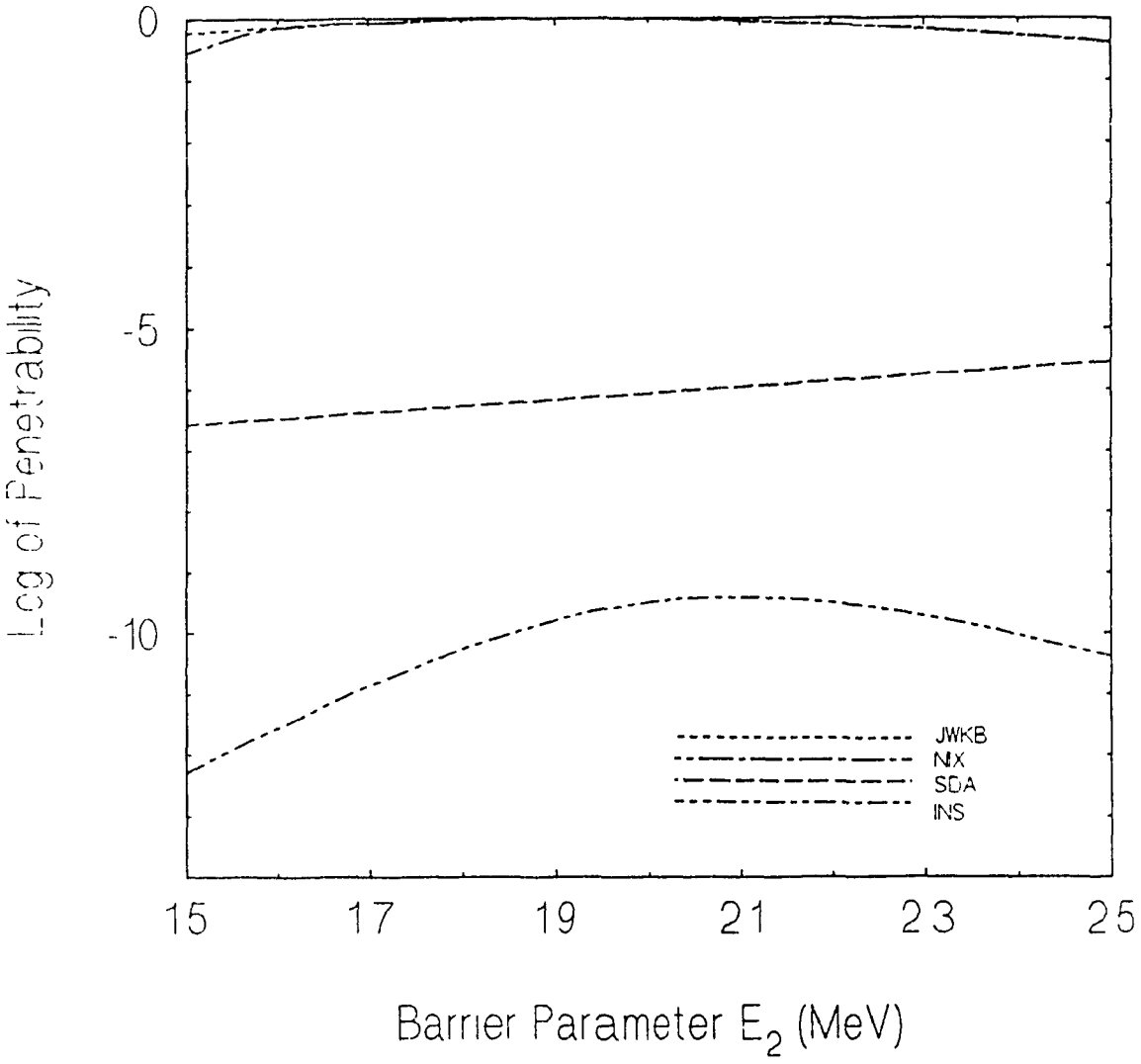

FIG. 44. Maximum Penetrability at resonance energy level L_1 for DATA I with changing barrier parameter E_2

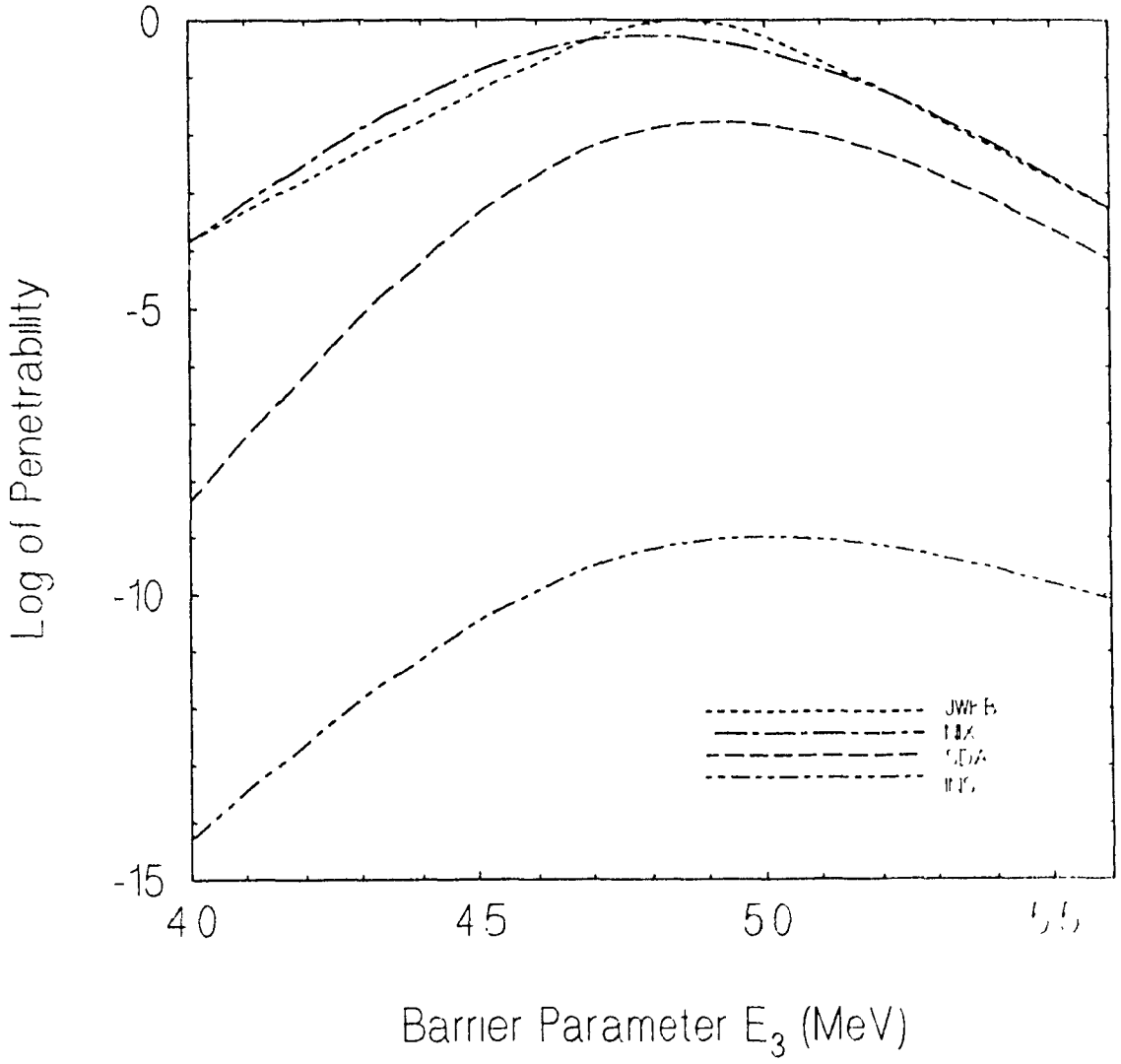

FIG. 45. Maximum Penetrability at resonance energy level L_1 for DATA I with changing barrier parameter E_3

The SDA and INS are more sensitive to changes in the barrier parameters and can vary by a factor of 10^{-12}. The smallest effects are felt by the JWKB and NIX, with a factor of 10^{-3}. Hence, the inclusion of reflection in the third barrier region of the double-humped barrier has the effect of sensitizing the maximum penetrability value at resonance with respect to barrier parameter fluctuations. The effect flattens out for $\hbar\omega_2$ and E_2 and are sharpest for $\hbar\omega_1, \hbar\omega_3$. For all methods, the penetrability variations are parabolic in nature, exhibiting one or two maxima. The JWKB graph for E_1 reveals two maxima. This is also present in the NIX graph for E_2.

The JWKB and NIX are notably very close in behaviour, with much higher peak maxima than SDA and INS. Although the INS probabilities are less than the SDA, and though the SDA are less than NIX and JWKB, the penetrabilities for SDA can sharply increase with fluctuations in $\hbar\omega_1$ (Fig. 40), even surpassing both NIX and JWKB.

8.3 Level Widths

Figs. 46 to 49 illustrate the resonance widths for Figs. 20 to 23. Resonance widths found for DATA I using JWKB, NIX, SDA, and INS reveal a consistent behaviour among methods. The resonance widths at half maximum (RWHM) increase for all barrier parameters except the barrier heights E_1 and E_3. For DATA I, the RWHMs for L_1 range from 10^{-10} to 10^{-17} for the JWKB and NIX methods and from 10^{-6} to 10^{-10} for the SDA and INS. For the highest bound state levels, for all methods, the RWHM is found to be in the tenth keVs.

NIX and JWKB are generally in agreement. The SDA and INS have greater widths at lower energy, in the order of 10^5 times. At high energies all methods are approximately in agreement.

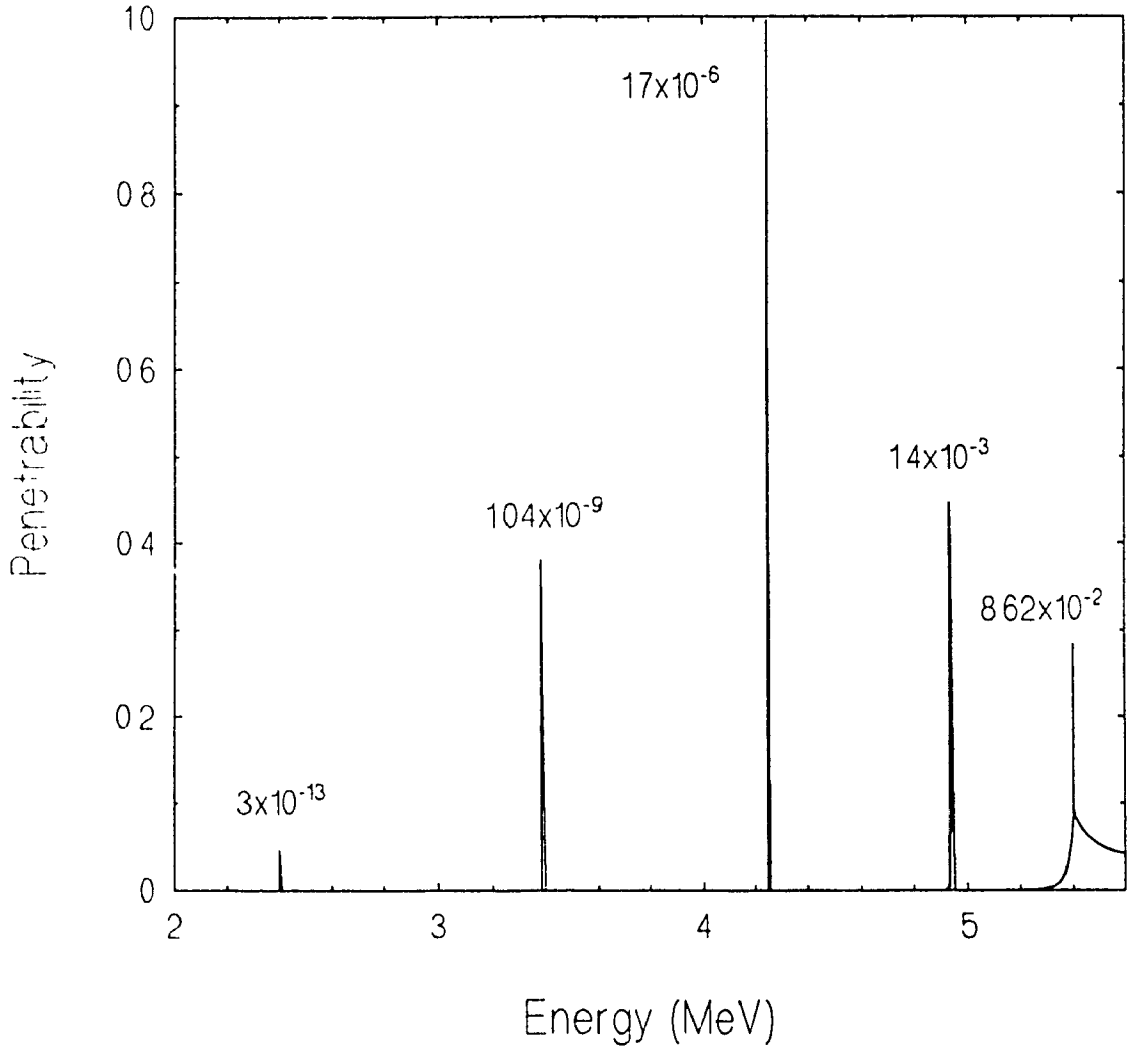

FIG. 46. Resonance widths at half maximum (RWHM) for resonances of Fig. 20.

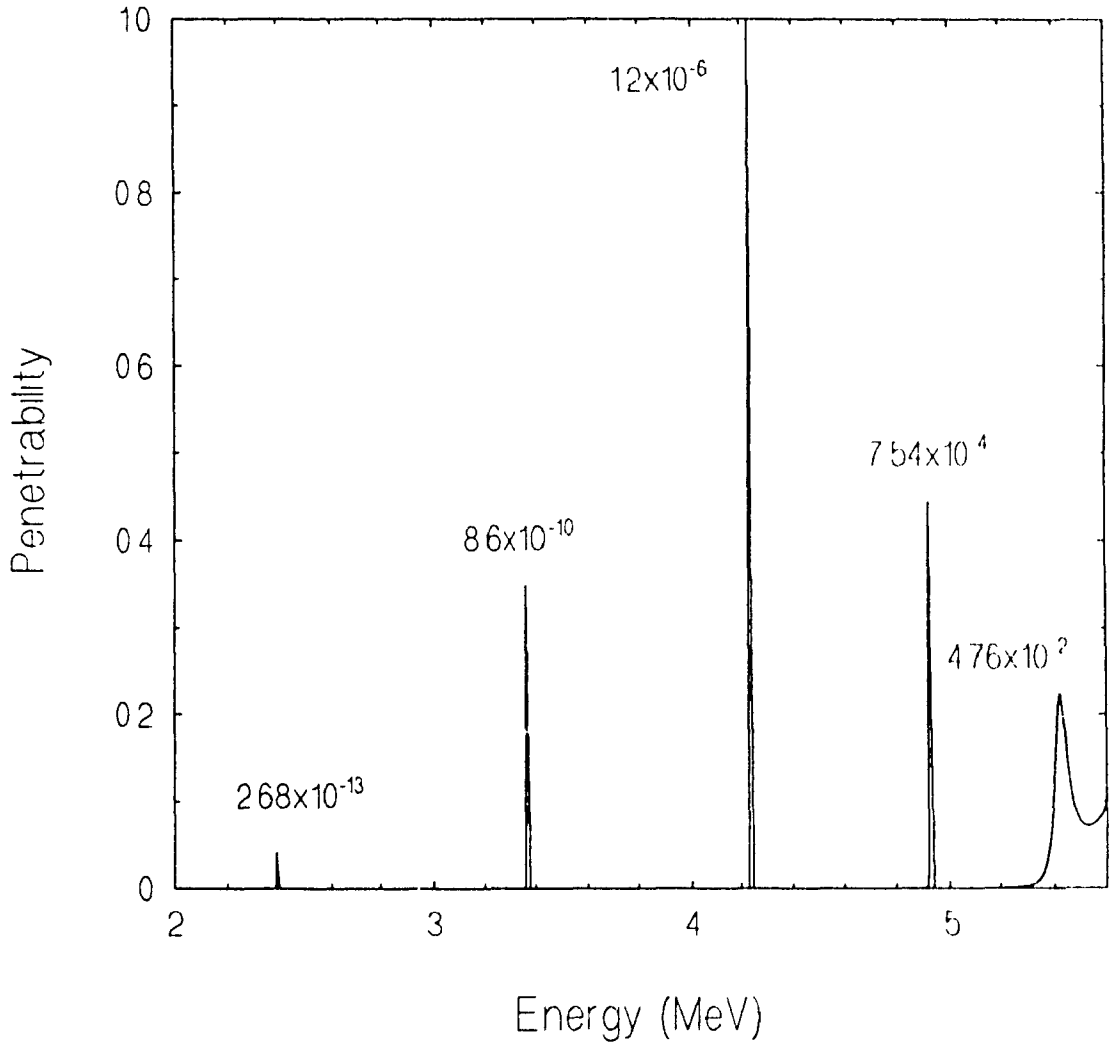

FIG. 47 Resonance widths at half maximum (RWHM) for resonances of Fig 21

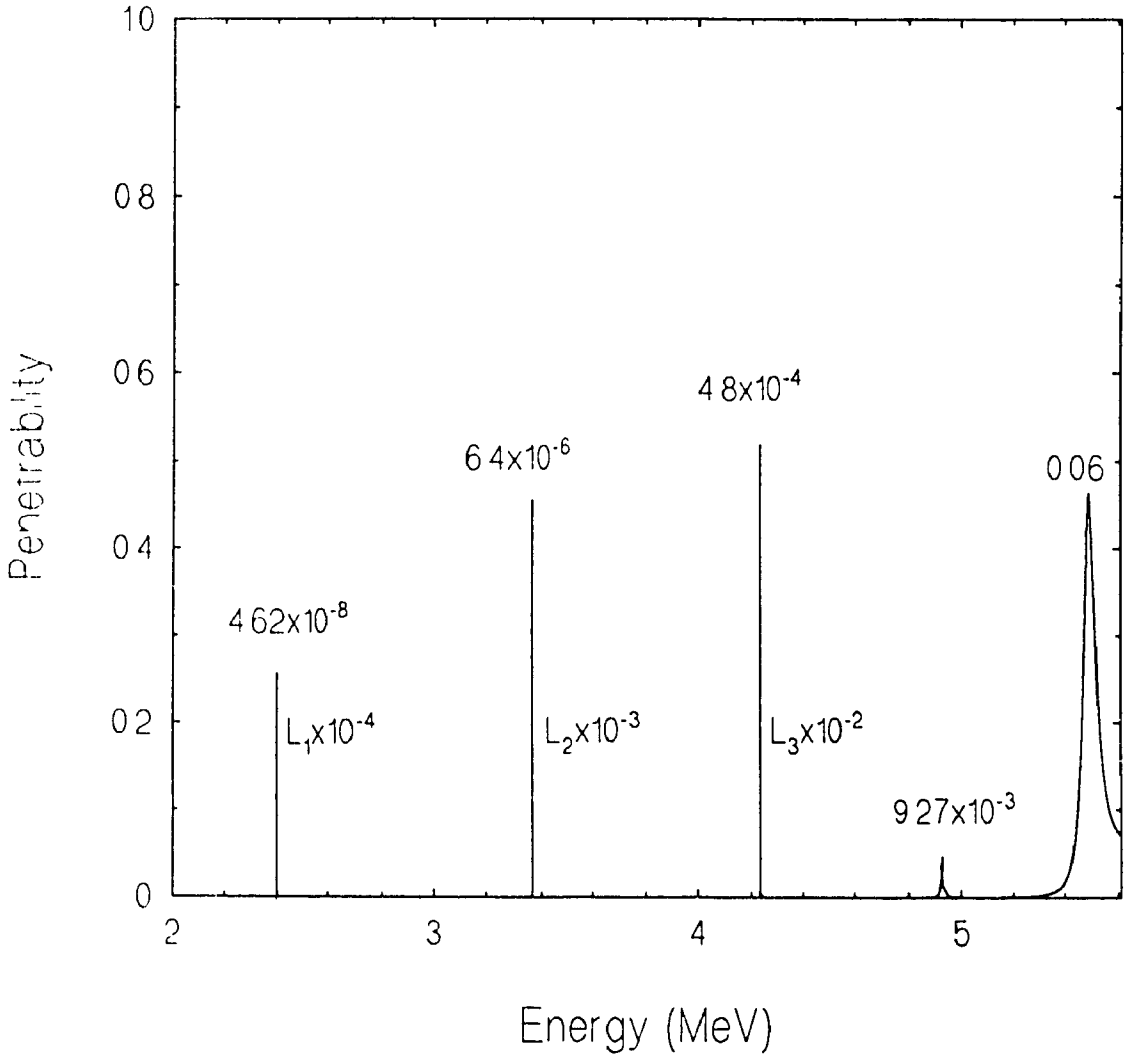

FIG. 48 Resonance widths at half maximum (RWHM) for resonances of Fig 22

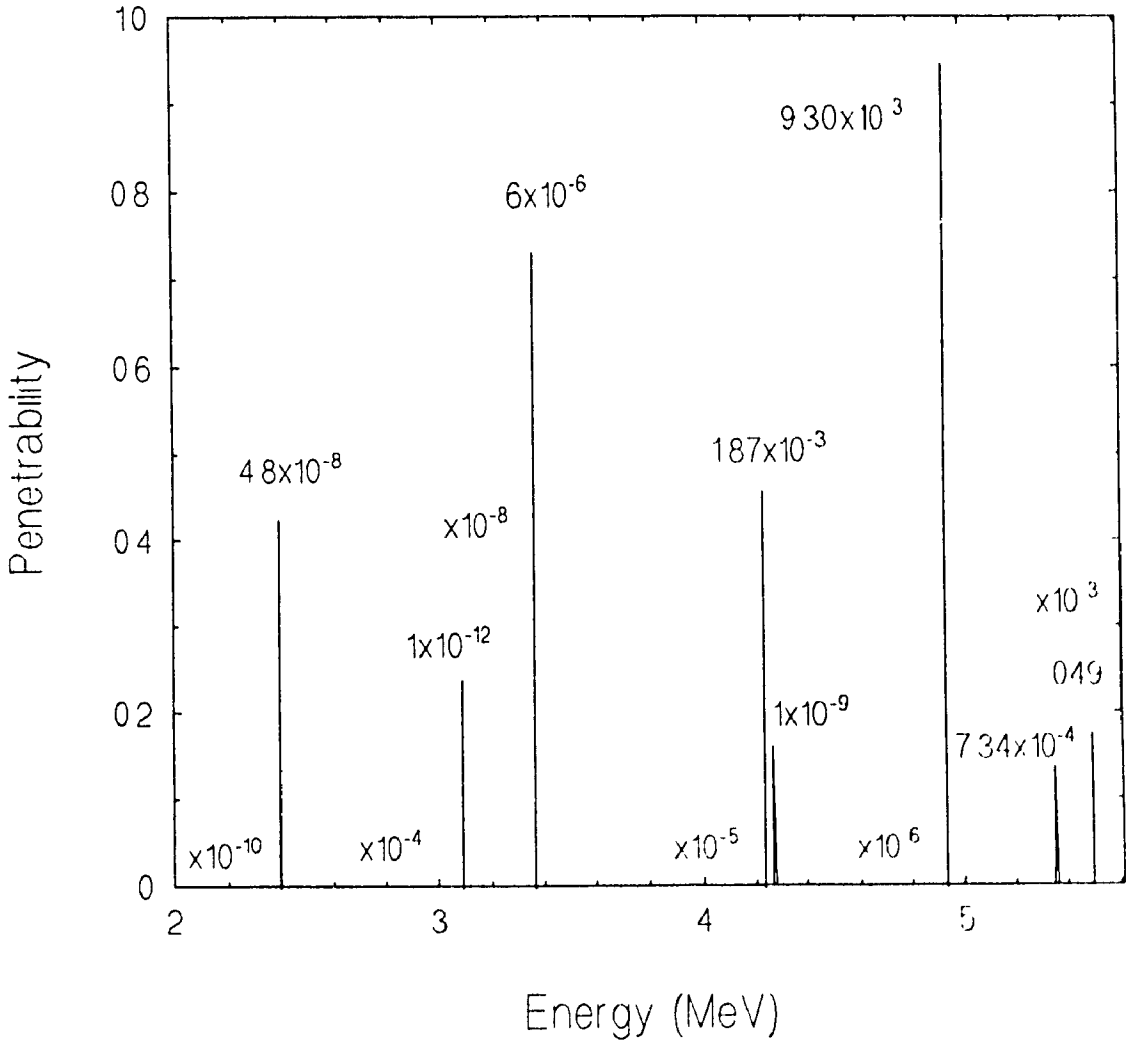

FIG. 49 Resonance widths at half maximum (RWHM) for resonances of Fig 23

8.4 Full-Barrier Penetrability from Ground State Energy

Equation 6.12 is the JWKB expression for tunnelling the complete double-humped barrier. For the exact methods, the spontaneous half-life is determined by calculating the penetrability from the ground-state deformation energy E_o=0. Equations 5.34 and 5.311 have the incident energy in the numerator. Consequently, they cannot be used to obtain the ground state energy, since they yield zero probabilities for non zero denominators. Fig. 50. is a plot of the full-barrier penetrability for SDA and INS. The penetrability approaches zero as the energy goes to zero.

Calculations of spontaneous fission based on DATA I reveal that an increase of 0.2 MeV in barrier height will decrease the penetrability by a factor of 5 to 10 times. Since E_1 and E_3 can vary upto 0.4MeV for U^{236} (TABLE I), it is possible to bring the JWKB and NIX values to agreement. This is true for any actinide nuclei. TABLE VI lists values for the spontaneous fission probability for JWKB and NIX. The values differ at least by a factor of 0.9 and at most by 184.1 for U^{236} whose experimental half-life is approximately $2x10^{16}$ years. Yet, by choosing E_1=5.73 and E_3=5.63 for JWKB and E_1=5.53 and E_3=5.43 for NIX, the penetrability become $3.593x10^{-43}$ and $7.109x10^{-44}$ consecutively. Therefore, the spontaneous fission half-life obtained by the JWKB has changes from being 184 times greater to 5 times.

TABLE VI. Comparison of JWKB and NIX values for the probability of spontaneous fission from it's ground state energy E = 0.

	JWKB $P(E_0)$	NIX $P(E_0)$	factor
am239	5.63830e-050	2.43910e-050	2.3
am240	8.03831e-062	9.09188e-062	0.9
am241	5.04382e-048	1.39576e-048	3.6
am242	9.93554e-064	8.70831e-064	1.1
am243	4.10219e-048	1.64321e-048	2.5
am244	8.03830e-062	9.09188e-062	0.9
am245	6.49145e-049	3.95747e-049	1.6
cm241	4.23776e-047	5.35302e-048	7.9
cm242	3.57330e-034	1.01141e-035	35.3
cm243	8.29216e-047	5.69867e-048	14.5
cm244	6.26389e-035	6.44015e-036	9.7
cm245	1.68263e-046	7.71778e-047	2.2
np237	4.50908e-048	4.66010e-048	1.0
pu235	3.11895e-047	2.16327e-047	1.4
pu237	3.88037e-048	2.44853e-048	1.6
pu238	1.04944e-038	2.53093e-039	4.1
pu239	7.54927e-051	4.63203e-051	1.6
pu240	5.20853e-039	8.78488e-040	5.9
pu241	1.94807e-049	4.57101e-050	4.3
pu242	5.72149e-039	1.21737e-039	4.7
pu243	1.59329e-046	9.59680e-047	1.7
pu244	1.44761e-038	3.88970e-039	3.7
pu245	1.65485e-045	1.19973e-045	1.4
u236	1.79184e-042	9.73139e-045	184.1
u238	2.55560e-042	3.73409e-043	6.8

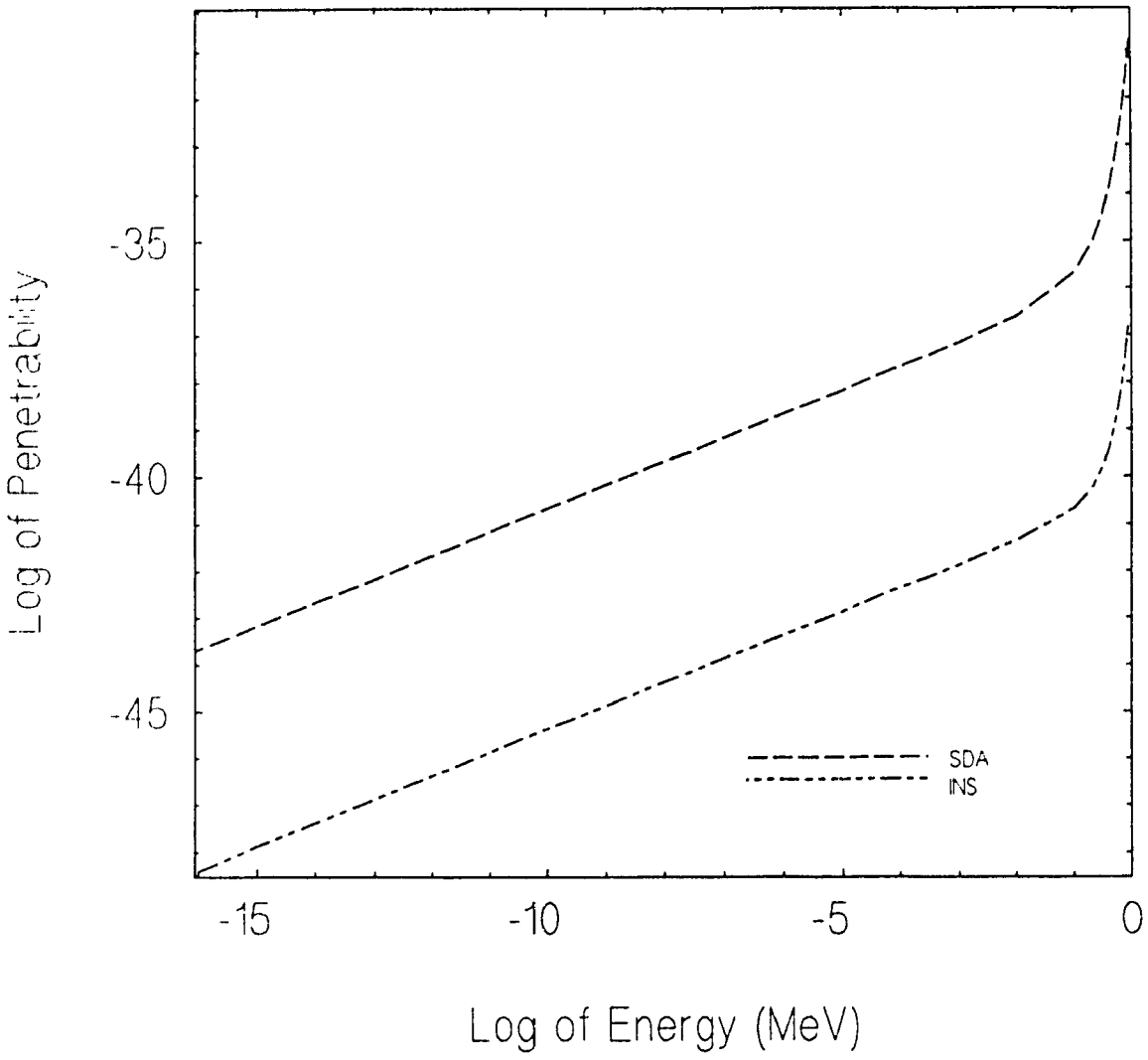

FIG. 50 Full-barrier penetrability from ground-state energy in SDA and INS calculations

8.5 Effect on Spontaneous and Isomeric Fission Half-Life

Equations 6.22 and 6.23 relate isomeric fission to the probability of penetrating the individual barrier of a double-humped barrier. It is well known that exact and JWKB expressions for the penetrability through a one-peaked barrier yield very good tunnelling values for both methods. Therefore, since only the isomeric energy is required from the JWKB, NIX, INS, and SDA methods and since they are very close in the actinide region, all methods will predict Isomeric half-lives very closely, with approximately 10% difference. Even though, it is possible to adjust the barrier parameters slightly, bringing the Exact and JWKB into agreement. Isomeric fission half-lives will exhibit greatest deviations for symmetric barriers with high values of $\hbar\omega_2$.

Experimentally, barrier parameters may deviate from ±0.2 to ±0.6 MeV. The differences in method used, in general, vary less for a particular set of data than differences due to changes in barrier parameters in the range ±0.2to ±0.6. This along with the sensitive nature on the SDA make it possible to adjust barrier parameters in favour of a particular method, as was done by Bhandhari[45], in his use of TABLE I. The same holds for spontaneous fission. It is relatively easy to adjust barrier parameters within its allowed tolerance, in favour of one method over another. Simply increasing the value of E_1 for U^{236} by 0.2 MeV will change the spontaneous fission half-live from $2x10^{16}$ yrs to $1x10^{17}$ yrs.

Conclusion

It is apparent that significant differences exist among the various exact and approximate penetrability expressions. However, the magnitude of numerical deviations among various methods are in general less than experimental error. This fact, coupled with the simplified assumption of the double-humped barrier as smoothly joined parabolas, makes it difficult to determine which method gives the best results when evaluating spontaneous and isomeric fission half-lives.

The isomeric energy does not differ among exact methods. The same is true for the asymptotic JWKB method and Lebeouf's use of the uni-directional connection formulas. As a result, isomeric half-lives differ only between Exact and JWKB methods. For the actinide nuclei, the greatest difference is found to be 10%. Yet, it is possible to adjust barrier parameters within 0 to 0.4MeV to obtain 0% difference, whereas experimental error can be as high as 48%. Nix's remark that the energy shifts increase at higher energies is only true away from resonances. At resonances, his observation is only valid for low $\hbar\omega_2$ values.

The exact methods of Sharma and Lebeouf yield penetrability expressions with smaller resonance widths at low energies, than the asymptotic JWKB and NIX expressions. At

higher energies the widths are comparable. Both the Nix and JWKB maximum penetrabilities at resonances are much higher and less sensitive to barrier fluctuations than Sharma and Lebeouf's exact methods. These results do not effect calculations of spontaneous and isomeric half-lives, therefore, it is left for future work to investigate what effect these differences will have on the various types of nuclear reaction cross-sections.

Spontaneous fission half-lives can differ by factors of upto 184 times for the actinide nuclei. However, once again, it is possible to adjust the barrier parameters, within its allowed experimental error, and obtain a 0% difference between the JWKB and NIX methods. Therefore, there does not appear to be any obvious advantages in using one penetrability expression over another for evaluating spontaneous and isomeric fission half-lives.

APPENDIX A

Requiring wave functions (5.17a-c) and their derivatives to be continuous at connecting points a and b gives

$$AE_a^*(\alpha_1,-u)+BE_a(\alpha_1,-u)=CU_a(\alpha_2,v)+DV_a(\alpha_2,v) \tag{A.1}$$

$$\begin{aligned} A[-u'E_a^{*(-u)}(\alpha_1,-u)]+B[-u'E_a^{(-u)}(\alpha_1,-u)]= \\ C[v'U_a^{(v)}(\alpha_2,v)]+D[v'V_a^{(v)}(\alpha_2,v)] \end{aligned} \tag{A.2}$$

$$CU_b(\alpha_2,v)+DV_b(\alpha_2,v)=TE_b(\alpha_3,w) \tag{A.3}$$

$$Cv'U_b^{(v)}(\alpha_2,v)+Dv'V_b^{(v)}(\alpha_2,v)=Tw'E_b^{(w)}(\alpha_3,w) \tag{A.4}$$

dividing by A gives

$$\frac{B}{A}(E_a(\alpha_1,-u))-\frac{D}{A}(V_a(\alpha_2,v))-\frac{C}{A}(U_a(\alpha_2,v))-0=E_a^*(\alpha_1,-u) \tag{A.5}$$

$$\frac{B}{A}\left(-u' E_a^{(-u)}(\alpha_1, -u)\right) - \frac{D}{A}\left(v' V_a^{(v)}(\alpha_2, v)\right) - \frac{C}{A}\left(v' U_a^{(v)}(\alpha_2, v)\right) - 0 = -u' E_a^{*}(\alpha_1, -u) \tag{A.6}$$

$$0 - \frac{D}{A}\left(V_b(\alpha_2, v)\right) - \frac{C}{A}\left(U_a(\alpha_2, v)\right) - \frac{T}{A}\left(E_b(\alpha_3, w)\right) = 0 \tag{A.7}$$

$$0 - \frac{D}{A}\left(v' V_b^{(v)}(\alpha_2, v)\right) - \frac{C}{A}\left(v' U_b^{(v)}(\alpha_2, v)\right) - \frac{T}{A}\left(w' E_b^{(w)}(\alpha_3, w)\right) = 0 \tag{A.8}$$

using Cramer's Rule

$$\frac{T}{A} = \frac{\det(A_3)}{\det(A)} \tag{A.9}$$

(A.10)

$$\det(A_3) = \begin{vmatrix} E_a(\alpha_1, -u) & -V_a(\alpha_2, v) & -U_a(\alpha_2, v) & E_a^{*}(\alpha_1, u) \\ -u' E_a^{(-u)}(\alpha_1, -u) & -v' V_a^{(v)}(\alpha_2, v) & v' U_a^{(v)}(\alpha_2, v) & -u' E_a^{*(u)}(\alpha_1, -u) \\ 0 & V_b(\alpha_2, v) & U_b(\alpha_2, v) & 0 \\ 0 & v' V_b^{(v)}(\alpha_2, v) & v' U_b^{(v)}(\alpha_2, v) & 0 \end{vmatrix}$$

(A.11)

$$\det(A_3) = u'v'[(E_a^*(\alpha_1,-u)\,E_a^{(-u)}(\alpha_1,-u)) - (E_a(\alpha_1,-u)\,E_a^{*(-u)}(\alpha_1,-u))]$$
$$[(U_b(\alpha_2,v)\,V_b^{(v)}(\alpha_2,v)) - (V_b(\alpha_2,v)\,U_b^{(v)}(\alpha_2,v))]$$

this can be rewritten using Wronskians

$$\det(A_3) = u'v'W[E^*(\alpha_1,-u)\,E(\alpha_1,-u)]\,W[U(\alpha_2,v),V(\alpha_2,v)] \quad (A.12)$$

$$\det(A) = \begin{vmatrix} E_a(\alpha_1,-u) & -V_a(\alpha_2,v) & -U_a(\alpha_2,v) & 0 \\ -u'E_a^{(-u)}(\alpha_1,-u) & -v'V_a^{(v)}(\alpha_2,v) & v'U_a^{(v)}(\alpha_2,v) & 0 \\ 0 & V_b(\alpha_2,v) & U_b(\alpha_2,v) & -E_b(\alpha_3,w) \\ 0 & v'V_b^{(v)}(\alpha_2,v) & v'U_b^{(v)}(\alpha_2,v) & -w'E_b^{(w)}(\alpha_3,w) \end{vmatrix} \quad (A.13)$$

Finally,

$$\frac{T}{A} = \frac{v'u'W[E^*(\alpha_1,-u),E(\alpha_1,-u)]\,W[U(\alpha_2,v),V(\alpha_2,v)]}{\begin{vmatrix} E_a(\alpha_1,-u) & -V_a(\alpha_2,v) & -U_a(\alpha_2,v) & 0 \\ -u'E_a^{(-u)}(\alpha_1,-u) & -v'V_a^{(v)}(\alpha_2,v) & v'U_a^{(v)}(\alpha_2,v) & 0 \\ 0 & V_b(\alpha_2,v) & U_b(\alpha_2,v) & -E_b(\alpha_3,w) \\ 0 & v'V_b^{(v)}(\alpha_2,v) & v'U_b^{(v)}(\alpha_2,v) & -w'E_b^{(w)}(\alpha_3,w) \end{vmatrix}} \quad (A.14)$$

APPENDIX B

$$\overline{a}(w) = \begin{pmatrix} a_1(w) \\ a_2(w) \end{pmatrix} \tag{B.1}$$

$$\overline{M}(w) = \frac{1}{2} i \begin{pmatrix} 1 & e^{-2iw} \\ -e^{2iw} & -1 \end{pmatrix} \tag{B.2}$$

$$\overline{\zeta}(z) = \begin{pmatrix} q(z)^{-1/2} \exp(iw(z)) \\ q(z)^{-1/2} \exp(-iw(z)) \end{pmatrix} \tag{B.3}$$

Connecting two points on opposite sides of an Overdense Potential

$$F(z, z_o) = \begin{pmatrix} -[1+O(\mu)]e^{2k} & i+O(\mu) \\ [i+O(\mu)]e^{2k} & 1+O(\mu) \end{pmatrix} \tag{B.4}$$

$$k = \int_{x^I}^{x^{II}} q(z)\, dz \tag{B.5}$$

Connecting two points on opposite sides of an Overdense Potential

$$\overline{F}(z, z_o) = \begin{pmatrix} -e^{2k} & e^{i\varphi}(1+e^{-2k1/2}) \\ e^{i\varphi}(1+e^{-2k1/2}e^{2k}) & 1 \end{pmatrix} \qquad \text{(B.6)}$$

APPENDIX C

Eqs. C.1-C.4 are expressions for the Weber Function W(a,x) and its derivative in terms of Airy Functions. The expressions involve solving for coefficients. This is a lengthy process and will only be done for the above mentioned weber function. Other functions U,V and their derivatives can be expressed in a similar way (see Olver[43]).

$$W(a,x) = -\frac{E(\mu)\,C(t(\mu),\zeta)\,D_1(\mu,\zeta)}{B(u)} \tag{C.1}$$

$$W(a,-x) = E(\mu)\,C(t(u),\zeta)\,D_3(\mu,\zeta)\,B(\mu) \tag{C.2}$$

$$W'(a,x) = \frac{-A(\mu)\,D_2(\mu,\zeta)}{B(\mu)\,C(t(\mu),\zeta)} \tag{C.3}$$

$$W'(a,-x) = \frac{A(\mu)\,D_4(\mu,\zeta)\,B(\mu)}{C(t(\mu),\zeta)} \tag{C.4}$$

The functions A,B,C,D_i, and E are ,

$$A(\mu) = \sqrt{\frac{\pi}{2}}\,\mu^{2/3} I(\mu) \tag{C.5}$$

$$B(\mu) = \sqrt{2}\, e^{\frac{1}{4}\pi\mu^2} \tag{C.6}$$

$$C(t(\mu),\zeta) = \left(\frac{\zeta}{t^2-1}\right)^{1/4} \tag{C.7}$$

$$D_1(\mu,\zeta) = B_1(-\mu^{3/4}\zeta)\sum_{s=0}^{\infty} -1^s \frac{a_s(\zeta)}{\mu^{4s}} + \frac{B_i'(-\mu^{4/3}\zeta)}{\mu^{8/3}}\sum_{s=0}^{\infty} -1^s \frac{b_s(\zeta)}{\mu^{4s}} \tag{C.8}$$

$$D_2(\mu,\zeta) = -B_1(-\mu^{3/4}\zeta)\sum_{s=0}^{\infty} -1^s \frac{c_s(\zeta)}{\mu^{4s}} + B_i'(-\mu^{4/3}\zeta)\sum_{s=0}^{\infty} -1^s \frac{d_s(\zeta)}{\mu^{4s}} \tag{C.9}$$

$$D_3(\mu,\zeta) = A_1(-\mu^{3/4}\zeta)\sum_{s=0}^{\infty} -1^s \frac{a_s(\zeta)}{\mu^{4s}} + \frac{A_i'(-\mu^{4/3}\zeta)}{\mu^{8/3}}\sum_{s=0}^{\infty} -1^s \frac{b_s(\zeta)}{\mu^{4s}} \tag{C.10}$$

$$D_4(\mu,\zeta) = -A_1(-\mu^{3/4}\zeta)\sum_{s=0}^{\infty} -1^s \frac{c_s(\zeta)}{\mu^{4s}} + A_i'(-\mu^{4/3}\zeta)\sum_{s=0}^{\infty} -1^s \frac{d_s(\zeta)}{\mu^{4s}} \tag{C.11}$$

$$E(\mu) = \sqrt{\pi}\,\mu^{1/3} I(\mu) \tag{C.12}$$

The arguments of the above functions are given as,

$$\mu=\sqrt{2a}, \quad t=\frac{x}{\sqrt{2}\mu} \tag{C.13a,b}$$

$$I(\mu)=\frac{2^{1/4}}{\mu^{1/2}}\left(1-\frac{1}{1152\mu^4}-\frac{16123}{39813120\mu^8}\right) \tag{C.14}$$

$$\zeta^{3/2}=\frac{3}{4}t(t^2-1)-\frac{3}{4}\ln[t+(t^2-1)^{1/2}] \tag{C.15}$$

The first two coefficients for a_s, b_s, c_s, d_s are,

$$a_0=m_0M_0 \tag{C.16a}$$

$$a_1=m_0M_2+m_1\zeta^{-3/2}M_1+m_2\zeta^{-3}M_0 \tag{C.16b}$$

$$b_0=\zeta^{-1/2}(-n_0M_1-n_1\zeta^{-3/2}M_0) \tag{C.17a}$$

$$b_1=\zeta^{-1/2}(-n_0M_3-n_1\zeta^{-3/2}M_2-n_2\zeta^{-3}M_1-n_3\zeta^{-9/2}M_0) \tag{C.17b}$$

$$c_0=\zeta^{1/2}(-m_0R_1-m_1\zeta^{-3/2}R_0) \tag{C.18a}$$

$$c_1=\zeta^{1/2}(-m_0R_3-m_1\zeta^{-3/2}R_2-m_2\zeta^{-3}R_1) \tag{C.18b}$$

$$d_0 = n_0 R_0 \qquad \text{(C.19a)}$$

$$d_1 = n_0 R_2 + n_1 \zeta^{-3/2} R_1 + n_2 \zeta^{-3} R_0 \qquad \text{(C.19b)}$$

The above coefficients require additional coefficients given as follows,

$$n_0 = 1\,,\; n_1 = \frac{5}{48}\,,\; n_2 = \frac{385}{4608}\,,\; n_3 = \frac{85085}{663553} \qquad \text{(C.20a,b,c)}$$

$$m_0 = 1\,,\; m_1 = -\frac{7}{48}\,,\; m_2 = -\frac{455}{4608}\,,\; m_3 = -\frac{95095}{663552} \qquad \text{(C.21a,b,c)}$$

$$M_0 = 1 \quad,\; M_1 = \frac{t^3 - 6t}{24\,(t^2-1)^{3/2}} \qquad \text{(C.22a,b)}$$

$$M_2 = \frac{-9t^4 + 249t^2 + 145}{1152\,(t^2-1)^3} \qquad \text{(C.22c)}$$

$$M_3 = \frac{-4042t^9 + 18189t^7 - 28287t^5 - 151995t^3 - 259290t}{414720\,(t^2-1)^{9/2}} \qquad \text{(C.22d)}$$

$$R_0=1 \quad , R_1=\frac{t^3+6t}{24(t^2-1)^{3/2}} \qquad \text{(C.23a,b)}$$

$$M_2=\frac{15t^4-327t^2-143}{1152(t^2-1)^3} \qquad \text{(C.23c)}$$

$$R_3=\frac{-4042t^9+18189t^7-36387t^5+238425t^3+259290t}{414720(t^2-1)^{9/2}} \qquad \text{(C.23d)}$$

The function A_i and B_i are Airy Functions.

REFERENCES

1 Fermi, E. (1934). Nature (London) **133**, 898

2 Hahn, O., and Strassmann, F. (1939). Naturwissenschaften **26**, 755.

3 Curie, I.J., and Savitch (1938).

4 Meitner, L. and Fisch, O.R. (1939). Nature (London) **143**, 239.

5 Bohr, N., and Wheeler, J.A. (1939). Phys. Rev. **56**, 426.

6 Mottelson, B,R., and Nillson, S.G. (1956). Klg. Dan. Vidensk. Selsk. Mat. Fys. Skr. **1**, No. 8.

7 Bes, D., and Szymanski, Z. (1961). Nucl. Phys. **28**, 42.

8 Strutinsky, V.M. (1967). Nucl. Phys. **A95**, 420.

9 Möller, P. and Nix, J.R., (1974), in Physics and Chemistry of Fission, Proceedings of a Conference at Rochester (IAEA, Vienna), Vol. 1, p.103.

10 Wong, C.Y., and Bang, J., Phys. Letters **29B**, 143 (1969), in Proceeding of the Second Symposium on the Physics and Chemistry of Fission, Vienna, Autstria, (1969) , (International Atomic Energy Agency, Vienna, Austria, 1969), p.923.

11 David, B., *Quantum Theory*, Prentice Hall, (1951).

12 Merzbacher, E., *Quantum Mechanics*, John Wiley & Sons., New York (1970).

13 Kemble, E.C., *The Fundamental Priciples of Quantum Mechanics*, McGraw Hill, New York, (1937).

14 Fromöm, N., and Fröman, P.O. (1965). *JWKB Approximation, Contributions to the theory* , North-Holland Publishing Company, Amsterdam.

15 Ignatyuk, A.V., Rabotnov, N.S., and Smirenkin, G.N., Phys. Letters **29B**, 209 (1969).

16 Bhandari, B.S., Ph.D. Thesis, Ohio University, (1974).

REFERENCES

17 Bhandari, B.S., Nucl. Phys. **A256**, 271 (1976).

18 Bhandari, B.S., Phys. Rev. **C19**, 1820 (1979); 22, 606 (1980).

19 Cramer, J.D., and Nix, J.R. (1970). Phys. Rev. **C2**, 1048.

20 Leboeuf, J.N. (1972). M.Sc. Thesis., Concordia University.

21 Sharma, R.C., and Leboeuf, J.N. (1975). Canadian Journal of Physics. Vol 53 Num 24, 2648-2653.

22 Sharma, R.C., and Leboeuf, J.N. (1976). Phys. Rev. **C14**, 6.

23 Swiatecki, W.J., and Bjornholm, S. (1972). Physics Reports. **4**, No. 6, 325-341.

24 Cohen, S., and Swiatecki, W.J. (1963). Ann. Phys. (N.Y.) **22**, 406.

25 Gamow, G.Z., Physik., 89 p.592, (1934).

26 Elsasser, W.J., Phys. Rad., 5 p.635, (1934).

27 Nillson, S.G., (1955). Kgl. Danske Videnskab. Selskab Mat. Fys. Medd. 29. [Intro., 8.3-9.4]

28 Brack, M., Dangaard, J., Jensen, A.S., Pauli, H.C., Rev of Modern Physics , vol 44 Num 2.

29 Larsson, S.E., and Leander, G. (1974), in Physics and Chemistry of Fission, Proceedings of a Conference at Rochester (IAEA, Vienna), Vol.1, p.177.

30 Flocard, H., Quentin, P., Vautherin, D., and Kerman, A.K., (1974), in Physics and Chemistry of Fission, Proceedings of a Conference at Rochester (IAEA, Vienna), Vol. 1, p.221.

31 Jeffreys, B.s., 1961, The asymptotic approximation method. Review article in: Quantum theory I, edited by Bates, D.R., (Academic Press, New York and London).

REFERENCES

32 Kramers, H.A., (1926). Z.f. Physik **39**, 828.

33 Morse, P.M., and Feshbach, H., (1953) *Methods of Theoretical Physics, Part II* (McGraw - Hill Book Company, Inc., New York and London).

34 Onley, D.S., *Lecture notes on Quantum Mechanics*, (1970).

35 Langer, R.E., (1937), Phys. Rev. **51**, 669.

36 Hecht, E.C., and Mayer, E.J., (1957), Phys. Rev. Vol 106 Num 6, 1156-1160.

37 Nix, J.R., and Walker, G.E., (1969), Nucl. Phys., **A132**, 60-74.

38 Polikanov, S.M., Druin, V.A., Karauchov, V.A., Mikheev, V.L., Pleve, A.A., Skobelev, N.K., Subotin, V.G., Ter-Akapian, G.M., and Fomichev, V.A., (1962), Zh. Eksp. Teor. Fiz. **42**, 1016.

39 Bjornholm, S., and Lynn, J.E., Rev. Mod. Phys. **52**, 725 (1980)

40 Miller, J.C.P., *Tables of Weber Parabolic Cylinder Funcions*. (1955), Her Majesty's Stationary Office.

41 National Bureau of Standards, 1949B. *TABLES OF THE Confluent Hypergeomtric Function $F(\frac{1}{2}n;\frac{1}{2};x)$ and Related Functions*. Applied Mathematical Series, 3. Washington, UnitedStates Government Printing Office.

42 Olver, F.W.J., *Uniform Asymptotic Expansions for Weber Parabolic Cylinder Functions of Large Orders*. (1959) Journal of Research of the National Bureau of Standards, Vol **63B** No. 2.

43 Lowan, A.N., and Horenstein, W., (1942), *On the Function $H(m,a,x) = exp(-ix)F(m+1-ia,2M+2;2ix)$*. Journal of Mathematics and Physics, **21**, 264-283.

44 Moshier, S.L., *Methods and Programs for Mathematical Functions*. (1989), John Wiley & Sons, N.Y.

45 Bhandari, B.S., (1989) Phys. Rev. Vol 42, Num 4, 1443.